SIMS STUDIES ON ISOTOPIC ABUNDANCE ANOMALIES OF MAGNESIUM IN PRIMITIVE METEORITES

BY

HIROSHI NISHIMURA

Institute of Geological Sciences
College of General Education
Osaka University

1982

PREFACE

The origin of the solar system has been interesting historically for a long period of time. For the study of the early solar system, extraterrestrial materials such as meteorites play an important role, because some of them contain informations about the primordial solar nebula.

Recently, isotopic studies on meteorites have brought fruitful results, among which, the most striking is on the idea of the multi-component solar nebula. First evidence was found by Clayton et al. through the study of the Allende meteorite which fell in 1969. They found the excess of ^{16}O in the meteorite, which was interpreted as the result of the injection of new component into the early solar nebula.

This paper describes results of study, which strongly supports the above mentioned idea, through the discovery of ^{24}Mg anomaly in the Allende and Yamato-74191 meteorites.

This paper consists of six sections and an appendix. Section one is a historical view and an introduction to the investigation of isotopic abundance anomaly of magnesium. Section two is a description of samples of meteorites and terrestrial minerals. Section three is a description of apparatus used in the present investigation, which are ion microprobe mass analyzers. In section four and section five, experimental procedures, results and discussion for magnesium isotopic abundance ratio measurements are described. Conclusion is stated in section six. In the appendix, computer programs developed by the author himself for a precise isotopic ratio measurement are listed.

CONTENTS

ABSTRACT

Isotopic abundance ratios of magnesium have been measured in the Allende (C3), Yamato-74191 (L3) and Yamato-75028 (H3) meteorites. Three Al-rich inclusions in Allende have been analyzed and excess ^{26}Mg due to the decay of now-extinct ^{26}Al has been found in the two of them. One of them has excess ^{26}Mg correlating with Al/Mg ratio. The other one has excess ^{26}Mg, but it is likely to diffuse out to the boundary layer by the heating after the specimen was formed. Al-correlated excess ^{26}Mg gives an estimate of $^{26}Al/^{27}Al$ ratio of $(2.8 \pm 2.2) \times 10^{-4}$ at the time when the minerals in the inclusion crystallized. This leads to the estimate of a time interval between the nucleosynthesis of ^{26}Al and the crystallization of the minerals of $(1.3\ ^{+1.6}_{-0.6}) \times 10^{6}$ years.

Excess ^{24}Mg has been discovered for Al-poor and Mg-rich matrix areas of both Allende and Yamato-74191. The excess ^{24}Mg is suggestive of the nucleosynthesis of almost pure ^{24}Mg and its injection into the pre-existed solar nebula. And this almost pure ^{24}Mg is expected to be synthesized in an explosive carbon burning process on the occasion of a supernova explosion.

These isotopic abundance anomalies of ^{24}Mg and ^{26}Mg experimentally found in this work together with ^{16}O excess reported by Clayton et al. can be strong evidences to support the hypothesis that the primordial solar nebula was inhomogeneous and composed of at least two components.

1. HISTORICAL VIEW AND INTRODUCTION

Isotopic abundance anomalies in primitive meteorites play an important role in the understanding of the origin and the early history of the solar nebula.

Before 1960's it had been accepted that the primordial solar nebula was a single component and isotopically homogeneous.[1-3] Meanwhile, isotopic abundance anomalies had long been searched in meteoritic and terrestrial samples in conjunction with the production of nuclei by the irradiation of energetic particles in the early history of the solar system.

In 1960, Reynolds[4] reported that the large excess of ^{129}Xe was ascribed to the radioactive decay of now extinct ^{129}I whose half life is 1.7×10^7 years. It was concluded that ^{129}I still existed at the time of the solidification of the chondrite. The time interval between the solidification and the nucleosynthesis was calculated to be $(3.5 \pm 0.6) \times 10^8$ years for Richardton assuming that the ratio of ^{129}I to ^{127}I at the termination of nucleosynthesis, $(^{129}I/^{127}I)_o$, is equal to unity. This time interval has been called "formation interval".

Magnesium isotopic anomalies have been investigated especially for the excess of ^{26}Mg due to the decay of now extinct ^{26}Al (half life = 7.2×10^5 y), since ^{26}Al was thought to be possible heat source in melting meteorite parent bodies.[5] In spite of the search for ^{26}Mg anomaly,

neither excess nor depletion exceeding statistical errors have been observed until 1972.

In 1964, Shima[7] reported no variation of magnesium isotopic abundance for three terrestrial and one chondritic samples.

In 1970, Clarke et al.[9] reported that Bruderheim and Kohr Temiki chondrites had 4 to 6 ‰ excess in ^{26}Mg. For the same samples, however, Schramm et al.[10] observed no anomaly of ^{26}Mg in 1970.

The Allende meteorite, which fell in Mexico in 1969,[11] has brought an unexpected development in the investigation of the origin of the primordial solar nebula through isotopic anomaly studies. This meteorite has been classified into C3 carbonaceous chondrite, and much examined since its fall. It was confirmed mineralogically[12,13] and isotopically[14-32] to contain primordial materials. The isotopic evidence of primitiveness firstly found was the anomaly of ^{16}O. The excess ^{16}O was observed for Ca-Al-rich white inclusions in Allende by Clayton et al.[14] They have described that the excess ^{16}O might be the result from the admixture of a component of almost pure ^{16}O. They thought that this component might represent interstellar material with a separate history of nucleosynthesis. Furthermore, ^{16}O anomalies have been found even in an ordinary chondrite ALHA-76004 of the type LL3 by Mayeda et al.[15]

The attempts of searching for the excess ^{26}Mg which was a decay product from ^{26}Al have been successively carried

out for Allende by several workers. Gray and Compston[16] showed in 1974 that the excess ^{26}Mg was found to be 0.41 % in a chondrule with high Al/Mg ratio, and it was concluded to be due to the decay of ^{26}Al. In the same year, Lee and Papanastassiou[17] reported the ^{26}Mg anomalies, but the anomalies did not correlate with Al/Mg, and did not appear to be due to ^{26}Al decay. Lee et al.[18] reexamined in 1976 a Ca-Al-rich inclusion of Allende and observed the enrichment of ^{26}Mg up to 1.3 %. This excess has correlated with Al/Mg ratio and would be due to the in situ decay of ^{26}Al. From the extent of the excess and Al/Mg ratio, the initial ratio of $^{26}Al/^{27}Al$ at the time of the solidification of the inclusion was estimated to be about 6×10^{-5}. In 1979, Lee et al. further observed a larger excess of ^{26}Mg up to 9.7 % for anorthite mineral separates by using their direct loading technique.[19,20] Esat et al. also reported[21] highly fractionated Mg and the negative anomaly of ^{26}Mg, which has been designated FUN anomaly, for two Allende inclusions. Stegmann and Begemann reported in 1981[22] the ^{26}Mg excess of 15 % correlating with Al concentration, and $^{26}Al/^{27}Al$ ratio at the time of solidification was estimated to be 5.9×10^{-5}.

The investigation mentioned above have been performed by using the method of thermal ionization mass spectrometry.

An ion microprobe mass spectrometric technique has been also used for the investigation of magnesium isotopic

abundance anomaly. Bradley et al.[23] reported the excess ^{26}Mg up to 40 % in an anorthite grain picked out of the Allende meteorite with an ion microprobe. The excess has correlated with Al/Mg ratio. Hutcheon et al.[24] reported that two anorthite specimens in Allende had ^{26}Mg excess of 7-18 %. Shimizu et al.[25] also reported that ca. 13 % excess ^{26}Mg was observed in an anorthite inclusion and 16 % excess in a hibonite inclusion from Leoville C3 carbonaceous chondrite. In 1979, Hutcheon et al.[26] showed that melilite and hibonite crystals from Allende had distinct ^{26}Mg excesses.

These data have been obtained by the use of ion microprobe techniques.

The discoveries of ^{16}O and ^{26}Mg anomalies in Ca-Al-rich inclusions of the Allende and Leoville carbonaceous chondrites have led to the search for more anomalies of other elements in order to clarify the special features of the Allende chondrite. In both 1977 and 1978, isotopic abundance anomalies of such elements as S,[27] Ba and Nd,[28] Ca,[29] Sr,[30] Sm[31] and Ag[32] have been observed one after another in the Allende meteorite.

The excess of ^{26}Mg correlating with Al/Mg ratio has been concluded to be due to the in situ decay of ^{26}Al, and a view that ^{26}Al existed at the time when the minerals in the inclusion crystallized has been generally accepted. This ^{26}Al has been thought to be synthesized shortly before the crystallization because of the short half life

(7.2×10^5 y) of ^{26}Al. The time interval between the synthesis of these isotopes and the crystallization has been estimated to be at most a few million years.[19,33] This time interval is very much different from the ^{129}I-^{129}Xe formationn interval of ca. 2×10^8 years observed for Allende inclusions.[34,35] In order to explain this difference consistently, it has been considered that ^{26}Al has a separate origin from ^{129}I. This idea led to a hypothesis as follows:

Two separate nucleosynthetic events were considered. One of them would be around 2×10^8 years before the crystallization of minerals and the other, a few million years before. Both of the events have been considered to be supernova explosions, although these would have considerably different conditions. A supernova explosion which synthesized such r-process nuclei as ^{129}I would be accompanied by larger amount of neutron flux, and another one which synthesized ^{26}Al and ^{16}O would be a supernova whose predominant nuclear process was an explosive carbon burning and the latter did not give so much neutron flux as ^{129}I could be formed. Because, if the latter supernova formed enough ^{129}I, ^{129}I-^{129}Xe and ^{26}Al-^{26}Mg formation intervals should be essentially the same values.

If such a latter supernova as in the above mentioned idea had exploded, this would have synthesized ^{20}Ne, ^{23}Na, ^{24}Mg and ^{28}Si together with ^{16}O and ^{26}Al, and these nuclei would be injected into the primordial solar nebula from the

theoretical considerations by Arnett[37] and Arnett and Truran.[38]

As a result of the formation and injection of these isotopes, their remnants may be kept in the primitive meteorites as in the case of ^{16}O and ^{26}Mg. The possibility led us to investigate not only ^{26}Mg isotopic abundance anomaly but also ^{24}Mg anomaly for primitive meteorites. We have investigated them with ion microprobe mass analyzers, because they are capable of an isotopic abundance measurement for a localized portion of the order of 100 μm size. This capability is essentially important for the study of such specimens as chondrites that are usually complex aggregates of various kinds of fine minerals.

In order to confirm the anomaly of ^{26}Mg and to obtain distribution of the anomaly on the sample surface, line analyses of magnesium isotopic ratios across three inclusions of the Allende meteorite have been carried out firstly. Secondly, a search for an excess ^{24}Mg, which has never been observed, was performed for many Al-poor and Mg-rich portions of matrix areas of a few primitive chondrites.

2. SAMPLES

Meteoritic samples used for the present investigation of isotopic abundance anomalies of ^{26}Mg and ^{24}Mg are listed in Table 2.1. Ten specimens of terrestrial mineral samples were also used and the list is in Table 2.2.

2.1 METEORITIC SAMPLES

Three meteoritic samples shown in Table 2.1 are chondrites. The classifications of those chondrites based on the categories proposed by Van Schmus and Wood[39] are also listed in the second column of the table. C, L and H represent the classification based on Fe/Si ratio and the degree of oxidation. The degree of oxidation becomes lower in this order. C corresponds to carbonaceous chondrite, L, ordinary chondrite of low iron group, H, ordinary chondrite of high iron group. There are two other groups of E (enstatite chondrite) and LL (low iron and low metal ordinary chondrite), although chondrites of these two groups were not used in the present work. The number after the group name, 3 in this case, means the petrologic type proposed by Van Schmus and Wood.[39] The petrologic type ranges from 1 to 6 (or recently 7) and represents the degree of metamorphism. The higher the number of petrologic type is, the more the metamorphism proceeds. A chondrite belonging to the petrologic type less than 3 is unequilibrated and is generally accepted to contain primordial

material, almost unaltered, although types 1 and 2 in H, L and LL groups have not been found.

2.1.1 Allende

A photomicrograph of a cut surface of the Allende (C3) carbonaceous chondrite is shown in Fig.2.1. Various kinds of inclusions, which are different in color, shape, size and texture, are embedded in black matrix. It has been reported that white inclusions are abundant in Al-rich refractory minerals, which are thought to have crystallized in the early stage of solidification from gaseous state[42,43] and to be primitive in case of the Allende chondrite.[12,13] Since white inclusions appear to have various thermal histories, judging from their profiles, the following three specimens with different shapes and textures were selected.

They are:

(1) an amoeboid whitish inclusion,

(2) a relatively small chondrule-like white inclusion surrounded by a ring-shaped boudary layer, and

(3) a large round white inclusion.

Photomicrographs of these specimens are shown in Figs. 2.2, 2.3 and 2.4, respectively. The specimen 1 may have been heated and once melted from the amoeboid shape. The specimen 2 has a ring-shaped boundary layer which has a microscopically different texture from the central inclusion part. The specimen 3 is similar in size and texture to the specimen investigated by Phinney et al.,[44] which contain

refractory-rich inclusions. These three specimens are abbreviated as AL0, AL1 and AL2, respectively, in this paper.

2.1.2 Yamato-74191

A photomicrograph of a cut surface of the Yamato-74191 (L3) chondrite is shown in Fig. 2.5. As is seen in the picture, most part of the surface is occupied by chondrules and there is a little matrix area which exists in the narrow portion among the chondrules.

This chondrule has been reported to be unequilibrated,[41,45] and to contain a large amount of trapped gases.[46] Thus it is expected to contain primordial materials. This chondrite is abbreviated as Y-74191.

2.1.3 Yamato-75028

A photomicrograph of a cut surface of the Yamato-75028 chondrite is shown in Fig. 2.6. This chondrite itself is reported to be a breccia of H3 and L3 matter with H5 clasts.[41] A specimen of H3 part of this chondrite was distributed by the National Institute of Polar Research. Since the petrologic type is 3, this specimen is thought to be less metamorphosed. This is abbreviated Y-75028.

2.2 TERRESTRIAL SAMPLES

Terrestrial mineral samples listed in Table 2.2 are all silicates. A forsterite in dunite from Ehime Pref., Japan was used as a laboratory standard. Four olivine samples in

lherzolite or spinel lherzolite were used as sub-standards. Using the samples of a hornblende, a vesuvianite, and a cordierite together with the forsterite, calibration curves for Al/Mg and Mg/Si ratios were formed in secondary ion mass spectrometry. An anorthite and a feldspar samples were used for the examination of the interference of sodium in mass spectra. The details of the examination will be separately described in the later section.

For the investigation of ^{26}Mg isotopic abundance anomaly, three inclusions of Allende were analyzed. For the study of ^{24}Mg anomaly, matrix parts of the three chondrites were analyzed.

3. APPARATUS

Two ion microprobe mass analyzers were used for magnesium isotopic analyses. One of them is a home-made apparatus and the other is a Hitachi IMA 2A apparatus.

3.1 ION MICROPROBE MASS ANALYZER

An ion microprobe mass analyzer has several merits. They are:

(1) Quantitative or semi quantitative elemental analysis of the localized portion of a solid sample is possible,

(2) Isotopic analysis is possible,

(3) No chemical treatment is necessary before the analysis except polishing and cleaning, and

(4) The consumption of a sample is extremely low compared with that by a wet chemical method.

These merits are expected to be advantageous to the isotopic analysis of chondritic materials, which are heterogeneous and are aggregates of various kinds of fine minerals, because the selection of analyzed area is quite easy.

Schematic diagrams of a home-made and a Hitachi's apparatus are shown in Figs. 3.1 and 3.2, respectively. These two apparatus are essentially the same constitutions. The apparatus consists of an ion source for producing primary ions, accelerating and focusing electrodes for primary ion beam, a sample holder and its moving device, accelerating and focusing electrodes for secondary ions, a double

focusing mass spectrometer, and pumping systems.

3.2 PRIMARY ION GUN AND FOCUSING SYSTEM

The primary ion gun is of a hollow cathode type. An example of the ion source of the home-made apparatus is illustrated in Fig. 3.3. Typical operating conditions of the ion guns of both apparatus are listed in Table 3.1.

The accelerating and focusing system for primary ion beam consists of a drawing out and accelerating electrodes, two sets of Einzel lenses (objective and condenser lenses) and deflecting electrodes.

Typical working conditions for magnesium isotopic analysis are tabulated in Table 3.2.

3.3 SAMPLE HOLDER

A sample mounting system of the home-made apparatus is illustrated in Fig. 3.4. A tantalum plate was used as a holder. Samples were mounted on the holder, and the surfaces of the samples were covered with a sheet of tantalum with a slit of about 2 mm wide and 20 mm long as shown in the figure. The holder was movable perpendicular to the primary ion beam in Z direction shown in Fig. 3.4. The incident angle of the primary ion beam to the surface of the sample was 45°, and the drawing out direction of the secondary ions was also 45° to the surface normal.

A sample mounting system of the Hitachi IMA 2A is shown in Fig. 3.5. Samples were mounted on a cylindrical holder

and, were covered with a sheet of tantalum with apertures of 3 mm in diameter, through which samples were bombarded by primary ions. The incident direction of the primary ion beam is perpendicular to the sample surface, and the drawing out direction of the secondary ions was 45° to the surface normal.

3.4 COLD FINGER

For the precise isotopic ratio measurement, it is a problem that molecular ions may overlap the subject mass peak at the same mass number. Large part of molecular ions which may interfere the isotopic ratio measurement are originated from volatile gas adsorbed on the sample surface. In order to remove the volatile gas in the sample chamber and to decrease the interferences, a liquid nitrogen cold finger was put aside the sample holder in both the apparatus. A schematic diagram of the installation is shown in Fig. 3.6. The details of the examination of interferences will be described in a later section.

3.5 ELECTRON SPRAY

When a sample is an insulator, charge-up effect due to the positive ion bombardment causes the instability of secondary ion current. In order to avoid the charge-up, an electron spray was utilized. As the result, enough stable secondary ion current could be obtained. A chart showing the stability of secondary ion current is shown in Fig. 3.7. In the figure, the peak top of $^{24}Mg^{+}$ for a terrestrial

forsterite sample was recorded for about one hour. A short period irregular fluctuation is found to be less than 0.4 % in this case, although a slow variation with time is observed to be about 1.5 % for one hour. Since the slow variation can be corrected by a data acquisition procedure, there is no problem about the isotopic ratio measurement.

3.6 MASS SPECTROMETER AND PUMPING SYSTEM

The mass spectrometer is of a double focusing type. Radii and deflection angles of electric and magnetic sectors are listed in Table 3.3. Width of each slit under the usual working conditions are also shown in the table. Resolutions of these mass spectrometers used in the present work are shown in the same table.

Two pumping systems of the same constitutions are used in the home-made apparatus. It consists of an oil diffusion pump with a liquid nitrogen cold trap followed by a rotary pump.

In case of the Hitachi's apparatus, two systems of a turbomolecular pump with a liquid nitrogen cold trap followed by a rotary pump, an oil diffusion pump followed by a rotary pump, and an ion pump are used as shown in Fig. 3.6.

3.7 DETECTING SYSTEM

Mass-analyzed secondary ions were amplified by a secondary electron multiplier followed by an amplifier and a pen recorder.

The secondary ion intensity has been measured as a peak height of a mass spectrum.

3.8 COMPUTER CONTROLLING SYSTEM

A computer controlling system has been developed with a microcomputer for a precise isotopic ratio measurement. The control of mass scannings as well as the calculations of isotopic ratios and the statistical procedures can be performed. A block diagram of this controlling system is shown in Fig. 3.8.

A CPU used in this system is 8080AFC. Interfaces constructed are:

(1) to operate a power supply of an electromagnet,

(2) to put on and off a recorder,

(3) to read the output DC voltage of an amplifier into computer as 3.5 digit BCD code,

(4) to control an AD converter,

(5) to switch sensitivities of detecting system by switching a feed back resistor of the amplifier, and

(6) to read out the data from the computer to a digital printer.

These interfaces are shown in Figs. 3.9, 3.10 and 3.11.

A software of this controlling system has been also developed by the author. This program consists of three parts. These are:

(1) a program of setting initial conditions which are re-

quired for the isotopic ratio measurement by the dialog between a computer and an operator through a CRT screen,

(2) a program of controlling the interfaces, and

(3) a program of calculating isotopic ratios and of a statistical procedure.

Programs (1) and (3) are written with BASIC and (2) is written with assembler. These programs are listed in Appendix.

The computer controlling system has been mainly used in Hitachi IMA 2A apparatus. The details of the working of this system will be stated in the later section.

4. EXPERIMENTAL

Isotopic abundance ratios of magnesium have been measured for the three chondritic samples comparing with those for terrestrial samples.

4.1 SAMPLE PREPARATION

Most samples shown in Table 2.1 and 2.2 were polished with emery papers and ultrasonically washed and cleaned in acetone. For some samples, freshly spalled surfaces were used without polishing and cleaning procedures.

Those samples were set on a holder as shown in Figs. 3.4 and 3.5.

4.2 EXAMINATION OF INTERFERENCES

Molecular and multiply-charged ions are usually formed as secondary ions by ion bombardment of a sample surface. Among these, ionic species overlapping a subject mass peak interfere the isotopic ratio measurement. Possible interfering ionic species at mass 24, 25 and 26 of subject ionic species of $^{24}Mg^+$, $^{25}Mg^+$ and $^{26}Mg^+$ are listed in the second column of Table 4.1.

These overlaps can be avoided in principle by making a mass resolution high enough to resolve these interfering species from the subject mass peak. Resolutions necessary to resolve each interfering ionic species are listed in the third column of Table 4.1. However, even if a high resolu-

tion is attained, the interfering peaks are in most cases masked by a tailing of the subject mass peak and they can be hardly detected, since the intensity of almost all interfering species are expected to be less than 1×10^{-3} of the subject peaks in the present work. Adding this, it is necessary to take an ion intensity as high as possible to minimize an error due to the statistical fluctuation of the intensity.

Taking this situation into account, we have carried out the measurements with low resolution mode and extensively examined the contributions of the interferences in the following manner.

4.2.1 $^{24}MgH^+$ and $^{25}MgH^+$

As described in the previous section, a liquid nitrogen cold finger was put aside the sample holder in order to decrease hydride ions. A remarkable effect of the cold finger was observed as shown in Table 4.2. The estimate was carried out according to eqs. (4.1) and (4.2) using the terrestrial forsterite and olivine samples.

$$\frac{I_{25}}{I_{24}} = \frac{A_{25}}{A_{24}}(1-\beta) + x \qquad \ldots\ldots (4.1)$$

$$\frac{I_{26}}{I_{24}} = \frac{A_{26}}{A_{24}}(1-\beta)^2 + \frac{A_{25}}{A_{24}}x \qquad \ldots\ldots (4.2)$$

where Im: secondary ion intensity at mass number m,

Am: natural isotopic abundance of ^{m}Mg,

β: mass discrimination factor,

x: hydride ion formation ratio for Mg.

The values of x and β were obtained by solving these equations. The value of x is shown in Table 4.2, which is the maximum value of x's for the samples of a terrestrial forsterite and terrestrial olivines in four lherzolites. The value of β was 0.014 with a standard deviation of 0.002.

4.2.2 $^{23}NaH^+$ and $^{23}NaH_2^+$

The contribution of $^{23}NaH^+$ to the peak at mass 24 was estimated from mass spectra obtained for a terrestrial sodium-rich feldspar sample in granodiorite from Hyogo Pref., Japan and an anorthite sample from Hokkaido, Japan. Since the peak at mass 24 essentially consisted of two components, $^{24}Mg^+$ and $^{23}NaH^+$, in this case, $^{23}NaH^+$ was evaluated by subtracting the contribution of $^{24}Mg^+$. $^{24}Mg^+$ was estimated as follows. Neglecting x in eqs. (4.1) and (4.2), and after eq. (4.2) is devided by the square of eq. (4.1), we can get

$$\frac{I_{26} \cdot I_{24}}{(I_{25})^2} = \frac{A_{26} \cdot A_{24}}{(A_{25})^2} \qquad \ldots\ldots (4.3)$$

The right term of eq. (4.3) is constant. Therefore, if I_{25} and I_{26} are substituted into eq. (4.3), then we can get I_{24}.

In almost all cases, no residue of the subtraction of

$^{24}Mg^+$ from the peak at mass 24 existed and the maximum value of $^{23}NaH^+/^{23}Na^+$ was found to be 5×10^{-5}. While $^{23}Na^+/^{24}Mg^+$ ratio was of the order of 1000 in case of the feldspar and anorthite samples, and the ratio was less than 0.05 in the usual case of chondrites, then the contribution of $^{23}NaH^+$ to $^{24}Mg^+$ was estimated to be less than 2.5×10^{-6}.

As for the contribution of $^{23}NaH_2^+$, even if the peak at mass 25 was all due to $^{23}NaH_2^+$ for the sodium-rich feldspar, the ratio of the intensity at mass 25 to that at mass 23 was less than 2.5×10^{-4}, although most part of the peak at mass 25 is observed to be originated from an impurity magnesium in the feldspar judging from the peak at mass 26 ($^{26}Mg^+$). Thus, $^{23}NaH_2^+/^{25}Mg^+$ in case of chondrite analysis was estimated to be much less than 1.5×10^{-4}.

4.2.3 $^{12}C_2^+$, $^{12}C^{13}C^+$, $^{13}C_2^+$, $^{12}C^{14}N^+$, $^{12}C^{13}CH^+$ and $^{12}C_2H_2^+$

The contributions of these ionic species were estimated from mass spectra obtained for five carbon-rich samples. The samples used are all terrestrial and are listed in the first column of Table 4.3. The contribution of $^{12}C_2H^+$ will be described in section 4.2.4.

Secondary ion intensities at masses 12, 12.5, 24, 25 and 26 were used for the estimate. The intensity of $^{12}C^+$ was evaluated by subtracting $^{24}Mg^{2+}$ estimated based on the intensity at mass 12.5 ($^{25}Mg^{2+}$) from the intensity at mass 12.

The diatomic ion formation ratio for carbon isotopes is evaluated as

$$^{12}C_2^+ : {}^{12}C^{13}C^+ : {}^{13}C_2^+ = 100:2.2:0.013 \quad \ldots\ldots (4.4)$$

from the arithmetic combination of the isotopic abundances of carbon. Assuming that

$$^{12}C_2^+ : (^{13}C_2^+ + {}^{12}C^{14}N^+ + {}^{12}C^{13}CH^+ + {}^{12}C_2H_2^+) = 100:y,$$

the following equations can be set up by neglecting the contributions of magnesium hydride ions as described in 4.2.1 and 4.2.2.

$$\frac{I_{25}-2.2k}{I_{24}-100k} = \frac{A_{25}}{A_{24}}(1-\beta) \quad \ldots\ldots (4.5)$$

$$\frac{I_{26}-yk}{I_{24}-100k} = \frac{A_{26}}{A_{24}}(1-\beta)^2 \quad \ldots\ldots (4.6)$$

where I_m: secondary ion intensity at mass m,

A_m: natural isotopic abundance of ^{m}Mg,

β: mass discrimination factor,

k: proportional constant.

If we substitute the mass discrimination factor of 0.014 into β, which was obtained for the terrestrial forsterite sample, then the simultaneous equations (4.5) and (4.6) for the variables k and y can be solved. Using the obtained values of k and y, intensities of $^{12}C_2^+$, $^{12}C^{13}C^+$ and $(^{13}C_2^+ + {}^{12}C^{14}N^+ + {}^{12}C^{13}CH^+ + {}^{12}C_2H_2^+)$ have been able to be evaluated. From the results, the molecular ion formation ratio of these ionic species to $^{12}C^+$ have been obtained as shown in the second and third columns in Table 4.3.

In cases of magnesium isotopic measurements for chondrite samples analyzed so far, the upper limit of the secondary ion intensity ratio of $^{12}C^+/^{24}Mg^+$ was 7×10^{-4}. From this value and the maximum value among the ratios listed in Table 4.3, the maximum contributions of $^{12}C^+$, $^{12}C^{13}C^+$ and $(^{13}C_2^+ + ^{12}C^{14}N^+ + ^{12}C^{13}CH^+ + ^{12}C_2H_2^+)$ to the respective subject peak were estimated as shown in Table 4.1.

4.2.4 $^{12}C_2H^+$

From the mass spectra obtained for the carbon-rich samples listed in Table 4.3, even if the peak appearing at mass 25 were all $^{12}C_2H^+$, the ratio of this intensity to $^{12}C^+$ was estimated to be less than 2×10^{-3}. Thus $^{12}C_2H^+/^{25}Mg^+$ was estimated to be less than 1×10^{-5} for the chondrite analysis.

4.2.5 $^{48}Ca^{2+}$

Calcium has six stable isotopes of masses 40, 42, 43, 44, 46 and 48. The doubly-charged ions of $^{40}Ca^{2+}$ appears at mass 20. The intensity ratios of $^{40}Ca^{2+}/^{40}Ca^+$ was observed to be less than 0.015 for the chondrite samples used. Since $^{48}Ca^{2+}/^{48}Ca^+$ would be equal to $^{40}Ca^{2+}/^{40}Ca^+$, the contribution of $^{48}Ca^{2+}$ to $^{24}Mg^+$ was calculated to be less than 2×10^{-5} from the intensities at masses 24 and 48.

4.2.6 $^{48}Ti^{2+}$ and $^{50}Ti^{2+}$

Titanium has five stable isotopes of masses 46, 47, 48,

49 and 50. Doubly-charged ions of $^{47}Ti^{2+}$ and $^{49}Ti^{2+}$ appear at mass numbers 23.5 and 24.5, respectively. In cases of the analyzed chondrites, no peaks exceeding the noise levels at those mass numbers were observed when the sensitivities at mass numbers 23.5 and 24.5 were 10^3 times higher than that at mass 24. Therefore, the noise levels were taken as maximum intensities of $^{47}Ti^{2+}$ and $^{49}Ti^{2+}$. Thus, $^{48}Ti^{2+}/^{24}Mg^{+}$ and $^{50}Ti^{2+}/^{25}Mg^{+}$ were estimated to be less than 7×10^{-5} and 4×10^{-5}, respectively.

4.2.7 $^{50}Cr^{2+}$ and $^{52}Cr^{2+}$

Chromium has four stable isotopes of masses 50, 52, 53 and 54. Doubly-charged ions of $^{53}Cr^{2+}$ appears at mass 26.5. No peak could be detected even with 10^3 times higher sensitivity than that at mass 24. From the noise level at mass 26.5, $^{50}Cr^{2+}/^{25}Mg^{+}$ and $^{52}Cr^{2+}/^{26}Mg^{+}$ were estimated to be less than 1×10^{-6} and 5×10^{-4}, respectively.

4.2.8 Summary

The estimate of the contribution of doubly-charged and molecular ions was done for the Hitachi IMA 2A apparatus as mentioned above. For the home-made apparatus, the same way of the estimate was used. The maximum contribution of these interfering ionic species to the subject peak are summarized in the fourth and fifth columns in Table 4.1. From the results, the extent of the interferences is found to be less than 1 permil as a whole for each subject peak of $^{24}Mg^{+}$, $^{25}Mg^{+}$ and $^{26}Mg^{+}$.

4.3 CALIBRATION CURVES FOR Al/Mg AND Mg/Si CONCENTRATION RATIOS

In order to estimate the concentration ratios of Al/Mg and Mg/Si from the secondary ion intensity ratios of $^{27}Al^+/^{24}Mg^+$ and $^{24}Mg^+/^{28}Si^+$, calibration curves for these elemental concentration ratios have been prepared. Samples used were terrestrial forsterite, hornblende, vesuvianite and cordierite. These four minerals are all silicates and their localities are listed in Table 2.2. The concentrations of Mg, Al and Si determined by the analysis of atomic absorption spectrometry were tabulated in Table 4.4 with their chemical formulae.

Figures 4.1 and 4.2 are the graphs of secondary ion intensity ratios versus concentration ratios. Plotted points fall well on a straight line with the slope of unity. These lines can be used to determine concentration ratios of Al/Mg and Mg/Si.

Al/Mg ratio can be a measure for aluminum concentration and Mg/Si ratio can be used in order to select a forsterite-rich portion.

4.4 MAGNESIUM ISOTOPIC ANALYSIS

Magnesium isotopic analyses have been carried out for the chondritic samples described in section 2. Mass scannings were repeated 40 to 90 times for one probed portion over the mass range from mass 24 to 26. A peak at mass 27 has also been taken as a measure of Al concentration at

least once in a run. Examples of mass spectra are shown in Figs. 4.3 and 4.4. Figure 4.3 shows a mass spectrum obtained for the white inclusion of AL2 with the home-made apparatus, and Fig. 4.4, for a portion of the matrix of Y-74191 with the Hitachi IMA 2A apparatus.

Because the contributions of the interfering peaks to mass 24, 25 and 26 were found to be less than 1 permil as described in section 4.2, and to be negligibly small, raw secondary ion intensity ratios of magnesium were calculated from the mass spectra.

4.4.1 Definition of the deviation of an isotopic ratio

The deviation of an isotopic ratio of $^{m}Mg/^{n}Mg$ for a sample from the ratio for a reference is usually defined as eq.(4.7).

$$\Delta_{m/n} = \left(\frac{(^{m}Mg/^{n}Mg)_{s}}{(^{m}Mg/^{n}Mg)_{r}} - 1 \right) \times 1000 \qquad \ldots\ldots (4.7)$$

where m and n are mass numbers of magnesium isotopes, and subscripts s and r represent "sample" and "reference", respectively.

The terrestrial forsterite (FO) in dunite from Ehime Pref., Japan was used to obtain the reference values of the isotopic ratios.

4.4.2 Automation of isotopic measurement by a microcomputer

The isotopic ratio has been measured automatically by

using a microcomputer. The hardware of the measuring system has been already described in section 3.6. Therefore, the details of the working of the system will be stated here mainly as to the software.

The working contains:

(1) Switching the scan speed, slow or fast, at the peak top and bottom, independently. In the usual case, the top was scanned slowly and the bottom, fastly.

(2) Reading the data into the memory by ten-point running mean method.

(3) Evaluating the peak height by the calculation of a top value minus a bottom value.

(4) Correcting the slow intensity variation with time during the scannings.

(5) Calculating the peak height ratios and Δ values. The formula of the calculation was preset in the computer.

(6) Taking statistical procedures that are the calculation of a mean, a standard deviation (σ) and a standard deviation of a mean (σ_m), the exclusion of data exceeding $\pm 2\sigma$, the re-calculation of a mean and errors, and the iteration of these procedures.

(7) Printing the data with a digital printer.

A flow chart of the procedure is shown in Fig. 4.5.

4.4.3 Analysis of terrestrial standard

In both the apparatus, the laboratory standard sample of terrestrial forsterite (FO) has been intermittently ana-

lyzed over about one year in order to check the reproducibility for magnesium isotopic ratio measurements in both the apparatus.

$\Delta_{25/24}$ and $\Delta_{26/24}$ values obtained with the home-made apparatus are plotted in Fig. 4.6 in the chronological order. The weighted means of all the data of $^{m}Mg/^{24}Mg$ were evaluated to be 0.12495 for m=25 and 0.13666 for m=26, and these values were used as reference values in eq. (4.7). The reproducibilities were evaluated to be ±3.5 ‰ for $\Delta_{25/24}$ and ±5.5 ‰ for $\Delta_{26/24}$ as ±2σ. These values are shown as error bars for the closed circles which correspond to the laboratory standard values mentioned above as weighted means.

In Fig. 4.7, are replotted these Δ values as a three isotope plot. A straight line with the slope of 1/2 in the figure corresponds to the normal mass fractionation line. The plotted points are along the straight line. This means that the scattering of the data was originated by the normal mass fractionation, and that these data can be corrected by the normalization for the mass fractionation.

In Fig. 4.7, two points symbolized by a closed triangle and a closed square are also plotted. These two points correspond to the absolute isotopic abundance ratios of magnesium reported by Catanzaro et al.[47] (CMGS 66) and Schramm et al.[9] (STW 70).

The weighted mean of our data (closed circle) deviates from these two data points by about 13 ‰ in $\Delta_{25/24}$. This

deviation can be thought to be mainly due to a mass discrimination effects. It is not necessary to correct the mass discrimination in comparing the isotopic abundance ratios obtained by one apparatus under the same experimental conditions with each other.

In order to clarify the anomaly of $\Delta_{26/24}$, it had better be corrected for the normal mass fractionation. For the correction, the isotopic ratios for the laboratory standard of the terrestrial forsterite (FO) was used as a reference values. The following equations were used for the calculation of a normalized isotopic abundance ratio of $(^{26}Mg/^{24}Mg)_n$ and its deviation, $\delta_{26/24}$, from the reference value:

$$\left(\frac{^{26}Mg}{^{24}Mg}\right)_n = \frac{(^{26}Mg/^{24}Mg)_s}{(1-\alpha)^2} \qquad \ldots\ldots (4.8)$$

$$1-\alpha = \frac{(^{25}Mg/^{24}Mg)_s}{(^{25}Mg/^{24}Mg)_r} = 1 + \frac{\Delta_{25/24}}{1000} \qquad \ldots\ldots (4.9)$$

$$\delta_{26/24} = \left(\frac{(^{26}Mg/^{24}Mg)_n}{(^{26}Mg/^{24}Mg)_r} - 1 \right) \times 1000 \qquad \ldots\ldots (4.10)$$

where α is the mass fractionation factor. A subscript of n denotes "after normalization", s, "sample", and r, "reference".

The $\delta_{26/24}$ values for the same data as those plotted in Fig. 4.6 are plotted in Fig. 4.8 also in the chronological order. The reproducibility for $\delta_{26/24}$ was found to be ±4.5 ‰ as ±2σ.

$\Delta_{24/25}$ and $\Delta_{26/25}$ values obtained by the Hitachi IMA 2A apparatus are plotted in Fig. 4.9 in the chronological order. These data were also obtained by the analysis of the FO sample. From these data, weighted means of $^{m}Mg/^{25}Mg$ values were calculated to be 8.0178 for m=24 and 1.0872 for m=26. Error bars for the closed circles in the figure represent reproducibilities as $\pm 2\sigma$. Those are ±2.8 ‰ for both the Δ values as shown in the figure.

The absolute isotopic abundance ratios of $^{24}Mg/^{25}Mg$ and $^{26}Mg/^{25}Mg$ are 7.89702 and 1.10404[9], respectively. The weighted means of the ratios obtained with the Hitachi apparatus also deviate from the absolute ones. This is again caused mainly by mass discrimination effects. Although the correction for the mass discrimination is possible, it is not necessary to correct in the case that only the deviations of the isotopic ratios are compared with each other. It is enough to take a correction for the normal mass fractionation in the same sense as stated above.

Therefore, the values shown in Table 4.5 obtained for the sample of the FO were used as the reference values.

Moreover, four other terrestrial olivines, SL45, SL46, MM and OK listed in Table 2.2 were analyzed as sub-standards with the Hitachi IMA 2A apparatus. The data normalized to the reference values for FO are plotted in Fig. 4.10. In the figure, a normal mass fractionation line whose slope is -1 through the origin is illustrated.

The plotted points for those terrestrial sub-standards

fall well along the normal mass fractionation line. These points deviate by 3 - 6 ‰ from the reference value. An explanation for the deviation guessed is as follows. The FO sample was taken from a rock of dunite and the four olivine samples were picked out of rocks of lherzolite or spinel lherzolite, and the localities of the rocks are all different. Because the differences of the types and the localities of rocks, the extent of mass fractionation may differ from one to another.

If the data for four olivine samples are corrected for the normal mass fractionation, the corrected values become consistent with that of FO standard within errors.

4.4.4 Search for ^{26}Mg anomaly

In order to search for ^{26}Mg anomaly, three specimens in the Allende carbonaceous chondrite, AL0, AL1 and AL2, have been used. There are descriptions about these three specimens. They all contain white or whitish inclusions which are expected to be composed of Al-rich refractory minerals such as hibonite, melilite and spinel.

Sketches of these inclusions are illustrated in Figs. 4.11, 4.12 and 4.13. The probed line for the magnesium isotopic analysis is shown in each figure. Photomicrographs of these inclusions have already been shown in section 2.

$\Delta_{m/24}$ values were calculated according to eq. (4.7) from raw secondary ion intensities. $^{27}Al^+/^{24}Mg^+$ ratio was also calculated. Furthermore, in order to obtain the extent

of ^{26}Mg anomaly, the normal mass fractionation was corrected by using the isotopic ratio for FO sample as the reference value. This correction was done by eqs. (4.8), (4.9) and (4.10).

4.4.5 Search for ^{24}Mg anomaly

In order to search for ^{24}Mg anomaly, the specimens of AL, Y-74191 and Y-75028 have been used. Al-poor and Mg-rich portions of matrix areas were analyzed in order to avoid the contribution from excess ^{26}Mg due to the decay of ^{26}Al. About 100 portions of matrix area were randomly analyzed for each specimen. An example of the probed portion is shown on the photograph in Fig. 2.1 by a red cross mark. Not only mass peaks at mass 24, 25 and 26 but also those at masses 27 and 28 were recorded at every probed portion.

$\Delta_{m/25}$ values were calculated by eq. (4.7). $^{27}Al^+/^{24}Mg^+$ and $^{24}Mg^+/^{28}Si^+$ ratios were also calculted. From Al/Mg ratio, portions with low aluminum concentrations could be found, and from Mg/Si ratio, forsterite-rich portions could be easily selected.

5. RESULTS AND DISCUSSION

5.1 ^{26}Mg ANOMALY

$\delta_{26/24}$ values obtained for the inclusions in the three specimens (AL0, AL1 and AL2) of the Allende chondrite are plotted in the chronological order in Figs. 5.1, 5.2, 5.3 and 5.4. The definition of the $\delta_{26/24}$ has appeared in the previous section and the $^{26}Mg/^{24}Mg$ ratio for FO was taken as the reference value.

The data in Fig. 5.3 correspond to the line analysis along AA' of the AL2 specimen in Fig. 4.13, and the data in Fig. 5.4, along BB' in the same specimen. In the lower part of Fig. 5.3, the data obtained for a terrestrial hornblende (HO) and vesuvianite (VE) are also shown.

These data for Allende are replotted in Figs. 5.5, 5.6, 5.7 and 5.8 as a function of the probed portion. $^{27}Al^{+}/^{24}Mg^{+}$ ratio for each probed portion is also shown as a measure of aluminum to magnesium concentration ratio.

5.1.1 Amoeboid whitish inclusion in AL0

As shown in Fig. 5.5, Al/Mg ratio is high in the area of this whitish inclusion. the anomaly of ^{26}Mg is not clear, although the mean value of $\delta_{26/24}$'s seems to be positive a little. The variation of $\delta_{26/24}$ does not correlate with that of Al/Mg ratio. Therefore, it was concluded that the excess ^{26}Mg could be hardly detected for this inclusion.

5.1.2 Chondrule-like white inclusion in AL1

The excess ^{26}Mg was observed rather in the ring-shaped boundary layer than in the white inclusion. There seems to be an anticorrelation between variations of $\delta_{26/24}$ and Al/Mg ratio except the data for the matrix area. From the variation of $\delta_{26/24}$ shown in Fig. 5.6, it may be considered that the white inclusion particle with ^{26}Al was firstly formed and after the formation of the particle, it was surrounded by the boundary layer. Then it was heated to enough high temperature not to melt but to recrystallize. During the recrystallization process, ^{26}Mg might be segregated toward the ring-shaped boundary layer. As the result of this segregation, excess ^{26}Mg was thought to be concentrated in the boundary layer.

5.1.3 Large white inclusion in AL2

This large white inclusion was analyzed along two different probed lines approximately perpendicular with each other. In both the analyses, excess ^{26}Mg more than 20 ‰ was observed, and the data showed the correlation with the Al/Mg ratio as shown in Figs. 5.7 and 5.8.

Figures 5.9 and 5.10 are three isotope plots of magnesium for the white inclusion along the probed lines of AA' and BB', respectively. The data for the matrix area are omitted in the figures. The ordinate represents $\Delta_{25/24}$, and the abscissa, $\Delta_{26/24}$, calculated according to eq. (4.7). In each figure, a normal mass fractionation line with the slope

of 1/2 is illustrated through the origin which was determined from the data for the laboratory standard (FO). All the data are found to clearly fall in the right hand side of the normal mass fractionation line.

The deviation in the direction of the abscissa between each data point and the normal mass fractionation line corresponds to the $\delta_{26/24}$ value corrected for the normal mass fractionation. The deviation to the right side clearly shows the positive anomaly of ^{26}Mg.

In order to quantify a correlation between the excess ^{26}Mg and Al/Mg ratio, these data are replotted as shown in Fig. 5.11. The upper graph of $\Delta_{26/24}$ versus Al/Mg clearly shows the correlation that $\Delta_{26/24}$ increases with the increase of Al/Mg ratio. On the contrary, $\Delta_{25/24}$ shows no systematic variation in a whole range of Al/Mg in this figure.

5.2 Al-CORRELATED EXCESS ^{26}Mg

the Al-correlated excess ^{26}Mg, which was observed in the large white inclusion in AL2 specimen of the Allende chondrite as shown in Fig. 5.11, can be thought to be originated from the in situ decay of ^{26}Al. Using the plot in Fig. 5.11, $^{26}Al/^{27}Al$ ratio at the time of the crystallization of Al-containing minerals from the remnant materials of the exploded supernova as stated in sections 1 and 2 can be estimated.

5.2.1 ^{26}Al at the time of primordial mineral crystallization

If the excess ^{26}Mg due to the in situ decay of ^{26}Al is written as $^{26}Mg^*$, ^{26}Mg existed in a specimen can be expressed in the following equation.

$$(^{26}Mg)_p = (^{26}Mg)_o + {}^{26}Mg^* \quad \ldots\ldots (5.1)$$

where subscript p represents "present", and o, "original" which means the initial magnesium originally existed.

When eq. (5.1) is devided by $(^{24}Mg)_o$,

$$\frac{(^{26}Mg)_p}{(^{24}Mg)_o} = \frac{(^{26}Mg)_o}{(^{24}Mg)_o} + \frac{^{26}Mg^*}{(^{24}Mg)_o} \quad \ldots\ldots (5.2)$$

Since $(^{24}Mg)_o$ would be equal to $(^{24}Mg)_p$ in this case, eq. (5.2) can be rewritten as

$$(\frac{^{26}Mg}{^{24}Mg})_p = (\frac{^{26}Mg}{^{24}Mg})_o + (\frac{^{26}Mg^*}{^{24}Mg})_p \quad \ldots\ldots (5.3)$$

From eq. (5.3),

$$\frac{(^{26}Mg^*/^{24}Mg)_p}{(^{26}Mg\ /^{24}Mg)_o} = \frac{(^{26}Mg/^{24}Mg)_p}{(^{26}Mg/^{24}Mg)_o} - 1 \quad \ldots\ldots (5.4)$$

is derived. The right side of eq. (5.4) is the same form as the definition of $\Delta_{26/24}$ and if this is put by $(\Delta_{26/24})_p$, then

$$\frac{(^{26}Mg^*/^{24}Mg)_p}{(^{26}Mg\ /^{24}Mg)_o} = \frac{(\Delta_{26/24})_p}{1000} \equiv (\Delta_{26/24}')_p \quad \ldots\ldots (5.5)$$

Since $^{26}Mg^*$ was originally ^{26}Al at the time of the primor-

dial material crystallization,

$$^{26}Mg^{*} = (^{26}Al)_{c} \qquad \text{..... (5.6)}$$

where subscript c means "crystallization".

Using eqs. (5.5) and (5.6),

$$(\Delta_{26/24'})_{p} = \frac{(^{26}Al)_{c}/(^{24}Mg)_{p}}{(^{26}Mg/^{24}Mg)_{o}}$$

$$= \frac{(^{26}Al/^{27}Al)_{c}((^{27}Al)_{c}/(^{24}Mg)_{p})}{(^{26}Mg/^{24}Mg)_{o}}$$

Since ^{27}Al is constant, so $(^{27}Al)_{c}=(^{27}Al)_{p}$, then

$$(\Delta_{26/24'})_{p} = \frac{(^{26}Al/^{27}Al)_{c}}{(^{26}Mg/^{24}Mg)_{o}} \times (\frac{^{27}Al}{^{24}Mg})_{p} \qquad \text{..... (5.7)}$$

As $(^{27}Al/^{24}Mg)_{p}$ can be expressed as $(^{27}Al/^{24}Mg)_{s}$, where subscript s means "specimen". Therefore eq. (5.7) becomes:

$$(\Delta_{26/24'})_{p} = \frac{(^{26}Al/^{27}Al)_{c}}{(^{26}Mg/^{24}Mg)_{o}} \times (\frac{^{27}Al}{^{24}Mg})_{s} \qquad \text{..... (5.8)}$$

By the calibration curve in Fig. 4.1, the concentration ratio of $(^{27}Al/^{24}Mg)_{s}$ can be related to the secondary ion intensity ratio as

$$(^{27}Al/^{24}Mg)_{s} = (^{27}Al^{+}/^{24}Mg^{+})_{s} \times 0.71 \qquad \text{..... (5.9)}$$

When eq. (5.9) is substituted into eq. (5.8), we can get

$$(\Delta_{26/24'})_{p} = \frac{(^{26}Al/^{27}Al)_{c}}{(^{26}Mg/^{24}Mg)_{o}} \times (\frac{^{27}Al^{+}}{^{24}Mg^{+}})_{s} \times 0.71 \qquad (5.10)$$

thus, using eqs. (5.5) and (5.10),

$$(\Delta_{26/24})_p = k \times \frac{(^{26}Al/^{27}Al)_c}{(^{26}Mg/^{24}Mg)_o} \times (\frac{^{27}Al^+}{^{24}Mg^+})_s \quad \cdots \quad (5.11)$$

where $k = 7.1 \times 10^2$.

In this equation, $k \times (^{26}Al/^{27}Al)_c/(^{26}Mg/^{24}Mg)_o$ is the slope of the straight line in $\Delta_{26/24}$ vs $(^{27}Al^+/^{24}Mg^+)_s$ plot of Fig. 5.11. If we put this slope g, then

$$g = k \times \frac{(^{26}Al/^{27}Al)_c}{(^{26}Mg/^{24}Mg)_o} \quad \cdots\cdots \quad (5.12)$$

and we can get an equation

$$(\frac{^{26}Al}{^{27}Al})_c = \frac{g}{k} \times (\frac{^{26}Mg}{^{24}Mg})_o \quad \cdots\cdots \quad (5.13)$$

where $(^{26}Mg/^{24}Mg)_o$ means the absolute isotopic abundance ratio of magnesium, and this $(^{26}Mg/^{24}Mg)_o$ can be replaced by the ratio reported by Catanzaro et al.[47] Then

$$(\frac{^{26}Al}{^{27}Al})_c = \frac{0.13932}{7.1 \times 10^2} g \quad \cdots\cdots \quad (5.14)$$

can be given.

From Fig. 5.11, the slope of $\Delta_{26/24}$ vs $^{27}Al^+/^{24}Mg^+$ plot, g, is evaluated to be 1.4 ± 1.1 by the least square fit. The obtained straight line by the least square fit is illustrated in the upper graph of Fig. 5.11 with a solid line. In the figure, the upper and lower limits obtained from the error of standard deviation are also illustrated with dashed lines.

The value of g and eq. (5.14) give the result that

$$\left(\frac{^{26}Al}{^{27}Al}\right)_c = (2.8 \pm 2.2) \times 10^{-4} \quad \ldots\ldots (5.15)$$

Lee et al.[18] reported that $(^{26}Al/^{27}Al)c$ is about 0.5×10^{-4}. This value is a little different from the present result, but in consideration of the error limit of our data, these two are barely consistent with each other.

If our 2.8×10^{-4} is valid for the white inclusion in AL2, it is about 4.5 times higher than that by Lee et al. A possible explanation for this discrepancy is that the minerals investigated at present had crystallized about 1.6×10^{6} years prior to the crystallization of the minerals for which Lee et al. have obtained their data.

5.2.2 Chronology from the viewpoint of ^{26}Al-^{26}Mg

The result stated in section 5.2.1 shows that ^{26}Al existed at the time of primordial mineral crystallization. Since the half-life of ^{26}Al is 0.72×10^{6} years, it can be considered that the time interval between the nucleosynthesis of ^{26}Al and the crystallization of Al-rich minerals was comparable with the half life. This time interval can be estimated by the same method as the case of ^{129}I-^{129}Xe chronology.

If we denote $^{26}Al/^{27}Al$ ratio at the time of nucleosynthesis as $(^{26}Al/^{27}Al)_o$, then

$$\left(\frac{^{26}Al}{^{27}Al}\right)_c = \left(\frac{^{26}Al}{^{27}Al}\right)_o \exp(-\lambda\Delta t) \qquad \ldots\ldots (5.16)$$

where λ: decay constant of ^{26}Al

Δt: time interval between the nucleosynthesis and the crystallization.

From eq. (5.16), we can get the following equation:

$$\Delta t = \frac{1}{\lambda}\left[\ \ln\left(\frac{^{26}Al}{^{27}Al}\right)_o - \ln\left(\frac{^{26}Al}{^{27}Al}\right)_c\ \right] \qquad \ldots\ldots (5.17)$$

$(^{26}Al/^{27}Al)_o$ ratio has been reported by many workers based on theoretical considerations. The reported ratios are listed in Table 5.1 in the order of the year of publication.

Four recent reports give the ratios around 1×10^{-3}. These theoretical data have been obtained by the consideration of an explosive burning nucleosynthesis with various nuclidic composition, temperature and density. Assuming that $(^{26}Al/^{27}Al)_o = 1 \times 10^{-3}$, and substituting this value into eq. (5.17), Δt is evaluated as

$$\Delta t = (1.3 \begin{smallmatrix} + 1.6 \\ - 0.6 \end{smallmatrix}) \times 10^6 \text{ years.}$$

This time interval is of the order of 10^5 to 10^6 years anyhow, and differs from what is called formation interval of 2×10^8 years estimated by ^{129}I-^{129}Xe chronology. These two different time intervals suggest that at least two different nucleosynthetic events had formed those extinct isotopes. And they were injected into the primordial solar nebula.

5.3 ^{24}Mg ANOMALY

5.3.1 Yamato-75028

Data for matrix areas of Y-75028 chondrite are shown in Fig. 5.12. These data were taken in portions where the concentration ratio of Al/Mg was less than 0.13 in consideration that aluminum concentration is enough low to avoid the contribution of $^{26}Mg^*$. The plotted points concentrate around the origin and distribute near the normal mass fractionation line. From the results, it is judged there is no anomaly of magnesium.

5.3.2 Allende

Plot of $\Delta_{26/25}$ versus $\Delta_{24/25}$ for matrix portions of Allende is shown in Fig. 5.13. Plotted points correspond to the data for the portions where the concentration ratio of Al/Mg was less than 0.13 and Mg/Si ratio was in the range of 1.5 to 2.5. About 20 percent of the analyzed portions satisfied these ranges of concentration ratios.

Anomaly of $\Delta_{24/25}$ is distinctly shown in the figure. The maximum excess of ^{24}Mg is about 20 ‰.

5.3.3 Yamato-74191

The data for Y-74191 are shown in Fig. 5.14. These data were obtained for narrow matrix portions among chondrules, because the Y-74191 chondrite is almost occupied with chondrules as shown in the picture of Fig. 2.5. Al/Mg concentration ratios were less than 0.13 for all portions plotted as data. Two kinds of data are included based on the difference of Mg/Si ratios. One of them is for the portions where Mg/Si ratio is less than 1.3 and the other,

Mg/Si ratio is higher than 1.5

Plotted points for the higher Mg/Si portions show the clear excess of ^{24}Mg. For lower Mg/Si portions, some points show the clear anomaly of ^{24}Mg, but, as a whole, the anomaly is not remarkable compared with that for the higher Mg/Si portions.

5.3.4 Excess ^{24}Mg

The excess of ^{24}Mg observed for Mg-rich and Al-poor portions of matrices in AL and Y-74191 can be explained in two ways. One of them is as the result of the addition of practically pure ^{24}Mg to the pre-existed solar nebula, the other is as the result of the depletions of ^{25}Mg and ^{26}Mg by nearly the same fractions. The latter case is considered to be less possible to happen, because any nuclear processes which decrease both ^{25}Mg and ^{26}Mg by the same fractions can be rarely expected. Therefore, only the former case will be discussed in the following.

5.4 Consistent explanation of excesses of ^{24}Mg and ^{26}Mg

It is necessary to explain both excesses of ^{26}Mg in a white inclusion of Allende and of ^{24}Mg in matrix areas of Allende and Y-74191 consistently. As was described in section 5.2, ^{26}Al, which resulted in the excess of ^{26}Mg, has been considered successfully to be formed in a nucleosynthesis on the occasion of a supernova explosion. And this supernova is estimated to have exploded a few million years prior to the crystallization of the primordial minerals based on the ratio of $(^{26}Al/^{27}Al)_c$ and the half life of ^{26}Al (7.2×10^5 y).

The formation interval from ^{129}I-^{129}Xe was 2×10^8 years, and for the same meteorite, ^{26}Al-^{26}Mg formation interval was 1-3 $\times$ 10^6 years. These two kinds of formation intervals are quite different with each other. If ^{129}I was formed in the late nucleosynthetic event, these two formation intervals should be the same values. Therefore, ^{129}I was not expected to be synthesized at the same time as the formation of ^{26}Al. The restriction leads to a prospect that neutron flux would be enough low in the case of the late nucleosynthetic event not to synthesize such r-process nuclei as ^{129}I. On the contrary, the explosion event of the previous supernova had synthesized ^{129}I through r-process under a condition of high neutron flux.

From the existence of the excess ^{24}Mg discovered for the matrices of Allende and Y-74191, it is thought that almost pure ^{24}Mg has been synthesized and injected into the pre-existed solar nebula.

This almost pure ^{24}Mg would be estimated to be synthesized through an explosive carbon burning process at the late supernova explosion according to the theoretical consideration by Arnett.[37] Possible conditions of the supernova is as follows:

Composition: 50 % ^{12}C, 50 % ^{16}O

Temperature: 1.8×10^9 K

Density: 10^7 g/cm^3

Among these conditions, temperature is the critical one. If the temperature is a little higher than this, for example 2×10^9 K, ^{24}Mg, ^{25}Mg and ^{26}Mg would have been formed in the abundances almost the same as the natural isotopic ones. Therefore, the discovery of the excess ^{24}Mg seems to rest-

rict the condition of the temperature of the late supernova. Moreover, the formations of almost pure ^{24}Mg and little ^{25}Mg and ^{26}Mg lead to the estimate that the late supernova explosion was of the type of low neutron flux, because the high neutron flux supernova must form not only ^{24}Mg but also ^{25}Mg and ^{26}Mg.

This low neutron condition is consistent with the aspect that r-process nucleus, ^{129}I, would not be synthesized in the late supernova explosion.

5.5 ^{20}Ne, ^{23}Na, and ^{28}Si

If the late supernova was exploded, ^{20}Ne, ^{23}Na and ^{28}Si wuold be also synthesized together with ^{16}O, ^{26}Al and ^{24}Mg. Among the elements of Ne, Na and Si, isotopic abundance anomaly of Si has been examined for the sample of Allende inclusions by Clayton and Mayeda,[50] but only normal mass fractionations have been observed.

Since Na has only one stable isotope, it is impossible to detect the isotopic anomaly.

In case of Ne, it is possible to detect the anomalous ^{20}Ne in principle. But because the wide range variety of the abundance of ^{20}Ne has been observed in many chondrites, it would be much difficult to detect the anomalous ^{20}Ne, which might be injected together with ^{24}Mg and ^{16}O, of the order of permil.[51]

6. CONCLUSION

The results stated in the previous section give the following points.

(1) Excess ^{26}Mg due to the in situ decay of now extinct ^{26}Al (half life = 7.2×10^5 y) has been detected in the Al-rich white inclusion in the Allende chondrite. The excess correlates with the concentration ratio of Al/Mg, and from the correlation, the ratio of $(^{26}Al/^{27}Al)_c$ at the primordial mineral crystallization could be determined. The value of $(^{26}Al/^{27}Al)_c$ was found to be $(2.8 \pm 2.2) \times 10^{-4}$ for this inclusion.

(2) The initial ratio of $(^{26}Al/^{27}Al)_o$ at the time of nucleosynthesis was estimated to be approximately 1×10^{-3} based on the theoretical considerations by Arnett[37], Truran and Cameron[48] and Arnett and Wefel.[49] Using the ratios of $(^{26}Al/^{27}Al)_c$ and $(^{26}Al/^{27}Al)_o$, a formation interval between the nucleosynthesis and the crystallization of the minerals could be estimated to be $(1.3 \,^{+\,1.6}_{-\,0.6}) \times 10^6$ years. This value is distinctly different from the ^{129}I-^{129}Xe formation interval which is 2×10^8 years.

(3) These results together with those reported by other workers on excess ^{26}Mg lead us to an explanation that at least two nucleosynthetic events had happened near the early solar nebula. The late event is considered to occur a few million years prior to the primordial mineral crystallization.

(4) The supernova explosion event would have formed ^{16}O, ^{20}Ne, ^{24}Mg, ^{26}Al and ^{28}Si through an explosive carbon burning process under a low neutron flux.

(5) Excess ^{24}Mg has been firstly found in Mg-rich and Al-poor portions in matrix areas of the Allende carbonaceous chondrite and the Yamato-74191 (L3) chondrite in the present work. The maximum excess of about 20 ‰ has been observed in case of Allende.

(6) This excess of ^{24}Mg can be explained as the result of the addition of practically pure ^{24}Mg formed in the late supernova event to the pre-existed solar nebula.

(7) The excess of ^{24}Mg discovered in the present work, together with the excess of ^{16}O found by Clayton et al. and that of ^{26}Mg found by the author and the other workers, can be strong evidences which support the hypothesis that the primordial solar nebula was inhomogeneous and composed of at least two components.

APPENDIX

Software developed by the author himself for a precise isotopic ratio measurement is described. This software consists of three parts. One is for controlling a power supply of electromagnet, relays to switch high registers of an amplifier through interfaces. This is written by assembler. The second is for setting various initial conditions for measurement, and the third is for calculating isotopic ratios and for taking statistical procedures. These are written by BASIC. The lists of these programs are from the next page.

Disassembling list of the controlling program

```
6000 CDA467 M0    CALL  IPR
6003 CDB767       CALL  IIF
6006 CDC267       CALL  ITM1
6009 CD8062       CALL  OFREC
600C CD7562       CALL  SLOW
600F AF           XRA   A
6010 320281       STA   SCCNT
6013 210058       LXI   H,PHSAV
6016 221081       SHLD  PHPNT
6019 21005C       LXI   H,TMSAV
601C 221281       SHLD  TMPNT
601F CDF167       CALL  ITM2
6022 CD7A62       CALL  ONREC
6025 1605         MVI   D,05H
6027 3E00    T0   MVI   A,00H
6029 CD7B63       CALL  TIM
602C 15           DCR   D
602D C22760       JNZ   T0
6030 CDD267 M1    CALL  IREG
6033 AF           XRA   A
6034 320381       STA   PKCNT
6037 3A0281       LDA   SCCNT
603A 3C           INR   A
603B 320281       STA   SCCNT
603E CD5162       CALL  SCAON
6041 3A0381 M11   LDA   PKCNT
6044 3C           INR   A
6045 320381       STA   PKCNT
6048 2A1481       LHLD  MXREG
604B EB           XCHG
604C 2A1681       LHLD  MNREG
604F CDDE62       CALL  INV
6052 19           DAD   D
6053 EB           XCHG
6054 2A1081       LHLD  PHPNT
6057 72           MOV   M,D
6058 23           INX   H
6059 73           MOV   M,E
605A 23           INX   H
605B 221081       SHLD  PHPNT
605E 2A1881       LHLD  TMREG
6061 EB           XCHG
6062 2A1281       LHLD  TMPNT
6065 72           MOV   M,D
6066 23           INX   H
6067 73           MOV   M,E
6068 23           INX   H
6069 221281       SHLD  TMPNT
606C 3A0381       LDA   PKCNT
606F 6F           MOV   L,A
6070 3A0081       LDA   PKSET
6073 BD           CMP   L
6074 DAE561       JC    E0
6077 2680         MVI   H,80H
6079 23           INX   H
607A 7E           MOV   A,M
607B 320C81       STA   SPPND
607E 2B           DCX   H
607F 7E           MOV   A,M
6080 320481       STA   SPPNT
6083 E60F         ANI   0FH
6085 FE07         CPI   07H
6087 CA9960       JZ    R7
608A FE08         CPI   08H
608C CAA160       JZ    R8
608F FE09         CPI   09H
6091 CAA960       JZ    R9
6094 FE0A         CPI   0AH
6096 CAB160       JZ    R10
6099 CD6663 R7    CALL  ON7
609C 1602         MVI   D,02H
609E C3B660       JMP   T3
60A1 CD6C63 R8    CALL  ON8
60A4 1602         MVI   D,02H
60A6 C3B660       JMP   T3
60A9 CD7163 R9    CALL  ON9
60AC 1603         MVI   D,03H
60AE C3B660       JMP   T3
60B1 CD7663 R10   CALL  ON10
60B4 1604    M2   MVI   D,04H
60B6 AF      T3   XRA   A
60B7 CD7B63       CALL  TIM
60BA 15           DCR   D
60BB C2B660       JNZ   T3
60BE CD3762       CALL  ADHL
60C1 CDCC62       CALL  BTB20
60C4 110800       LXI   D,0008H
60C7 19           DAD   D
60C8 220A81       SHLD  BARGU
60CB CDD267       CALL  IREG
60CE AF           XRA   A
60CF 320581       STA   UDPNT
60D2 3A0481       LDA   SPPNT
60D5 E620         ANI   20H
60D7 CC7062       CZ    FAST
60DA C47562       CNZ   SLOW
60DD 3E07    M4   MVI   A,07H
60DF 320781       STA   COUNT
60E2 CD3762 M5    CALL  ADHL
60E5 CDCC62       CALL  BTB20
60E8 CD1C63       CALL  MNMX
60EB EB           XCHG
60EC 2A0A81       LHLD  BARGU
60EF CDDE62       CALL  INV
60F2 19           DAD   D
60F3 7C           MOV   A,H
60F4 E680         ANI   80H
60F6 C2DD60       JNZ   M4
60F9 3A0781       LDA   COUNT
60FC 3D           DCR   A
60FD 320781       STA   COUNT
6100 C2E260       JNZ   M5
6103 3E20    M60  MVI   A,20H
6105 320781       STA   COUNT
6108 CD3762 M6    CALL  ADHL
610B CDCC62       CALL  BTB20
610E CD1C63       CALL  MNMX
6111 EB           XCHG
```

continued

```
6112 C5          PUSH B
6113 0611        MVI  B,11H
6115 0E00        MVI  C,00H
6117 CD8562      CALL BCTBI
611A C1          POP  B
611B CDDE62      CALL INV
611E 19          DAD  D
611F 7C          MOV  A,H
6120 E680        ANI  80H
6122 CA0862      JZ   00
6125 D5          PUSH D
6126 2A0A81      LHLD BARGU
6129 111200      LXI  D,0012H
612C 19          DAD  D
612D CDDE62      CALL INV
6130 D1          POP  D
6131 19          DAD  D
6132 7C          MOV  A,H
6133 E680        ANI  80H
6135 C29F61      JNZ  M8
6138 2A2A81      LHLD TRRG8
613B CDDE62      CALL INV
613E 19          DAD  D
613F 7C          MOV  A,H
6140 E680        ANI  80H
6142 C26C61      JNZ  M7
6145 7C          MOV  A,H
6146 FE00        CPI  00H
6148 C20861      JNZ  M6
614B 7D          MOV  A,L
614C E6E0        ANI  E0H
614E C20861      JNZ  M6
6151 3A0581 M13  LDA  UDPNT
6154 FE01        CPI  01H
6156 CA0861      JZ   M6
6159 3A0481      LDA  SPPNT
615C E610        ANI  10H
615E CC7062      CZ   FAST
6161 C47562      CNZ  SLOW
6164 3E01        MVI  A,01H
6166 320581      STA  UDPNT
6169 C30861      JMP  M6
616C D5      M7  PUSH D
616D 2A1481      LHLD MXREG
6170 EB          XCHG
6171 2A1681      LHLD MNREG
6174 CDDE62      CALL INV
6177 19          DAD  D
6178 0604        MVI  B,04H
617A CD5D63  M9  CALL HALF
617D 05          DCR  B
617E C27A61      JNZ  M9
6181 EB          XCHG
6182 2A0A81      LHLD BARGU
6185 19          DAD  D
6186 CDDE62      CALL INV
6189 D1          POP  D
618A 19          DAD  D
618B 7C          MOV  A,H
618C E680        ANI  80H
618E CA0361      JZ   M60
6191 3A0C81      LDA  SPPND
6194 E620        ANI  20H
6196 CC7062      CZ   FAST
6199 C47562      CNZ  SLOW
619C C30861      JMP  M6
619F 3A0581  M8  LDA  UDPNT
61A2 FE00        CPI  00H
61A4 CACF61      JZ   M10
61A7 3A0C81      LDA  SPPND
61AA E620        ANI  20H
61AC CC7062      CZ   FAST
61AF C47562      CNZ  SLOW
61B2 2A0A81      LHLD BARGU
61B5 CDDE62      CALL INV
61B8 19          DAD  D
61B9 7C          MOV  A,H
61BA E680        ANI  80H
61BC CA0361      JZ   M60
61BF CD7562      CALL SLOW
61C2 3A0781      LDA  COUNT
61C5 3D          DCR  A
61C6 320781      STA  COUNT
61C9 C20861      JNZ  M6
61CC C34160      JMP  M11
61CF 2A2A81  M10 LHLD TRRG8
61D2 CDDE62      CALL INV
61D5 19          DAD  D
61D6 7C          MOV  A,H
61D7 E680        ANI  80H
61D9 C26C61      JNZ  M7
61DC C30861      JMP  M6
61DF 00          NOP
61E0 00          NOP
61E1 00          NOP
61E2 00          NOP
61E3 00          NOP
61E4 00          NOP
61E5 3A0181  E0  LDA  SCSET
61E8 47          MOV  B,A
61E9 3A0281      LDA  SCCNT
61EC B8          CMP  B
61ED CAFE61      JZ   E1
61F0 CD3162      CALL KEY
61F3 CA0362      JZ   E2
61F6 3AFC7D      LDA  7DFCH
61F9 3E03        MVI  A,03H
61FB C30A62      JMP  E3
61FE 3E00    E1  MVI  A,00H
6200 C30A62      JMP  E3
6203 3E01    E2  MVI  A,01H
6205 C30A62      JMP  E3
6208 3E02    00  MVI  A,02H
620A 320681  E3  STA  EPNT
620D CD7163      CALL ON9
6210 CD7562      CALL SLOW
6213 3A0681      LDA  EPNT
6216 FE02        CPI  02H
```

```
6218 CA2562        JZ    01
621B 1606          MVI   D,06H
621D AF      T1    XRA   A
621E CD7B63        CALL  TIM
6221 15            DCR   D
6222 C21D62        JNZ   T1
6225 CD6162  01    CALL  SCAOF
6228 3A0681        LDA   EPNT
622B FE01          CPI   01H
622D C48062        CNZ   OFREC
6230 C9            RET
6231 3AFE7D  KEY   LDA   7DFEH
6234 E620          ANI   20H
6236 C9            RET
6237 CD4362  ADHL  CALL  ADON
623A 3E10          MVI   A,10H
623C CD7B63        CALL  TIM
623F 2A047C        LHLD  7C04H
6242 C9            RET
6243 3E0B    ADON  MVI   A,0BH
6245 32077C        STA   7C07H
6248 CD8963        CALL  TIMB
624B 3E0A          MVI   A,0AH
624D 32077C        STA   7C07H
6250 C9            RET
6251 3E09    SCAON MVI   A,09H
6253 32037C        STA   7C03H
6256 3E50          MVI   A,50H
6258 CD7B63        CALL  TIM
625B 3E08          MVI   A,08H
625D 32037C  SCA1  STA   7C03H
6260 C9            RET
6261 3E0B    SCAOF MVI   A,0BH
6263 32037C        STA   7C03H
6266 3E50          MVI   A,50H
6268 CD7B63        CALL  TIM
626B 3E0A          MVI   A,0AH
626D C35D62        JMP   SCA1
6270 3E0D    FAST  MVI   A,0DH
6272 C35D62        JMP   SCA1
6275 3E0C    SLOW  MVI   A,0CH
6277 C35D62        JMP   SCA1
627A 3E09    ONREC MVI   A,09H
627C 32077C  REC1  STA   7C07H
627F C9            RET
6280 3E08    OFREC MVI   A,08H
6282 C37C62        JMP   REC1
6285 C5      BCTBI PUSH  B
6286 D5            PUSH  D
6287 F5            PUSH  PSW
6288 210000        LXI   H,0000H
628B 3E02          MVI   A,02H
628D 37            STC
628E F5      BTB1  PUSH  PSW
628F 78            MOV   A,B
6290 D29762        JNC   BTB2
6293 0F            RRC
6294 0F            RRC
6295 0F            RRC
6296 0F            RRC
6297 E60F    BTB2  ANI   0FH
6299 C2A562        JNZ   BTB3
629C B4            ORA   H
629D B5            ORA   L
629E CAB662        JZ    BTB5
62A1 AF            XRA   A
62A2 C3AA62        JMP   BTB4
62A5 FE0A    BTB3  CPI   0AH
62A7 F2C662        JP    BTB6
62AA 54      BTB4  MOV   D,H
62AB 5D            MOV   E,L
62AC 29            DAD   H
62AD 29            DAD   H
62AE 19            DAD   D
62AF 29            DAD   H
62B0 85            ADD   L
62B1 6F            MOV   L,A
62B2 7C            MOV   A,H
62B3 CE00          ACI   00H
62B5 67            MOV   H,A
62B6 F1      BTB5  POP   PSW
62B7 3F            CMC
62B8 D28E62        JNC   BTB1
62BB 41            MOV   B,C
62BC 3D            DCR   A
62BD C28E62        JNZ   BTB1
62C0 F1            POP   PSW
62C1 37            STC
62C2 3F            CMC
62C3 D1            POP   D
62C4 C1            POP   B
62C5 C9            RET
62C6 F1      BTB6  POP   PSW
62C7 F1            POP   PSW
62C8 37            STC
62C9 D1            POP   D
62CA C1            POP   B
62CB C9            RET
62CC C5      BTB20 PUSH  B
62CD 7C            MOV   A,H
62CE F5            PUSH  PSW
62CF E61F          ANI   1FH
62D1 47            MOV   B,A
62D2 4D            MOV   C,L
62D3 CD8562        CALL  BCTBI
62D6 F1            POP   PSW
62D7 E640          ANI   40H
62D9 CCDE62        CZ    INV
62DC C1            POP   B
62DD C9            RET
62DE 37      INV   STC
62DF 3F            CMC
62E0 7D            MOV   A,L
62E1 2F            CMA
62E2 C601          ADI   01H
62E4 6F            MOV   L,A
62E5 7C            MOV   A,H
62E6 2F            CMA
```

continued

```
62E7 CE00          ACI   00H
62E9 67            MOV   H,A
62EA C9            RET
62EB C5      SUM   PUSH  B
62EC D5            PUSH  D
62ED 210000        LXI   H,0000H
62F0 011C81        LXI   B,TRRG1
62F3 3E0A          MVI   A,0AH
62F5 F5      SUM1  PUSH  PSW
62F6 0A            LDAX  B
62F7 5F            MOV   E,A
62F8 03            INX   B
62F9 0A            LDAX  B
62FA 57            MOV   D,A
62FB 03            INX   B
62FC 19            DAD   D
62FD F1            POP   PSW
62FE 3D            DCR   A
62FF C2F562        JNZ   SUM1
6302 D1            POP   D
6303 C1            POP   B
6304 C9            RET
6305 C5      ROTRG PUSH  B
6306 D5            PUSH  D
6307 E5            PUSH  H
6308 0612          MVI   B,12H
630A 211C81        LXI   H,TRRG1
630D 111E81        LXI   D,TRRG2
6310 1A      ROTR1 LDAX  D
6311 77            MOV   M,A
6312 23            INX   H
6313 13            INX   D
6314 05            DCR   B
6315 C21063        JNZ   ROTR1
6318 E1            POP   H
6319 D1            POP   D
631A C1            POP   B
631B C9            RET
631C E5      MNMX  PUSH  H
631D CD0563        CALL  ROTRG
6320 222E81        SHLD  TRRGA
6323 CDEB62        CALL  SUM
6326 EB            XCHG
6327 2A1681        LHLD  MNREG
632A CDDE62        CALL  INV
632D 19            DAD   D
632E 7C            MOV   A,H
632F E680          ANI   80H
6331 CA3A63        JZ    MNMX1
6334 EB            XCHG
6335 221681        SHLD  MNREG
6338 E1            POP   H
6339 C9            RET
633A 2A1481  MNMX1 LHLD  MXREG
633D CDDE62        CALL  INV
6340 19            DAD   D
6341 7C            MOV   A,H
6342 E680          ANI   80H
6344 C25B63        JNZ   MNMX2
6347 EB            XCHG
6348 221481        SHLD  MXREG
634B 3E80          MVI   A,80H
634D 320F7C        STA   7C0FH
6350 3A0E7C        LDA   7C0EH
6353 6F            MOV   L,A
6354 3A0E7C        LDA   7C0EH
6357 67            MOV   H,A
6358 221881        SHLD  TMREG
635B E1      MNMX2 POP   H
635C C9            RET
635D 37      HALF  STC
635E 3F            CMC
635F 7C            MOV   A,H
6360 1F            RAR
6361 67            MOV   H,A
6362 7D            MOV   A,L
6363 1F            RAR
6364 6F            MOV   L,A
6365 C9            RET
6366 3E00    ON7   MVI   A,00H
6368 32007C  ON70  STA   7C00H
636B C9            RET
636C 3E03    ON8   MVI   A,03H
636E C36863        JMP   ON70
6371 3E05    ON9   MVI   A,05H
6373 C36863        JMP   ON70
6376 3E09    ON10  MVI   A,09H
6378 C36863        JMP   ON70
637B C5      TIM   PUSH  B
637C 47            MOV   B,A
637D 0E00          MVI   C,00H
637F 0D      TIMO  DCR   C
6380 C27F63        JNZ   TIMO
6383 05            DCR   B
6384 C27F63        JNZ   TIMO
6387 C1            POP   B
6388 C9            RET
6389 3E80    TIMB  MVI   A,80H
638B 3D      TIMBO DCR   A
638C C28B63        JNZ   TIMBO
638F C9            RET
```

continued

```
66FC 2A1081 K0     LHLD PHPNT
66FF 223081 K00    SHLD PHTMP
6702 C9            RET
6703 2A1281 L0     LHLD TMPNT
6706 C3FF66        JMP  K00
6709 2A3081 K1     LHLD PHTMP
670C 2B            DCX  H
670D 7E            MOV  A,M
670E 323381        STA  PHTM2
6711 2B            DCX  H
6712 7E            MOV  A,M
6713 323281        STA  PHTM1
6716 223081        SHLD PHTMP
6719 C9            RET
671A F5      NOLF  PUSH PSW
671B 3A7984        LDA  PRPNT
671E FE0D          CPI  0DH
6720 CA2B67        JZ   NOLF1
6723 FE0A          CPI  0AH
6725 CA2B67        JZ   NOLF1
6728 CD2F67        CALL LPRI
672B F1      NOLF1 POP  PSW
672C C9            RET
672D 3E0A    LFPR  MVI  A,0AH
672F 320881  LPRI  STA  PRPN1
6732 3A127C  PRINT LDA  7C12H
6735 E604          ANI  04H
6737 C23267        JNZ  PRINT
673A 3A0881        LDA  PRPN1
673D 32107C        STA  7C10H
6740 3E0C          MVI  A,0CH
6742 32137C        STA  7C13H
6745 3C            INR  A
6746 32137C        STA  7C13H
6749 C9            RET
674A F5      HDCPY PUSH PSW
674B 3A7984        LDA  PRPNT
674E FE0D          CPI  0DH
6750 CA5667        JZ   HDCP1
6753 CD2F67        CALL LPRI
6756 F1      HDCP1 POP  PSW
6757 C9            RET
6758 00            NOP
6759 00            NOP
675A 00            NOP
675B 00            NOP
675C 3E07    BEL   MVI  A,07H
675E C32F67        JMP  LPRI
6761 3E08    BS    MVI  A,08H
6763 C32F67        JMP  LPRI
6766 3E0B    VT    MVI  A,0BH
6768 C32F67        JMP  LPRI
676B 3E0C    FF    MVI  A,0CH
676D C32F67        JMP  LPRI
6770 3E0D    CR    MVI  A,0DH
6772 C32F67        JMP  LPRI
6775 3E0E    SO    MVI  A,0EH
6777 C32F67        JMP  LPRI
677A 3E0F    SI    MVI  A,0FH
677C C32F67        JMP  LPRI
677F 3E11    DC1   MVI  A,11H
6781 C32F67        JMP  LPRI
6784 3E12    DC2   MVI  A,12H
6786 C32F67        JMP  LPRI
6789 3E13    DC3   MVI  A,13H
678B C32F67        JMP  LPRI
678E 3E14    DC4   MVI  A,14H
6790 C32F67        JMP  LPRI
6793 3E1B    ESC   MVI  A,1BH
6795 C32F67        JMP  LPRI
6798 00            NOP
6799 00            NOP
679A 00            NOP
679B 00            NOP
679C CD9367  ESCE  CALL ESC
679F 3E45          MVI  A,45H
67A1 C32F67        JMP  LPRI
67A4 211A67  IPR   LXI  H,NOLF
67A7 3EC3    I1    MVI  A,C3H
67A9 32EC84        STA  84ECH
67AC 22ED84        SHLD 84EDH
67AF 21137C        LXI  H,7C13H
67B2 3681          MVI  M,81H
67B4 360D          MVI  M,0DH
67B6 C9            RET
67B7 3E81    IIF   MVI  A,81H
67B9 32037C        STA  7C03H
67BC 3E93          MVI  A,93H
67BE 32077C        STA  7C07H
67C1 C9            RET
67C2 210F7C  ITM1  LXI  H,7C0FH
67C5 3634          MVI  M,34H
67C7 3674          MVI  M,74H
67C9 36B4          MVI  M,B4H
67CB C9            RET
67CC 214A67  CHNG  LXI  H,HDCPY
67CF C3A767        JMP  I1
67D2 160A    IREG  MVI  D,0AH
67D4 CD3762  I2    CALL ADHL
67D7 CDCC62        CALL BTB20
67DA CD0563        CALL ROTRG
67DD 222E81        SHLD TRRGA
67E0 15            DCR  D
67E1 C2D467        JNZ  I2
67E4 CDEB62        CALL SUM
67E7 221481        SHLD MXREG
67EA 21FF0F        LXI  H,0FFFH
67ED 221681        SHLD MNREG
67F0 C9            RET
67F1 210E7C  ITM2  LXI  H,7C0EH
67F4 AF            XRA  A
67F5 77            MOV  M,A
67F6 77            MOV  M,A
67F7 2B            DCX  H
67F8 3632          MVI  M,32H
67FA 77            MOV  M,A
67FB 2B            DCX  H
67FC 77            MOV  M,A
67FD 3650          MVI  M,50H
67FF C9            RET
```

List of BASIC controlling program

```
  5 CALL 17A4H: CALL 17B7H
 10 DATA TI,HOG54,5,46,7.99,47,7.32,48,73.99,49,5.46,50,5.25
 20 DATA SI,TAB(7),3,28,92.23,29,4.67,30,3.1
 30 DATA MG,STW70,3,24,1,25,.12663,26,.139805,CU,TAB(7),2,63,69.2,65,30.8
 40 DATA NI,BAR73,5,58,68.274,60,26.095,61,1.134,62,3.593,64,.904
 50 DATA CR,ICA80,4,50,4.35,52,83.79,53,9.5,54,2.36
 60 DATA FE,JAM79,4,54,5.8,56,91.77,57,2.15,58,.28
 70 DATA GE,TAB(7),5,70,20.5,72,27.4,73,7.8,74,36.5,76,7.8
 80 DATA MO,TAB(7),5,94,9.3,95,15.9,96,16.7,97,9.6,98,24.1
 90 DATA AG,TAB(7),2,107,51.83,109,48.17,OT,X,1,1,1
100 DIM A(5),B(5),C(5),D(5),E(5),F(25),H(5),I(5),J(5),K(5),L(5),M(4,5),N(50)
110 DIM P(25,5),Q(25,5),S(5),T(25,5),U(25,5),X(50,5),Y(50,5),Z(50,5)
120 LET A=1,B=0,D=A+A: CLEAR : PRINT "<AUTO SCAN>": PRINT
130 PRINT "INITIAL": GOSUB 1460: IF A$="Y" THEN  POKE 80A0H,B
140 LET B$="C",V=B,E0=-120,P0=2.5,X3=5933,X4=34348,N4=PEEK(80A0H)
150 PRINT "POLARITY": PRINT "SCAN SPEED": PRINT "SENS.SWITCH": GOSUB 1460: IF
A$<>"Y" THEN 150
160 PRINT "": INPUT "DATE"N$
170 INPUT "NAME"D$: IF B$="N" THEN 830
180 INPUT "ELEMENT"F$: RESTORE
190 READ E$,G$,N: FOR I=A TO N: READ J(I),L(I): LET D(I)=J(I),E(I)=L(I): NEXT
I: IF E$="OT" THEN 230
200 IF E$<>F$ THEN 190
210 LET J1=N
220 CLEAR : PRINT G$: FOR I=A TO N: PRINT J(I);F$," :",L(I): NEXT I: GOSUB 146
0: IF A$="Y" THEN  LET N1=N: GOTO 260
230 IF LEN(F$)>D THEN  LET F$=LEFT(F$,D)
240 INPUT "PEAK NO."N: IF E$<>"OT" THEN  GOSUB 1880: GOTO 220
250 FOR I=A TO N: INPUT "MASS"J(I),"ABUNDANCE"L(I): NEXT I: INPUT "REF."G$: GO
TO 220
260 INPUT "NORMALIZED TO MASS"T: FOR I=1 TO N: IF T=J(I) THEN  LET E=I
270 NEXT I: LET E$=F$: FOR I=A TO N: LET K(I)=L(I)/L(E): NEXT I: POKE 8100H,N:
 IF B$="T" THEN 830
280 PRINT "SELECT FROM (7,8,9,10)": FOR I=A TO N1
290 PRINT J(I);E$;: INPUT " SENSITIVITY="N: IF N>=7 THEN  IF N<=10 THEN 310
300 GOTO 290
310 LET C=32768+I,A(I)=N: POKE C,N: NEXT I
320 GOSUB 1460: IF A$<>"Y" THEN 280
```

continued

```
  330 LET H$="*PEAK",A1=A: GOSUB 1790: LET H$="*BASE",A1=D: GOSUB 1790
  340 LET C=C+A: POKE C,B: IF B$="Z" THEN 830
  350 INPUT "SCAN NO.(1<N<25)"N2: GOSUB 1460: IF A$<>"Y" THEN 350
  360 LET N=N2+A: POKE 8101H,N: POKE 8102H,B: IF B$="X" THEN 830
  370 INPUT "RUN NO."N5: GOSUB 1460: IF A$<>"Y" THEN 370
  380 IF B$="Y" THEN 830
  390 PRINT "INTERPO.AT": FOR I=A TO N1: PRINT J(I);E$: NEXT I: GOSUB 1490: FOR
I=A TO N1: IF N=J(I) THEN  LET E1=I
  400 NEXT I: IF B$="I" THEN 830
  410 PRINT "ON-LINE": GOSUB 1460: LET N3=A: IF A$<>"Y" THEN  LET N3=B
  420 PRINT "GRAPH": GOSUB 1460: LET N7=A: IF A$<>"Y" THEN  LET N7=D
  430 PRINT "INITIAL SCAN POINT": GOSUB 1460: IF A$<>"Y" THEN 430
  440 CLEAR : GOSUB 1850: PRINT "": PRINT "--START": GOSUB 1460: IF A$<>"Y" THEN
 670
  450 IF V=B THEN  LET N6=A: GOTO 470
  460 IF N6>A THEN  LET N6=N6-A
  470 IF V<>D THEN  LET N4=N4+A: POKE 80A0H,N4
  480 FOR J=B TO N1: LET X(N4,J)=B,Y(N4,J)=B: NEXT J: LET N(N4)=B: IF N3=B THEN
560
  490 CALL 1784H: POKE X4,55H: CALL 1775H: GOSUB 1570: CALL X3: CALL 17A4H
  500 CALL 17CCH: GOSUB 1470: CALL 17A4H: PRINT "(",G$,")": GOSUB 1480: IF N1>D+
D THEN  CALL 177AH
  510 PRINT E$,"   ": FOR I=A TO N1: PRINT #9,L(I): NEXT I: FOR I=A TO N1: IF I<
>E THEN  PRINT #12,K(I)
  520 NEXT I: CALL X3: CALL X3: PRINT " #   ": FOR I=A TO N1: PRINT #9,J(I): NEX
T I: FOR I=A TO N1: IF I=E THEN 550
  530 PRINT J(I);"/";J(E);: IF J(I)>99 THEN  PRINT " ": GOTO 550
  540 PRINT "   "
  550 NEXT I: CALL X3: CALL X3: POKE X4,56H
  560 CLEAR : GOSUB 1570: PRINT "": GOSUB 1470: CURSOR 10,11: PRINT "< TOTAL > <
 NOW >"
  570 CURSOR A,13: PRINT "< RUN  >   ",#5,N5,"     ",N6
  580 CURSOR A,15: PRINT "< SCAN >   ",#5,N2: GOSUB 1500: IF V=B THEN  CALL 1000
H: GOTO 600
  590 CALL 1022H
  600 LET V=PEEK(8106H): IF V=D THEN  POKE 8102H,W: GOTO 650
  610 IF N3=A THEN  GOSUB 850
  620 IF V=A+D THEN 830
```

continued

```
  630 IF V=B THEN 940
  640 GOSUB 1500: CALL 1030H: GOTO 600
  650 CLEAR : PRINT "--OVER FLOW, DOWN EMT VOLT": PRINT
  660 IF V<>B THEN  PRINT "<C>CONT."
  670 PRINT "<R>REPEAT": PRINT "<B>BUFFERING": PRINT "<S>STAT.": GOSUB 1850
  680 PRINT "<L>LIST": PRINT "<U>SUMMARY": PRINT "<E>END": INPUT "WHICH"I$
  690 FOR Q=A TO LEN(I$): LET B$=MID(I$,Q,A): IF B$="C" THEN 560
  700 IF B$="R" THEN  LET P0=2.5,E0=-120: POKE 8102H,B: GOTO 450
  710 IF B$="B" THEN  LET N(N4)=A: GOTO 830
  720 IF B$="X" THEN 350
  730 IF B$="Z" THEN 280
  740 IF B$="N" THEN 170
  750 IF B$="S" THEN 950
  760 IF B$="T" THEN 180
  770 IF B$="Y" THEN 370
  780 IF B$="I" THEN 390
  790 IF B$="U" THEN 1330
  800 IF B$="L" THEN 1330
  810 IF B$="E" THEN  STOP
  820 CLEAR : GOTO 660
  830 IF V<>B THEN 820
  840 NEXT Q: GOTO 820
  850 CALL 16FCH: FOR I=N1 TO A STEP -A: GOSUB 1450: LET P(W,I)=(P1*256+P2)*INT(
10^(10-A(I))+.5): NEXT I
  860 CALL 1703H: FOR I=N1 TO A STEP -A: GOSUB 1450: LET T(W,I)=P1*256+P2: NEXT
I: IF W=B THEN  RETURN
  870 LET E2=W: IF E1<>A THEN  LET E2=W-A
  880 FOR I=A TO N1
  890 LET U(W,I)=P(W,I)+(T(E2,E1)-T(W,I))*(P(W-A,I)-P(W,I))/(T(W-A,I)-T(W,I)): N
EXT I
  900 FOR I=A TO N1: LET Q(W,I)=U(W,I)/U(W,E): NEXT I
  910 POKE X4,55H: PRINT #5,W: FOR I=A TO N1: PRINT #9,INT(U(W,I)+.5): NEXT I
  920 FOR I=A TO N1: IF I<>E THEN  PRINT #12,Q(W,I)
  930 NEXT I: CALL X3: POKE X4,56H: RETURN
  940 IF N3=B THEN 1310
  950 CLEAR : PRINT "--STATISTICS,WAIT A MINUTE"
  960 FOR I=A TO W: FOR J=A TO N1: LET P(I,J)=(Q(I,J)/K(J)-A)*1000: NEXT J: NEXT
 I
```

continued

```
  970 FOR I=A TO W: LET F(I)=B: NEXT I: LET L=B,Y=A
  980 FOR J=A TO N1: LET S(J)=B,C(J)=B,K=B: FOR I=A TO W: IF F(I)=B THEN  LET S(
J)=S(J)+Q(I,J),K=K+A
  990 NEXT I: LET M(A,J)=S(J)/K,M(A+D,J)=(M(A,J)/K(J)-A)*1000: NEXT J
 1000 FOR J=A TO N1: FOR I=A TO W: IF F(I)=B THEN  LET C=Q(I,J)-M(A,J),C(J)=C(J)
+C*C
 1010 NEXT I: LET C=C(J)/K,U=SQR(C)*D,M(D,J)=SQR(C/(K-A)),H(J)=M(A,J)+U,I(J)=M(A
,J)-U
 1020 LET M(D+D,J)=M(D,J)/K(J)*1000: NEXT J: IF L=K THEN 1170
 1030 POKE X4,55H: IF N1>D+D THEN  CALL 177AH
 1040 PRINT "NO.OF DATA =",#4,K,"--*--": IF Y=A THEN 1070
 1050 PRINT " (": FOR I=A TO W: IF F(I)=Y-A THEN  PRINT I;","
 1060 NEXT I: PRINT ")"
 1070 CALL X3: FOR J=A TO D+D: GOSUB 1540: ON J GOSUB 1510,1520,1530,1520
 1080 FOR I=A TO N1: IF I<>E THEN  PRINT #12,M(J,I)
 1090 NEXT I: CALL X3: NEXT J: IF L=B THEN 1120
 1100 FOR J=A TO N1: IF B(J)<M(D+D,J) THEN 1170
 1110 NEXT J
 1120 FOR I=A TO W: IF F(I)<>B THEN 1160
 1130 FOR J=A TO N1: IF Q(I,J)<=H(J) THEN  IF Q(I,J)>=I(J) THEN 1150
 1140 LET F(I)=Y
 1150 NEXT J
 1160 NEXT I: FOR J=A TO N1: LET B(J)=M(D+D,J): NEXT J: LET L=K,Y=Y+A: GOTO 980
 1170 GOSUB 1480: IF N6<N5 THEN  IF V=B THEN  CALL 127AH
 1180 LET I=N4,M0=120,M1=-120: FOR J=A TO N1
 1190 LET X(I,J)=M(A+D,J),Y(I,J)=M(D+D,J): IF M(A+D,J)<M0 THEN  LET M0=M(A+D,J)
 1200 IF M(A+D,J)>M1 THEN  LET M1=M(A+D,J)
 1210 LET Z(I,J)=J(J): NEXT J: LET X(I,B)=N1,Y(I,B)=E,P=2.5
 1220 IF 10*P<M1-M0 THEN  LET P=D*P: GOTO 1220
 1230 IF P0<P THEN  LET P0=P
 1240 LET E3=P*(D-INT(M0/P)): IF E3>E0 THEN  LET E0=E3
 1250 IF N7=D THEN 1300
 1260 GOSUB 1530: CALL X3: CALL 177AH: GOSUB 1580: GOSUB 1590
 1270 FOR I=A TO W: CALL 16E7H: FOR J=A TO N1: LET Z=P(I,J),C=64+J: IF F(I)<>B T
HEN  LET C=63
 1280 GOSUB 1600: NEXT J: CALL 16D0H: NEXT I: CALL X3: GOSUB 1590: CALL X3: CALL
 16E7H: LET I=N4: GOSUB 1410
 1290 GOSUB 1590: GOSUB 1580: POKE X4,56H: CALL 176BH
```

continued

```
 1300 IF V=A+D THEN 830
 1310 IF N6>=N5 THEN 820
 1320 LET N6=N6+A,V=B: POKE 8102H,B: GOTO 470
 1330 INPUT "START #"N9,"END #"N8: CALL 177AH: LET E3=E0,P=P0
 1340 POKE X4,55H: CALL 1775H: IF B$="U" THEN  PRINT "SUMMARY (": GOTO 1360
 1350 PRINT "LIST ("
 1360 PRINT N9;"-";N8;") ",N$: CALL X3: GOSUB 1620: IF B$="L" THEN 1400
 1370 FOR I=N9 TO N8: CALL 16E7H: LET NO=N1,N1=X(I,B),E4=E,E=Y(I,B): GOSUB 1410:
LET N1=NO,E=E4
 1380 IF N(I)=A THEN  GOSUB 1590
 1390 NEXT I: GOSUB 1590: GOSUB 1580: CALL 1784H: GOSUB 1530: CALL X3
 1400 POKE X4,56H: CALL 176BH: GOTO 830
 1410 FOR J=A TO N1: IF J=E THEN 1440
 1420 LET C=45,Z=X(I,J)-Y(I,J)
 1430 GOSUB 1600: LET Z=Z+P*.1: IF Z<=X(I,J)+Y(I,J) THEN 1430
 1440 NEXT J: FOR J=A TO N1: LET Z=X(I,J),C=64+J: GOSUB 1600: NEXT J: CALL 16D0H
: RETURN
 1450 CALL 1709H: LET P1=PEEK(8132H),P2=PEEK(8133H): RETURN
 1460 INPUT "<Y/N>"A$: RETURN
 1470 FOR I=A TO N1: PRINT J(I);E$;" = 10 E",#4,A(I): NEXT I: RETURN
 1480 CALL 1784H: FOR I=A TO 13: PRINT "--*--": NEXT I: CALL X3: RETURN
 1490 INPUT "WHICH ONE"N: RETURN
 1500 LET W=PEEK(8102H): CURSOR 22,15: PRINT #4,W: CURSOR 30,15: RETURN
 1510 PRINT " MEAN    ": RETURN
 1520 PRINT "ERROR    ": RETURN
 1530 PRINT "DELTA %.": RETURN
 1540 LET F=9*N1-A-D
 1550 FOR G=A TO F: PRINT " ";: NEXT G: RETURN
 1560 LET C=32768+I,A5=PEEK(C),B5=A5+N*16: POKE C,B5: RETURN
 1570 PRINT N$," #",N4;"(",D$,")": RETURN
 1580 FOR I=B TO 12*P STEP P: PRINT #10,I-E3: NEXT I: CALL X3: RETURN
 1590 FOR J=A TO 13: PRINT "-+---------": NEXT J: CALL X3: RETURN
 1600 LET N=32785+INT(10*(Z+E3)/P+.5): IF N>=32785 THEN  IF N<=32917 THEN  POKE
N,C
 1610 RETURN
 1620 GOSUB 1590: LET I0=N9: FOR H=N9 TO N8: LET S=X(H,B),E5=Y(H,B): IF I0<>H TH
EN 1690
 1630 PRINT " #       ": FOR I=A TO D+D: GOSUB 1530: PRINT " +-  ": GOSUB 1520: P
RINT "      "
```

continued

```
 1640 NEXT I: CALL X3: PRINT "          ": FOR I=A TO S: IF I=E5 THEN 1680
 1650 PRINT Z(H,I);"/";Z(H,E5);: IF Z(H,I)>99 THEN  LET F=15: GOTO 1670
 1660 LET F=17
 1670 GOSUB 1550
 1680 NEXT I: CALL X3: CALL X3
 1690 PRINT #8,H: FOR J=A TO S: IF J<>E5 THEN  PRINT #12,X(H,J),Y(H,J),"   "
 1700 NEXT J: CALL X3: IF B$<>"L" THEN  IF N(H)=A THEN  GOSUB 1730
 1710 NEXT H: LET H=H-A: IF N(H)=B THEN  GOSUB 1730: CALL X3
 1720 RETURN
 1730 CALL X3: PRINT "G MEAN  ": FOR J=A TO S: LET S(J)=B,C(J)=B: NEXT J
 1740 FOR J=A TO S: IF J=E5 THEN 1780
 1750 LET K=B: FOR R=I0 TO H: LET S(J)=S(J)+X(R,J),K=K+A: NEXT R: LET M=S(J)/K
 1760 FOR R=I0 TO H: LET C=X(R,J)-M,C(J)=C(J)+C*C: NEXT R
 1770 LET O=SQR(C(J)/K/(K-A)),X(B,J)=M,Y(B,J)=O: PRINT #12,M,O,"   "
 1780 NEXT J: CALL X3: GOSUB 1590: LET I0=H+A: RETURN
 1790 PRINT H$+" SPEED*": PRINT "<0>ALL FAST": PRINT "<1>ALL SLOW": PRINT "<2>EA
CH SET"
 1800 GOSUB 1490: IF N>D THEN 1790
 1810 IF N<>D THEN  LET N=A1*N: FOR I=A TO N1: GOSUB 1560: NEXT I: RETURN
 1820 CLEAR : PRINT "<0>FAST": PRINT "<1>SLOW": FOR I=A TO N1: IF A1=D THEN  PRI
NT J(I)-A;"-";
 1830 PRINT J(I): INPUT "SPEED="N: IF N>=D THEN 1820
 1840 LET N=A1*N: GOSUB 1560: NEXT I: RETURN
 1850 PRINT "<T>ELEMENT (";E$;")": PRINT "<N>NAME     (",D$,")": PRINT "<X>SCAN #
  (";N2;")"
 1860 PRINT "<Y>RUN #    (";N5;")": PRINT "<Z>SENS.    (";: FOR I=A TO N1: PRINT A
(I);: NEXT I: PRINT ")"
 1870 PRINT "<I>INTERPO.(";E1;")": RETURN
 1880 FOR I=A TO N
 1890 INPUT "MASS"JO: FOR J=A TO J1: IF JO=D(J) THEN  LET J(I)=JO,L(I)=E(J): GOT
O 1910
 1900 NEXT J: PRINT JO;"IS MISTAKE": GOTO 1890
 1910 NEXT I: RETURN
```

ACKNOWLEDGMENTS

The author expresses his sincere thanks to Professor J. Okano of Osaka University for his encouragement and invaluable discussion throughout the work.

He is grateful to Professor K. Ogata of Okayama University of Science for his encouragement. Thanks are also given to Professor N. Takaoka of Yamagata University and Dr. K. Nagao of Okayama University of Science for providing the Allende specimens and for the discussion about this study. He is indebted to Professor T. Nagata of National Institute of Polar Research for the permission to use the Yamato meteorite samples. The author thanks Professor M. Honda and Dr. M. Shima for their encouragement. The author also thanks Dr. I. Kaneoka of the University of Tokyo for providing the samples of terrestrial lherzolites. He thanks Dr. Y. Uno for providing the terrestrial hornblende.

He is also much grateful to Professor H. Matsuda, Professor M. Date, Professor S. Miyamoto and Professor K. Katori for their useful advices and invaluable comments to prepare this paper.

He also thanks Miss M. Mizumoto for her help of preparing the manuscript.

REFERENCES

1) E.M. Burbidge, G.R. Burbidge, W.A. Fowler and F. Hoyle, Synthesis of the elements in stars, Rev. Mod. Phys., 29 (1957) 547-650.

2) W.A. Fowler, J.L. Greenstein and F. Hoyle, Nucleosynthesis during the early history of the solar system, Geophys. J., 6 (1962) 148-220.

3) J.A. Wood, On the origin of chondrules and chondrites, Icarus, 2 (1963) 152-180.

4) J.H. Reynolds, Determination of the age of the elements, Phys. Rev. Lett., 4 (1960) 8-10.

5) R.A. Fish, G.G. Goles and E. Anders, The record in the meteorites III. On the development of meteorites in asteroidal bodies, Astrophys. J., 132 (1960) 243-258.

6) H. Reeves and J. Audouze, Early heat generation in meteorites, Earth Planet. Sci. Lett., 4 (1968) 135-141.

7) M. Shima, The isotopic composition of magnesium in terrestrial samples, Bull. Chem. Soc. Japan, 37 (1964) 284-285.

8) N. Takematsu, S. Matsuo and S. Sato, Isotopic composition of magnesium in upper mantle materials and a meteorite, Geochem. J., 1 (1967) 51-54.

9) W.B. Clarke, J.R. DeLaeter, H.P. Schwarcz and K.C. Schane, Aluminum 26 - magnesium 26 dating of feldspar in meteorites, J. Geophys. Res., 75 (1970) 448-462.

10) D.N. Schramm, F. Terra and G.J. Wasserburg, The isotopic abundance of ^{26}Mg and limits on ^{26}Al in the early solar system, Earth Planet. Sci. Lett., 10 (1970) 44-59.

11) E.A. King, Jr., E. Schonfeld, K.A. Richardson and J.S. Eldridge, Meteorite fall at Pueblito de Allende, Chihuahua, Mexico: Preliminary information, Science, 163 (1969) 928-929.

12) U.B. Marvin, J.A. Wood and J.S. Dickey, Jr., Ca-Al rich phases in the Allende meteorite, Earth Planet. Sci. Lett., 7 (1970) 346-350.

13) L. Grossman, Petrography and mineral chemistry of Ca-rich inclusions in the Allende meteorite, Geochim. Cosmochim. Acta, 39 (1975) 433-454.

14) R.N. Clayton, L. Grossman and T.K. Mayeda, A component of primitive nuclear composition in carbonaceous meteorites, Science, 182 (1973) 485-488.

15) T.K. Mayeda, R.N. Clayton and E.J. Olsen, Oxygen isotopic anomalies in an ordinary chondrite, Meteoritics, 15 (1980) 330-331.

16) C.M. Gray and W. Compston, Excess ^{26}Mg in the Allende meteorite, Nature, 251 (1974) 495-497.

17) T. Lee and D.A. Papanastassiou, Mg isotopic anomalies in the Allende meteorite and correlation with O and Sr effects, Geophys. Res. Lett., 1 (1974) 225-228.

18) T. Lee, D.A. Papanastassiou and G.J. Wasserburg, Determination of ^{26}Mg excess in Allende and evidences for ^{26}Al, Geophys. Res. Lett., 3 (1976) 109-112.

19) T. Lee, D.A. Papanastassiou and G.J. Wasserburg, Aluminum-26 in the early solar system: fossil or fuel ?, Astrophys. J., 211 (1977) L107-L110.

20) T. Lee, D.A. Papanastassiou and G.J. Wasserburg, Mg and

Ca isotopic study of individual microscopic crystals from the Allende meteorite by the direct loading technique, Geochim. Cosmochim. Acta, 41 (1977) 1473-1485.

21) T.M. Esat, T. Lee, D.A. Papanastassiou and G.J. Wasserburg, Search for Al effects in the Allende FUN inclusion C1, Geophys. Res. Lett., 5 (1978) 807-810.

22) W. Stegmann and F. Begemann, Al-correlated ^{26}Mg excess in a large Ca-Al-rich inclusion of the Leoville meteorite, Earth Planet Sci. Lett., 55 (1981) 266-272.

23) J.G. Bradley, J.C. Huneke and G.J. Wasserburg, Ion microprobe evidence for the presence of excess ^{26}Mg in an Allende anorthite crystal, J. Geophys. Res., 83 (1978) 244-254.

24) I.D. Hutcheon, I.M. Steele, R.N. Clayton and J.V. Smith, An ion microprobe study of Mg isotopes in two Allende inclusions, Meteoritics, 13 (1978) 498-499.

25) N. Shimizu, M.P. Semet and C.J. Allegre, Geochemical applications of quantitative ion microprobe analysis, Geochim. Cosmochim. Acta, 42 (1978) 1321-1334.

26) I.D. Hutcheon, G.J. MacPherson, I.M. Steele and L. Grossman, A petrographic and ion probe isotopic study of type A coarse-grained inclusions, Meteoritics, 14 (1979) 427.

27) C.E. Rees and H.G. Thode, A ^{33}S anomaly in the Allende meteorite, Geochim. Cosmochim. Acta, 41 (1977) 1679-1682.

28) M.T. McCulloch and G.J. Wasserburg, Barium and neodymium isotopic anomalies in the Allende meteorite, Astrophys. J., 220 (1978) L15-L29.

29) T. Lee, D.A. Papanastassiou and G.J. Wasserburg, Calcium isotopic anomalies in the Allende meteorite, Astrophys. J., 220 (1978) L21-L25.

30) D.A. Papanastassiou and G.J. Wasserburg, Strontium isotopic anomalies in the Allende meteorite, Geophys. Res. Lett., 5 (1978) 595-598.

31) M.T. McCulloch and G.J. Wasserburg, More anomalies from the Allende meteorite: samarium, Geophys. Res. Lett., 5 (1978) 599-602.

32) W.R. Kelly and G.J. Wasserburg, Evidence for the existence of ^{107}Pd in the early solar system, Geophys. Res. Lett., 5 (1978) 1079-1082.

33) D.N. Schramm, Supernovae and the formation of the solar system, Protostars and Planets (ed. T. Gehrels) Univ. of Arizona Press, (1978) 384-398.

34) F.A. Podosek and R.S. Lewis, ^{129}I and ^{244}Pu abundances in white inclusions of the Allende meteorite, Earth and Planet. Sci. Lett., 15 (1972) 101-109.

35) A. Zaikowski, I-Xe dating of Allende inclusions: antiquity and fine structure, Earth Planet. Sci. Lett., 47 (1980) 211-222.

36) A.G.W. Cameron and J.W. Truran, The supernova trigger for formation of the solar system, Icarus, 30 (1977) 447-461.

37) W.D. Arnett, Explosive nucleosynthesis in stars, Astrophys. J., 157 (1969) 1369-1380.

38) W.D. Arnett and J.W. Truran, Carbon-burning nucleosynthesis at constant temperature, Astrophys. J., 157

(1969) 339-365.

39) W.R. VanSchmus and J.A. Wood, A chemical-petrologic classification for the chondrites, Geochim. Cosmochim. Acta, 31 (1967) 747-765.

40) J.T. Wasson, Meteorites; Classification and Properties. Berlin, Springer, (1974), 316p. (Mineral and Rocks, Vol. 10).

41) K. Yanai, comp. Catalog of Yamato Meteorites, 1st ed. Tokyo, Natl. Inst. Polar Res., (1979), 188p.

42) M. Blander and J.L. Katz, Condensation of primordial dust, Geochim. Cosmochim. Acta, 31 (1967) 1025-1034.

43) L. Grossman, Condensation in the primitive solar nebula, Geochim. Cosmochim. Acta, 36 (1972) 597-619.

44) D. Phinney, B. Whitehead and D. Anderson, Li, Be and B in minerals of a refractory-rich Allende inclusion, Proc. Lunar Planet. Sci. Conf. 10th (1979) 885-905.

45) M. Kimura, K. Yagi and K. Onuma, Opaque minerals in the Yamato-74191 chondrite, Mem. Natl. Inst. Polar Res., Spec. Issue (1980) 95-103.

46) N. Takaoka and K. Nagao, Neutron capture effects in Yamato-74191 and rare gas composition in Yamato-75258, Mem. Natl. Inst. Polar Res., Spec. Issue (1980) 210-218.

47) E.J. Catanzaro, T.J. Murphy, E.L. Garner and W.R. Shields, Absolute isotopic abundance ratios and atomic weight of magnesium, J. Res. Natl. Bureau Stds., 70A (1966) 453-458.

48) J.W. Sruran and A.G.W. Cameron, ^{26}Al production in explosive carbon burning, Astrophys. J., 219 (1978) 226-229.

49) W.D. Arnett and J.P. Wefel, Aluminum-26 production from a stellar evolutionary sequence, Astrophys. J., 224 (1978) L139-L142.

50) R.N. Clayton and T.K. Mayeda, Isotopic fractionation of silicon in Allende inclusion, Proc. Lunar Planet. Sci. Conf., 9th (1978) 1267-1278.

51) K. Nagao and N. Takaoka, private communication.

Table 2.1 Meteoritic samples used in the present work with their classifications and abbreviations

Sample	Classification	Abbreviation
Allende	C3	AL0, AL1, AL2
Yamato-74191	L3	Y-74191
Yamato-75028	H3	Y-75028

Table 2.2 Terrestrial samples used in the present work with their localities and abbreviations

Sample	Locality	Abbreviation
Forsterite in Dunite	Ehime Pref. Japan	FO
Olivine in Lherzolite	Salt Lake, Hawaii	SL46
Olivine in Lherzolite	Oki Island, Japan	OK
Olivine in Lherzolite	McMurdo, Antarctica	MM
Olivine in Spinel lherzolite	Salt Lake, Hawaii	SL45
Hornblende	Fukui Pref., Japan	HO
Vesuvianite	Chihuahua, Hawaii	VE
Cordierite	Kyoto Pref., Japan	CO
Anorthite	Hokkaido, Japan	AN
Feldspar in Granodiorite	Hyogo Pref., Japan	FE

Table 3.1 Typical operating conditions of the hollow cathode ion gun

	Hitachi IMA 2A	Home-made
Ionic species	Oxygen	Oxygen
Discharge voltage	400 V	1600 V
Discharge current	75 mA	30 mA

Table 3.2 Typical working conditions for magnesium isotopic analysis

	Hitachi IMA 2A	Home-made
Primary ion		
Energy	12-17 keV	8-9 keV
Beam diameter	70-200 μm	100-200 μm
Beam current	0.2-2 μA	0.2-0.8 μA
Secondary ion		
Accelerating voltage	3 kV	1 kV
Pressure		
Ultimate	3×10^{-5} Pa	6×10^{-5} Pa
during measurement	8×10^{-5} Pa	2×10^{-3} Pa

Table 3.3 Geometric parameters of mass spectrometers and resolutions

	Hitachi IMA 2A	Home-made
Electrostatic sector		
Radius	15 cm	10 cm
Deflection angle	90°	63.6°
Magnetic sector		
Radius	12.5 cm	10 cm
Deflection angle	90°	90°
Slits		
Main slit	equal to beam dia.	0.3×4 mm^2
β slit	0.5×6 mm^2	1.0×6 mm^2
Collector slit	0.5×8 mm^2	0.5×4 mm^2
Resolution*	150	100

* Resolutions shown here are those for magnesium isotopic analysis.

Table 4.1 Intrferences of possible molecular and doubly-charged ions to the subject ionic species

Subject ionic species	Possible interfering ionic species	Resolving* power	Maximum contribution to the subject peak	
			Home-made	Hitachi IMA
$^{24}Mg^+$	$^{12}C^{2+}$	1600	4×10^{-4}	3×10^{-5}
	$^{23}NaH^+$	1910	1×10^{-6}	2.5×10^{-6}
	$^{48}Ca^{2+}$	2730	4×10^{-4}	2×10^{-5}
	$^{48}Ti^{2+}$	2170	6×10^{-5}	7×10^{-5}
$^{25}Mg^+$	$^{12}C^{13}C^+$	1430	8×10^{-5}	5×10^{-6}
	$^{12}C_2H^+$	1140		1×10^{-5}
	$^{23}NaH_2^+$	1280		1.5×10^{-4}
	$^{50}Ti^{2+}$	1860	3×10^{-5}	4×10^{-5}
	$^{50}Cr^{2+}$	1950	6×10^{-5}	1×10^{-6}
	$^{24}MgH^+$	3560	1×10^{-3}	4×10^{-4}
$^{26}Mg^+$	$^{13}C_2^+$	1080	8×10^{-5}	7×10^{-6}
	$^{12}C^{14}N^+$	1270		
	$^{12}C^{13}CH^+$	910		
	$^{12}C_2H_2^+$	790		
	$^{52}Cr^{2+}$	2110	5×10^{-4}	5×10^{-4}
	$^{25}MgH^+$	2350	3×10^{-4}	5×10^{-5}

* Resolving power necessary to resolve an interfering ionic species from the subject one.

Table 4.2 Hydride ion formation ratio in cases without and with a cold finger of liquid nitrogen aside the sample holder

Liq. N_2	$^{24}MgH^+/^{24}Mg^+$ (=x)	$^{24}MgH^+/^{25}Mg^+$
without	$\sim 4 \times 10^{-3}$	$\sim 3 \times 10^{-2}$
with	$< 5 \times 10^{-5}$	$< 4 \times 10^{-4}$

Table 4.3 Secondary ion formation ratios of $^{12}C_2^+/^{12}C^+$ and $(^{13}C_2^+ + ^{12}C^{14}N^+ + ^{12}C^{13}CH^+ + ^{12}C_2H_2^+)/^{12}C^+$ for five carbon-containing terrestrial samples

Sample	$^{12}C_2^+/^{12}C^+$	$Y^*/^{12}C^+$
Graphite	0.054	0.0013
Calcite	0.003	0.0001
Silicon carbide	0.016	0.0004
Dolomite	$\sim$0	$\sim$0
Charcoal	0.040	0.0010

* $Y=(^{13}C_2^+ + ^{12}C^{14}N^+ + ^{12}C^{13}CH^+ + ^{12}C_2H_2^+)$

Table 4.4 Concentrations of Mg, Al and Si in four mineral samples determined by atomic absorption analysis (wt.%) and chemical formulae of the minerals

Sample	Mg	Al	Si	Chemical formula
Forsterite	31.1	0.2	16.9	Mg_2SiO_4
Hornblende	6.2	7.3	18.4	$(Ca,Na)_{2-3}(Mg,Fe,Al)_5[OH\cdot(Si,Al)_4O_{11}]_2$
Vesuvianite	2.7	8.0	15.4	$Ca_{10}(Mg,Fe)_2Al_4[(OH)_4\cdot(SiO_4)_5\cdot(Si_2O_7)_2]$
Cordierite	1.3	13.3	20.2	$Mg_2Al_3[AlSi_5O_{18}]$

Table 4.5 Isotopic ratios of magnesium obtained for the sample of terrestrial forsterite (FO) and used as the reference values

	Home-made	Hitachi IMA 2A
$^{25}Mg/^{24}Mg$	0.12495	0.12472
$^{26}Mg/^{24}Mg$	0.13666	0.13560
$^{24}Mg/^{25}Mg$	8.0032	8.0178
$^{26}Mg/^{25}Mg$	1.0937	1.0872

Table 5.1 $^{26}Al/^{27}Al$ ratio at the time of nucleosynthesis, $(^{26}Al/^{27}Al)_o$, based on theoretical invesitgations

$(^{26}Al/^{27}Al)_o$	Reference
1.2×10^{-3}	R.A. Fish et al. (1960)[5]
3.3×10^{-4}	W.A. Fowler et al. (1962)[2]
6.6×10^{-6}	H. Reeves and J. Audouze (1968)[6]
9.0×10^{-4}	W.D. Arnett (1969)[37]
1.3×10^{-3}	W.D. Arnett (1969)[37]
$0.4\text{-}2.0 \times 10^{-3}$	J.W. Truran and A.G.W. Cameron (1978)[48]
$1\ \text{-}2\ \times 10^{-3}$	W.D. Arnett and J.P. Wefel (1978)[49]

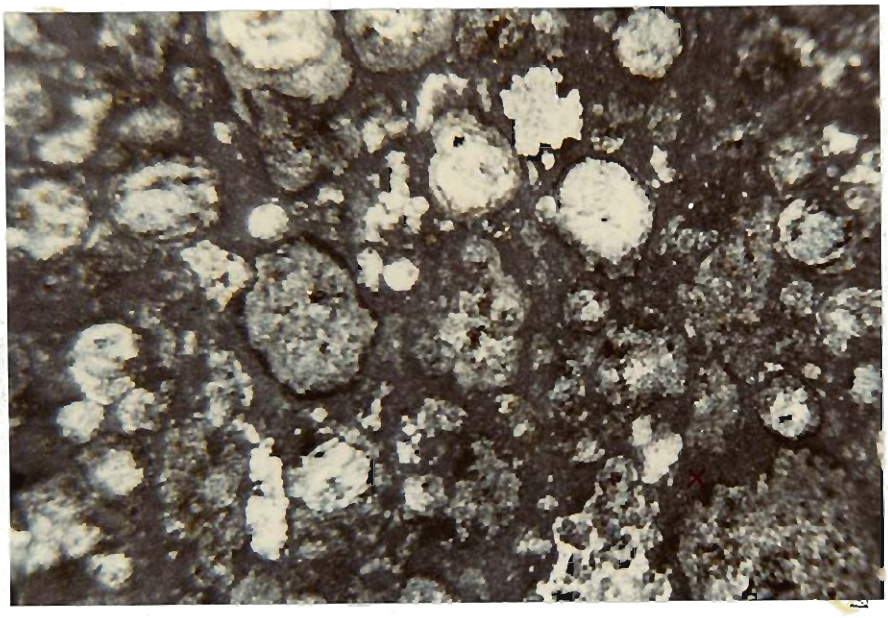

Fig. 2.1 Photomicrograph of a cut surface of the Allende carboanceous chondrite.

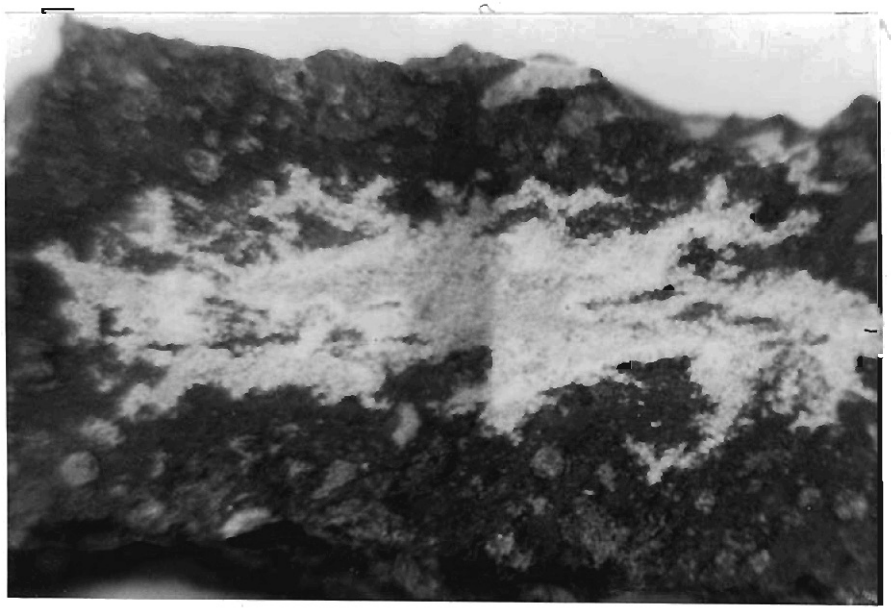

1 mm

Fig. 2.2 Photomicrograph of a cut surface of Allende including an amoeboid whitish inclusion.

1 mm

Fig. 2.3 Photomicrograph of a cut surface of Allende including a chondrule-like white inclusion surrounded by ring-shaped boundary layer.

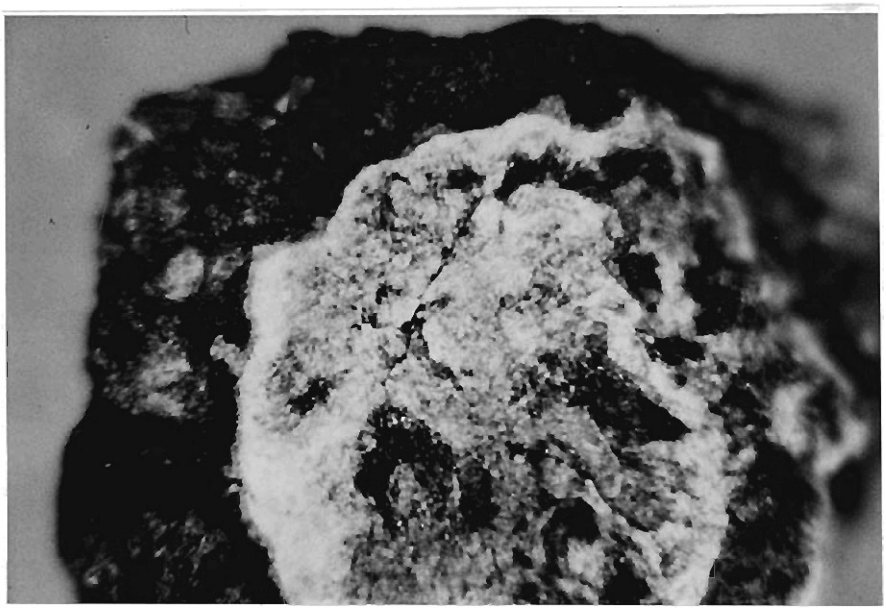

1 mm

Fig. 2.4 Photomicrograph of a cut surface of Allende including a large white inclusion.

1 mm

Fig. 2.5 Photomicrograph of a cut surface of Yamato-74191 (L3) chondrite.

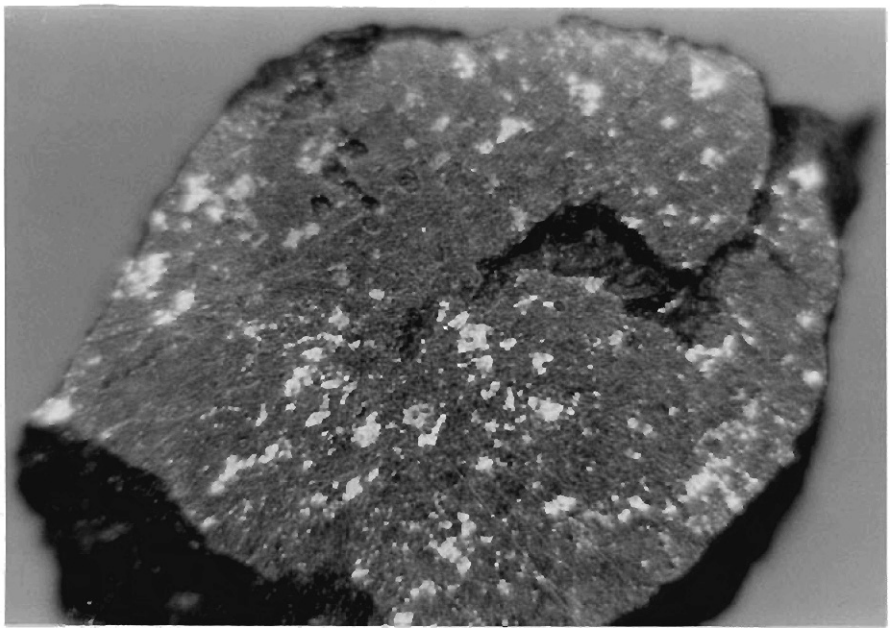

Fig. 2.6 Photomicrograph of a cut surface of Yamato-75028 brecciated chondrite. H3 part is taken in this picture.

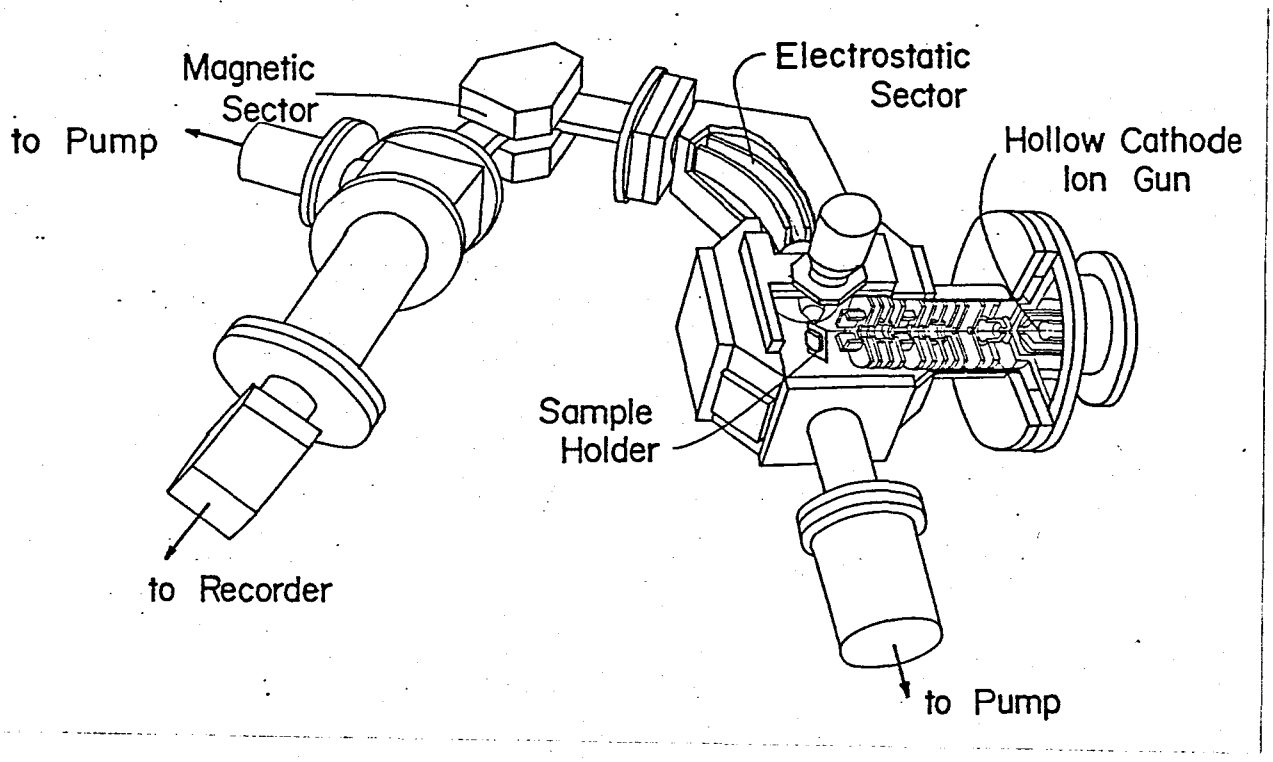

Fig. 3.1 Schematic diagram of a home-made ion microprobe mass analyzer.

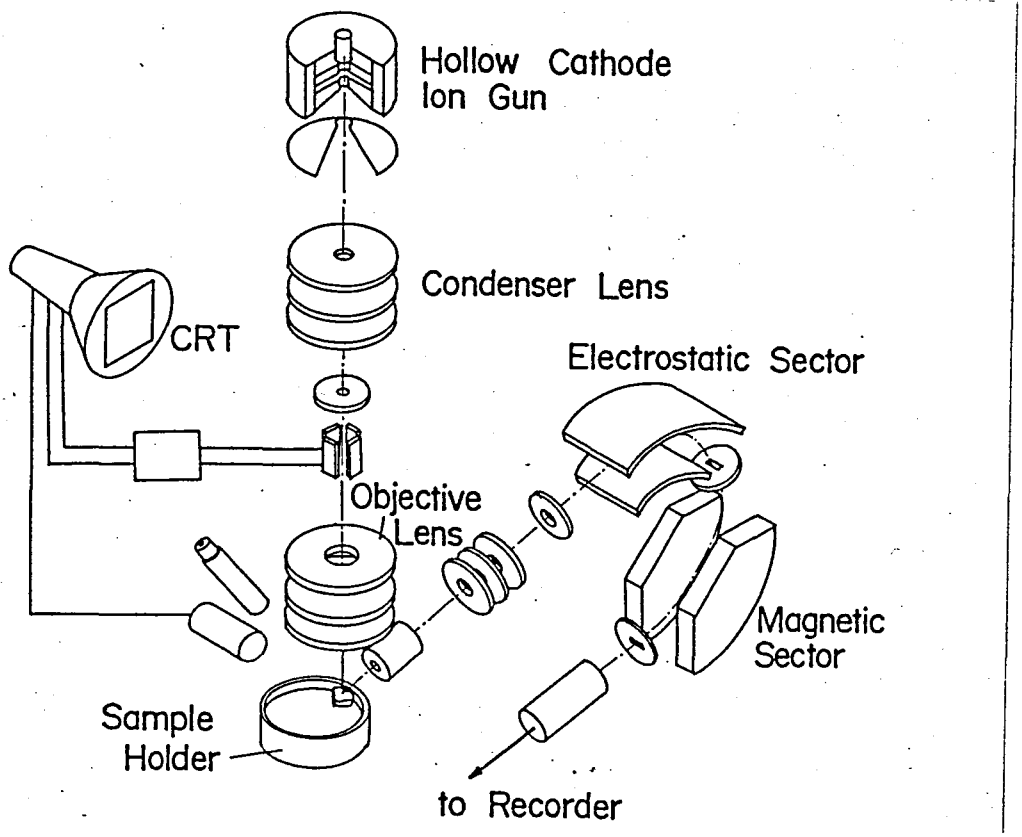

Fig. 3.2 Schematic diagram of a Hitachi IMA 2A ion microprobe mass analyzer.

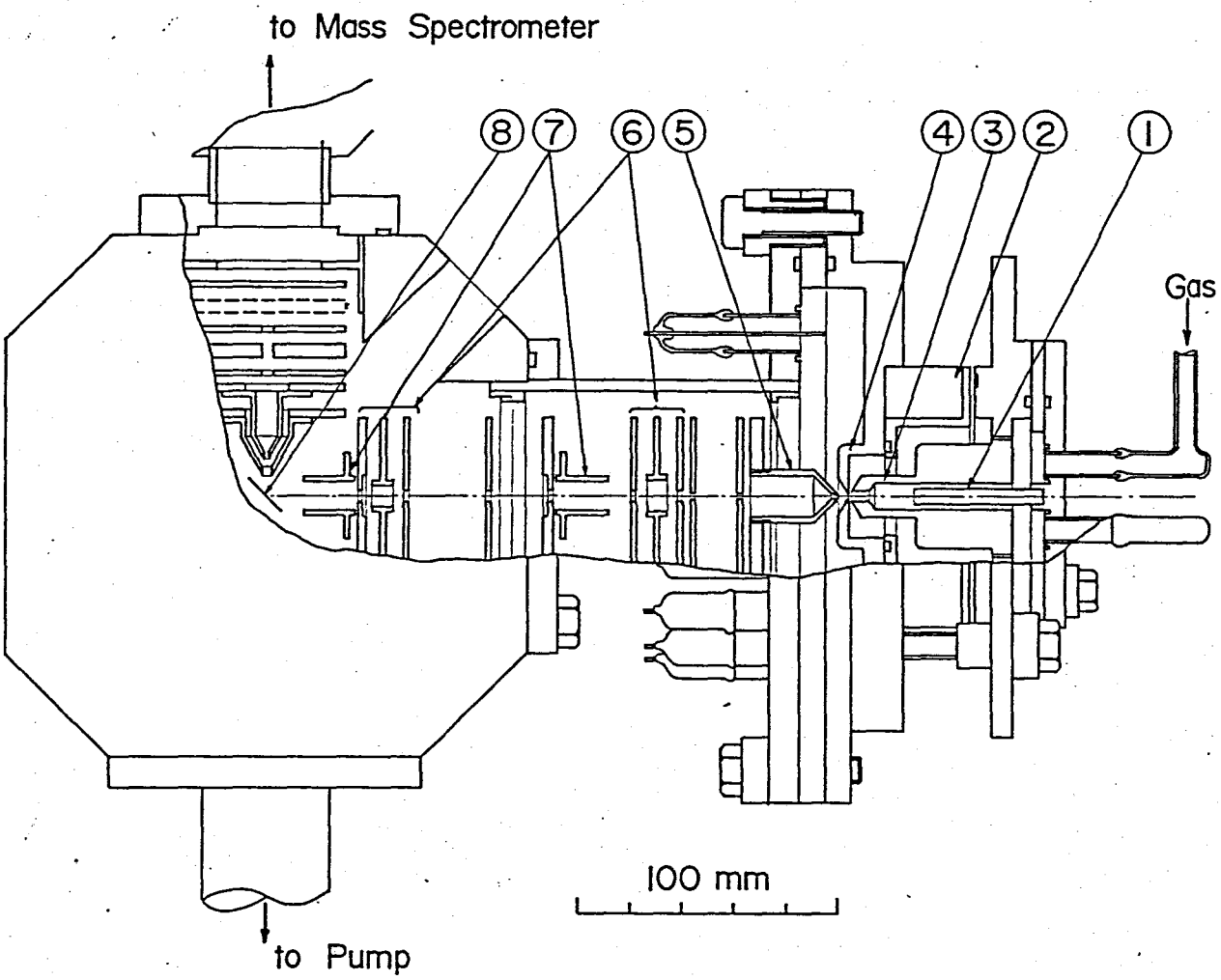

Fig. 3.3 Schematic diagram of a primary ion gun and accelerating and focusing system for the primary ion beam and for the secondary ions.

① hollow cathode
② ferrite parmanent magnet
③ intermediate electrode
④ anode
⑤ drawing out and accelerating electrode
⑥ Einzel lens
⑦ deflector
⑧ sample holder

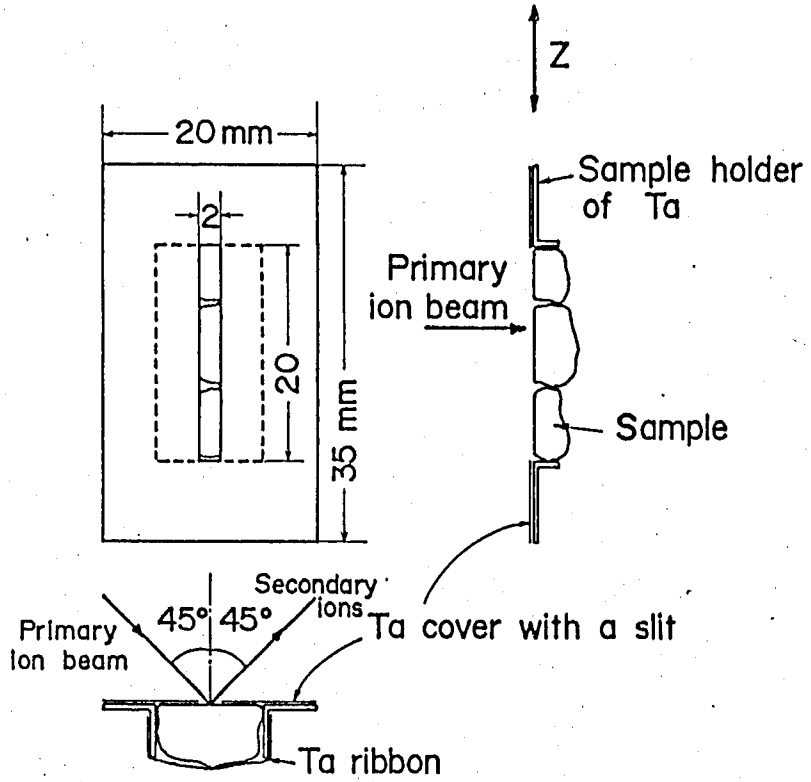

Fig. 3.4 Sample mounting system of the home-made apparatus. This is movable in the Z direction.

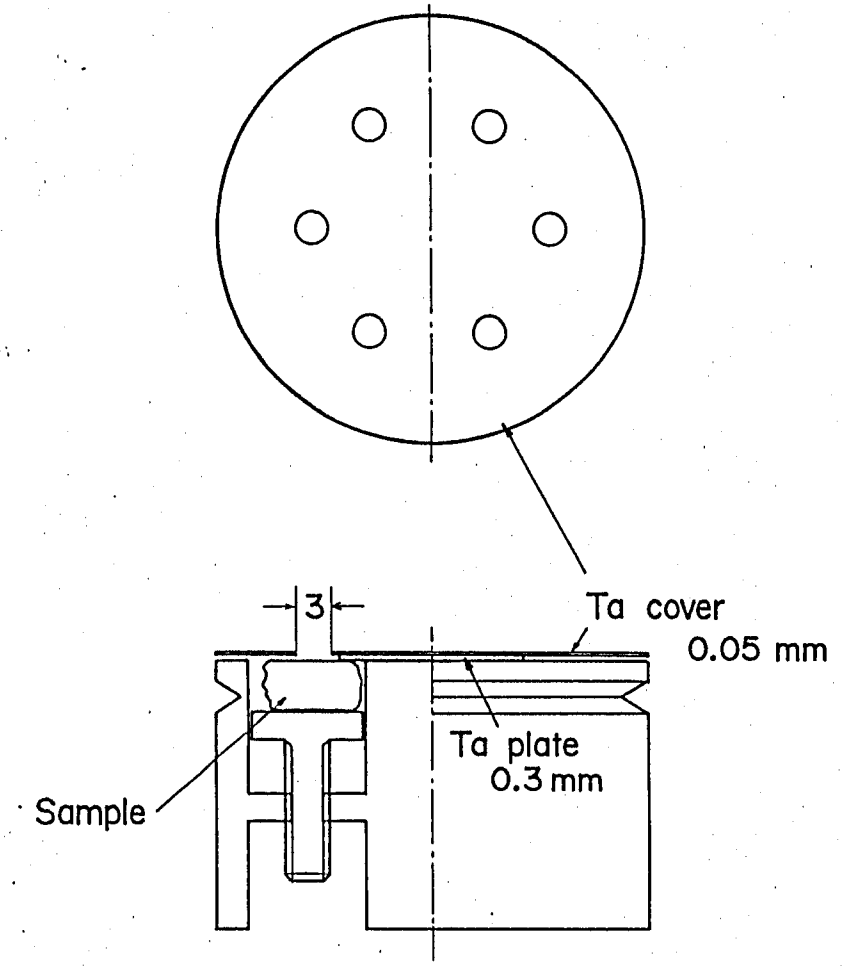

Fig. 3.5 Sample mounting system of the Hitachi IMA 2A apparatus.

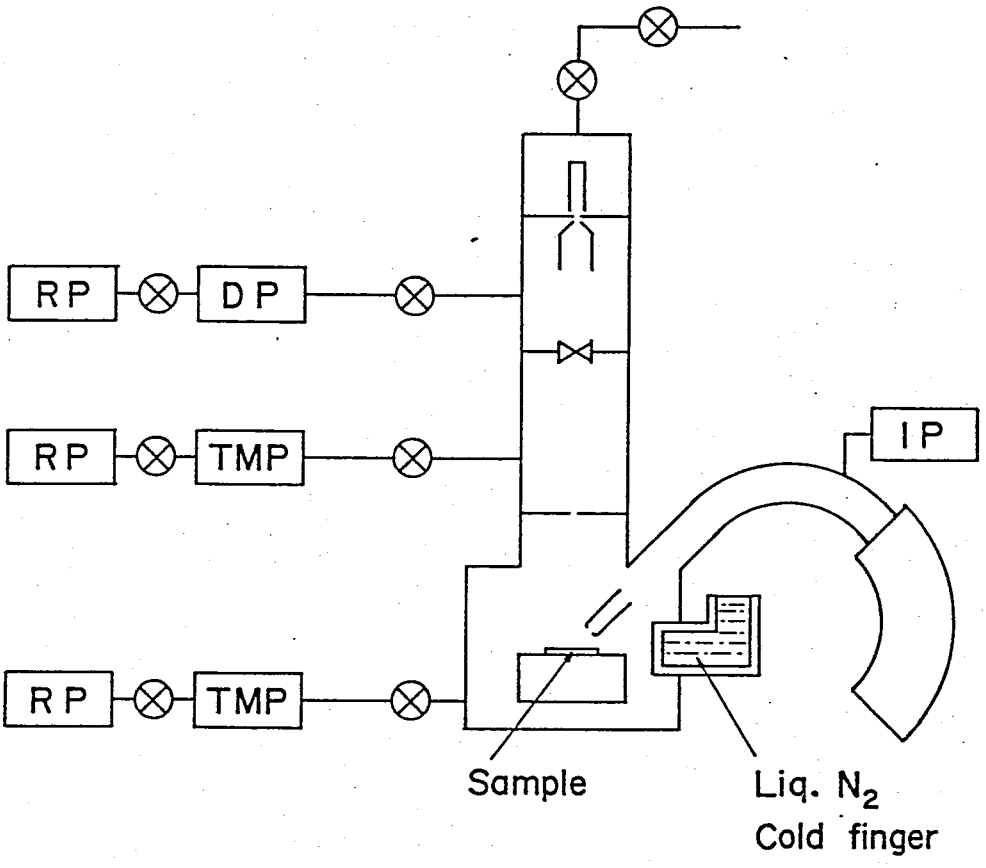

Fig. 3.6 Schematic diagram of the installation of a cold finger of liquid nitrogen, and pumping systems.
RP: Oil rotary pump, DP: Oil diffusion pump, TMP: Turbo-molecular pump, IP: Ion pump

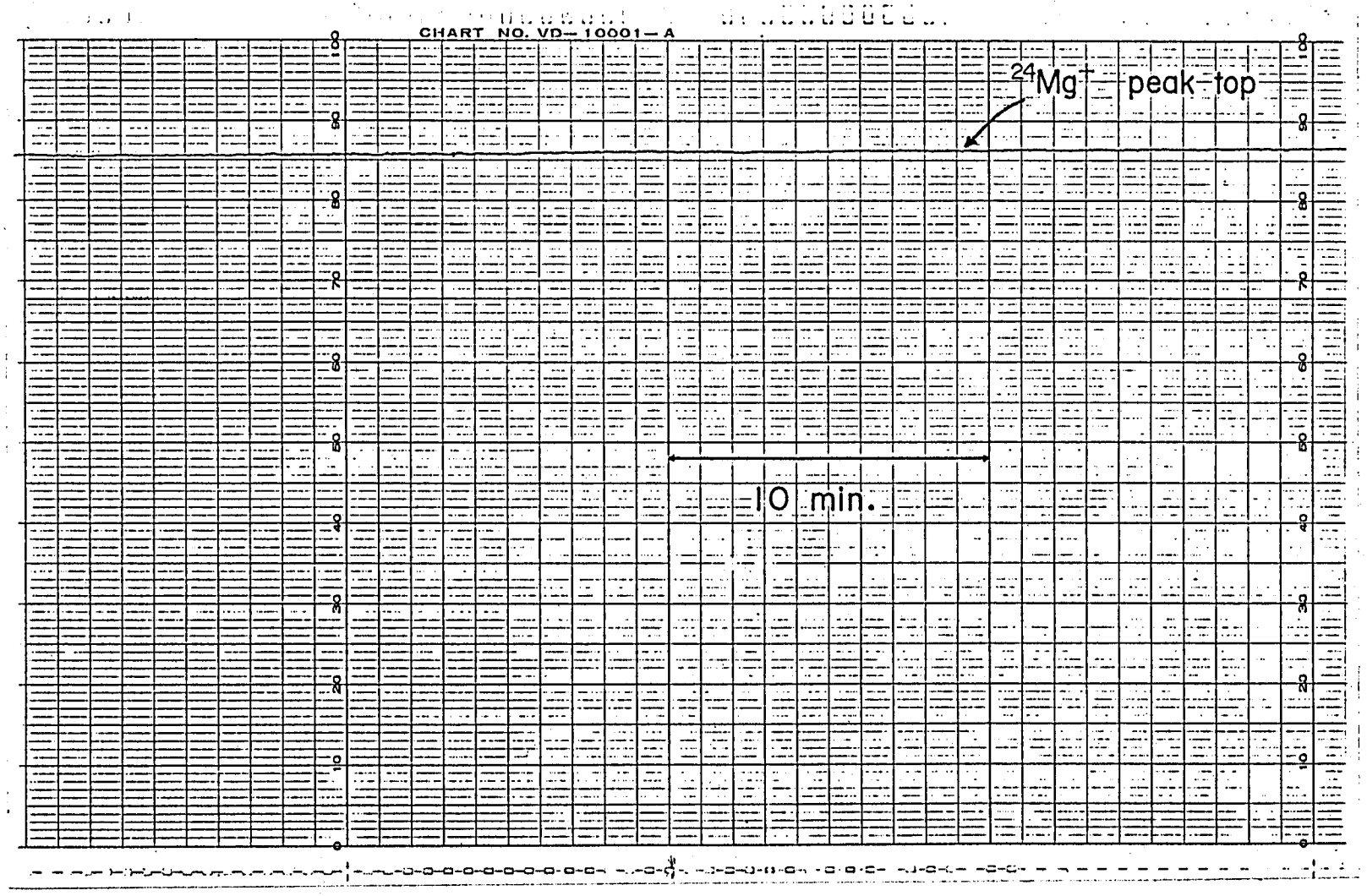

Fig. 3.7 Chart recording the peak top of $^{24}Mg^{+}$ for a terrestrial forsterite sample. This shows the stability of secondary ion current.

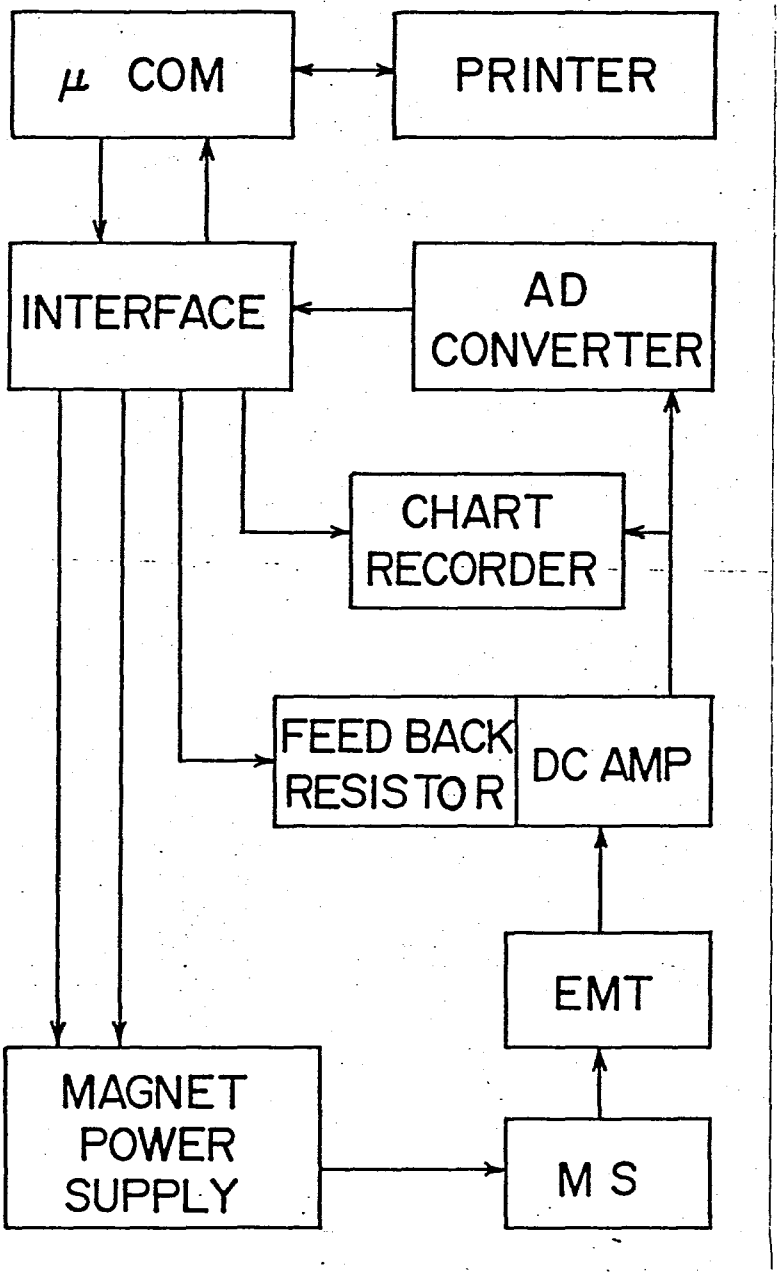

Fig. 3.8 Block diagram of a controlling system using a microcomputer.

μCOM: microcomputer with 8080AFC as CPU

EMT: secondary electron multiplier

MS: mass spectrometer

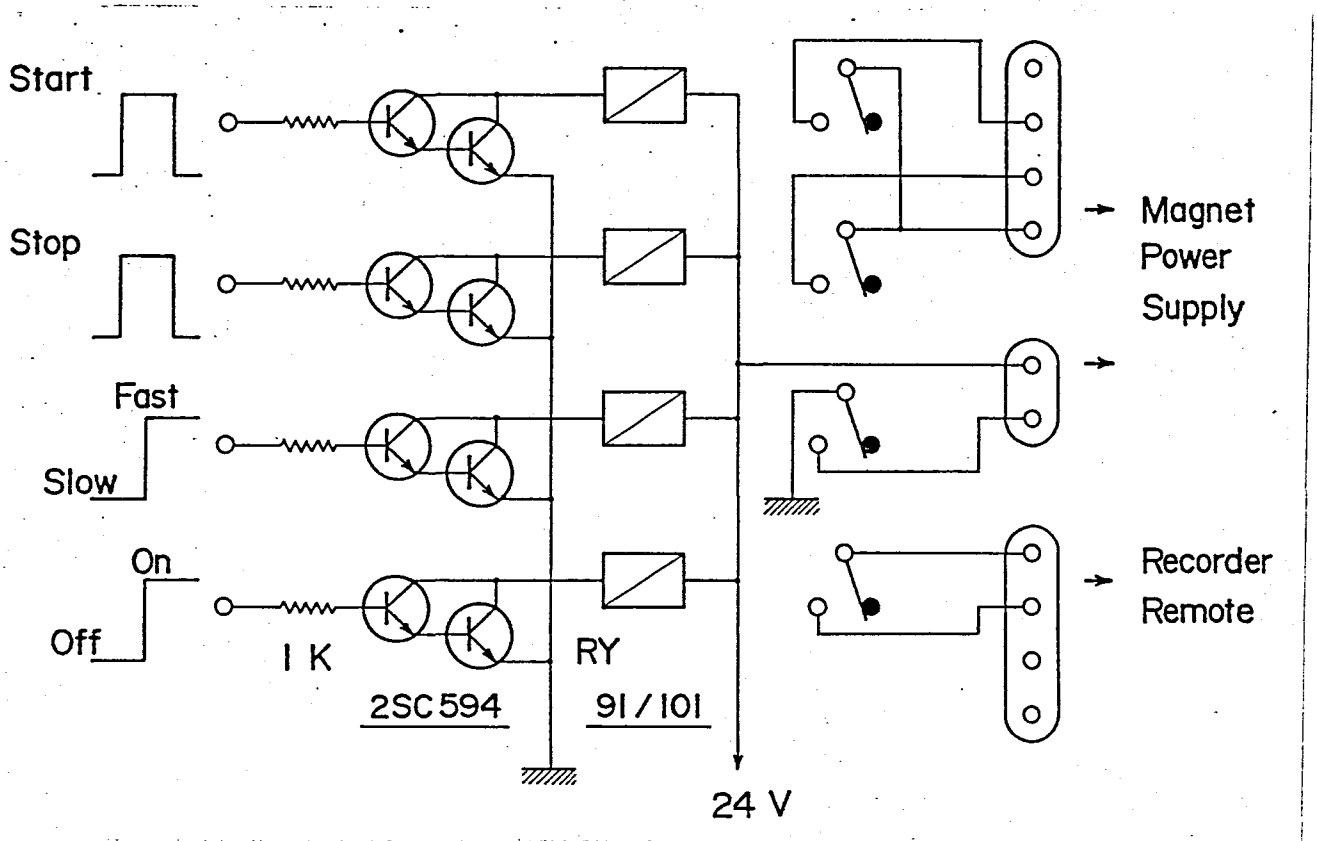

Fig. 3.9 Interfaces for a magnet power supply and a chart recorder.

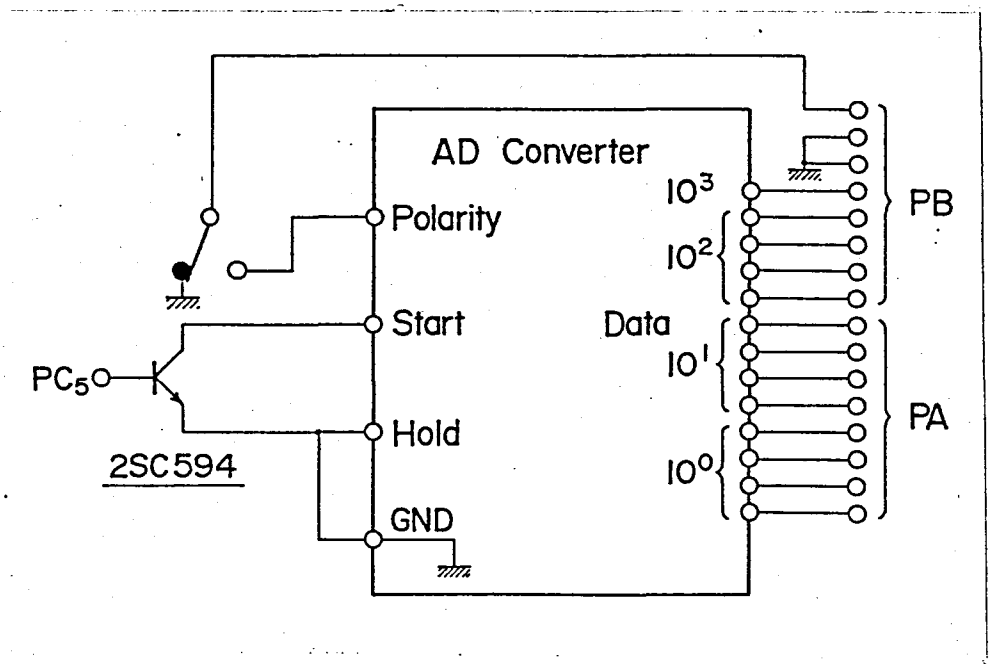

Fig. 3.10 Diagram of connections between an AD converter and a microcomputer.

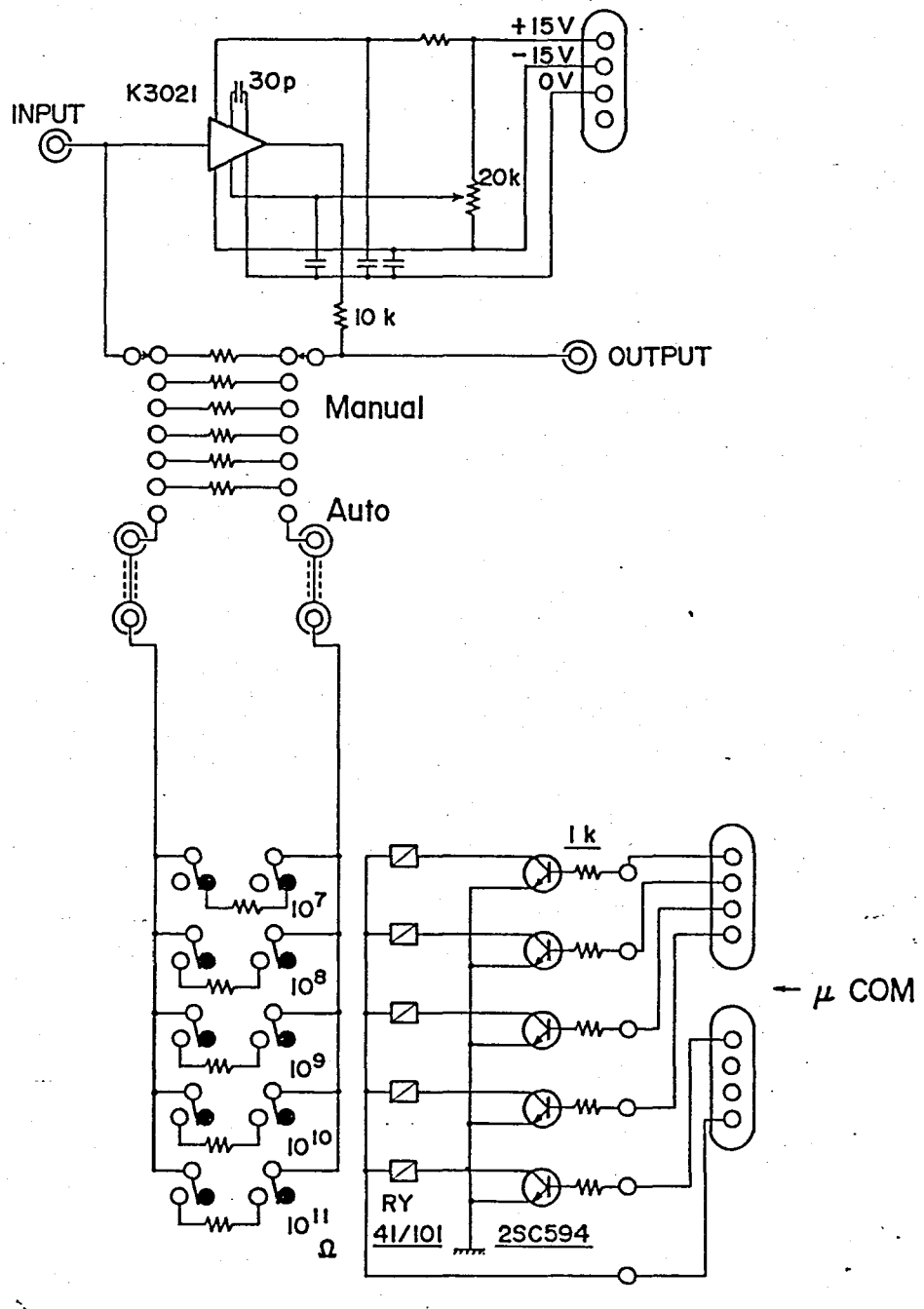

Fig. 3.11 Circuit for switching sensitivities of detecting system by switching a feed back resistor of an amplifier (K3021).

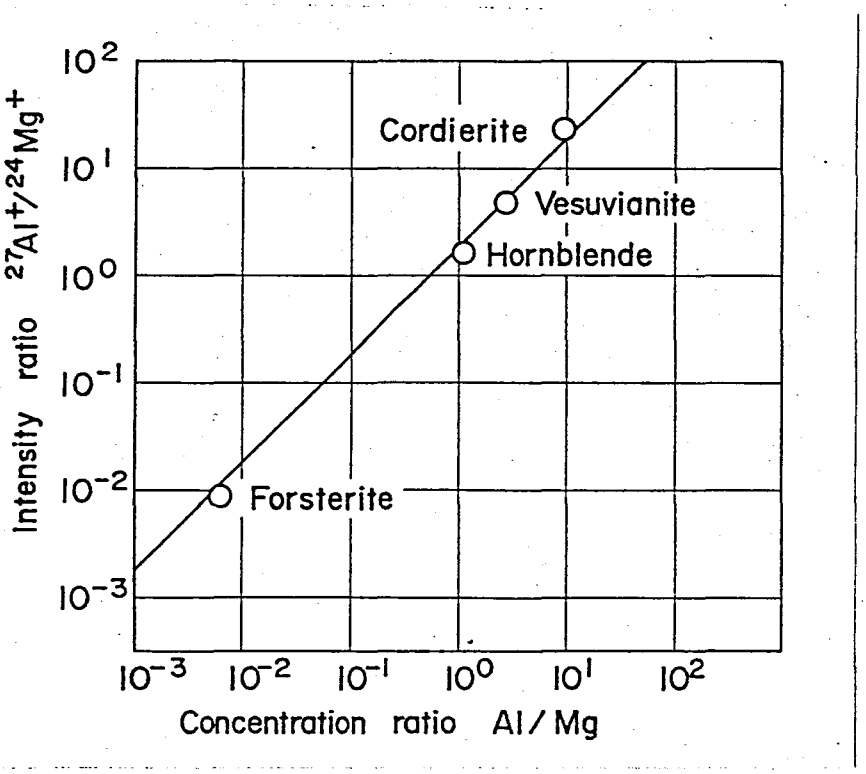

Fig. 4.1 Calibration curve for Al/Mg ratio. Elemental concentration was measured by atomic absorption analysis. The localities and the chemical formulae of the minerals are shown in Tables 2.2 and 4.4.

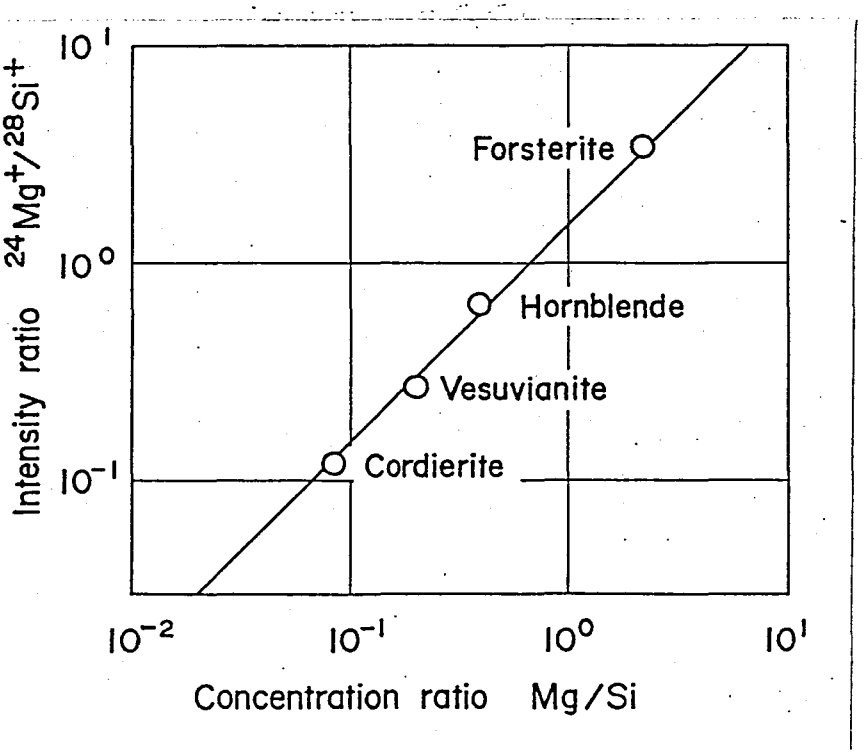

Fig. 4.2 Calibration curve for Mg/Si ratio. Elemental concentration was measured by atomic absorption analysis. The localities and the chemical formulae of the minerals are shown in Tables 2.2 and 4.4.

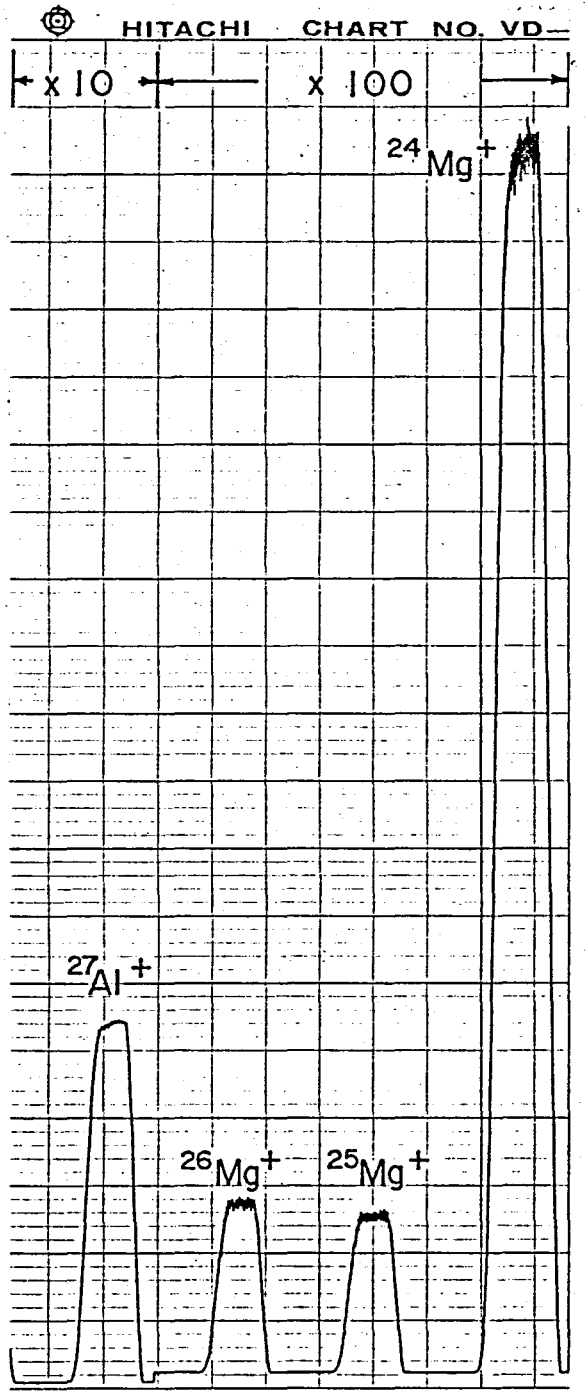

Fig. 4.3 Mass spectrum obtained for the white inclusion AL2 with the home-made apparatus. The sensitivities are shown in the upper part.

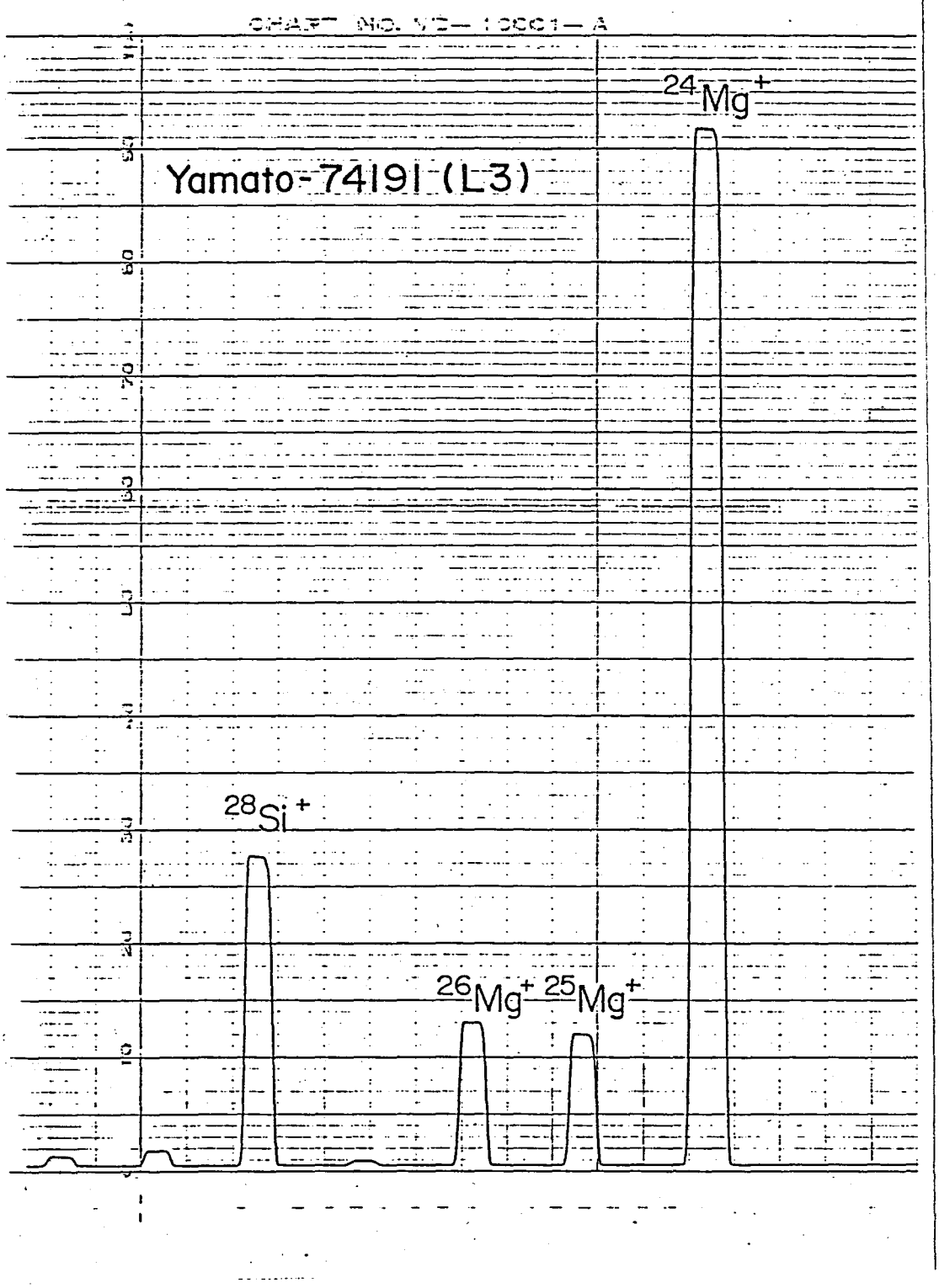

Fig. 4.4 Mass spectrum obtained for a portion of the matrix of Yamato-74191 chondrite with the Hitachi IMA 2A apparatus.

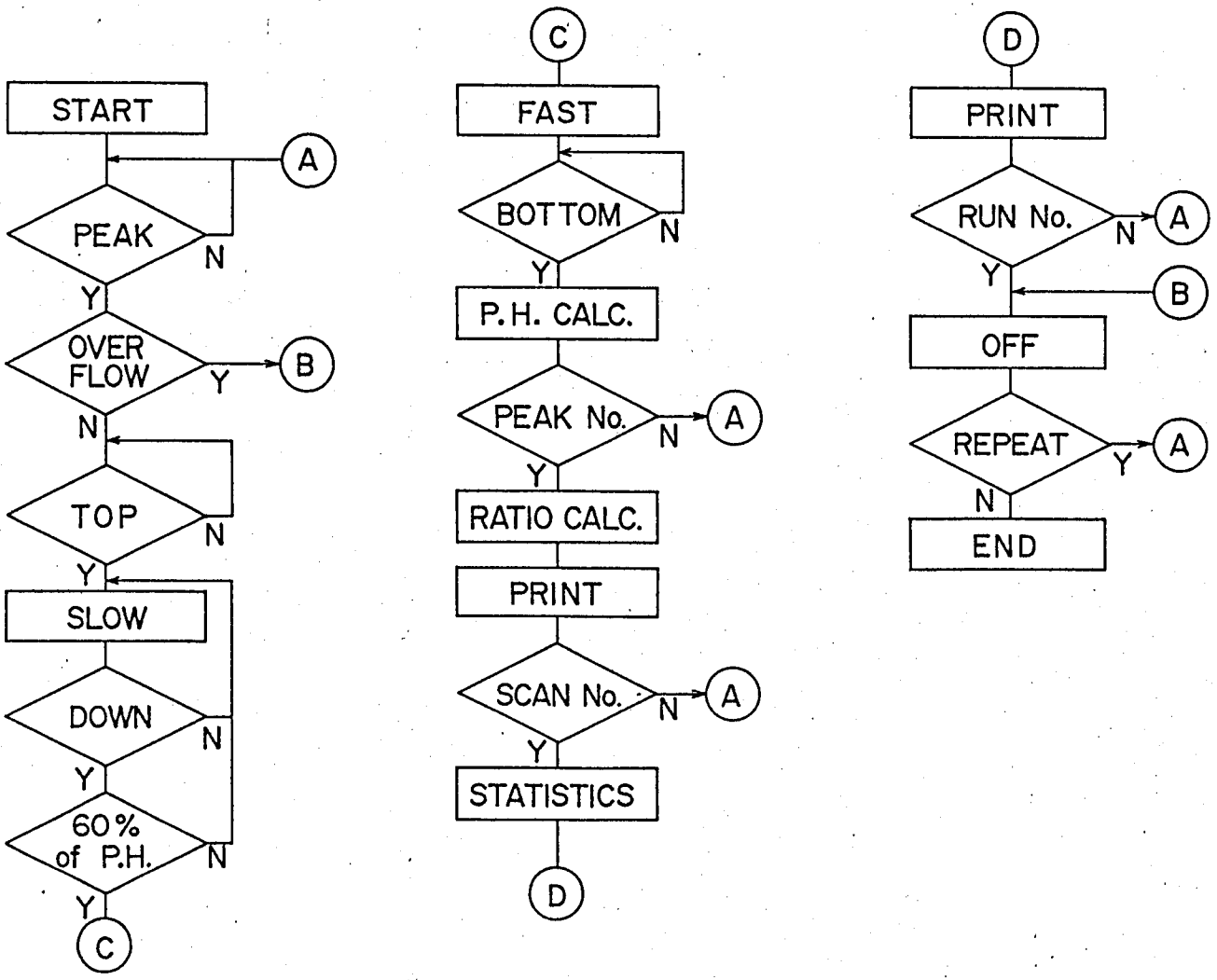

Fig. 4.5 Flow chart of obtaining isotopic ratios by using a microcomputer.

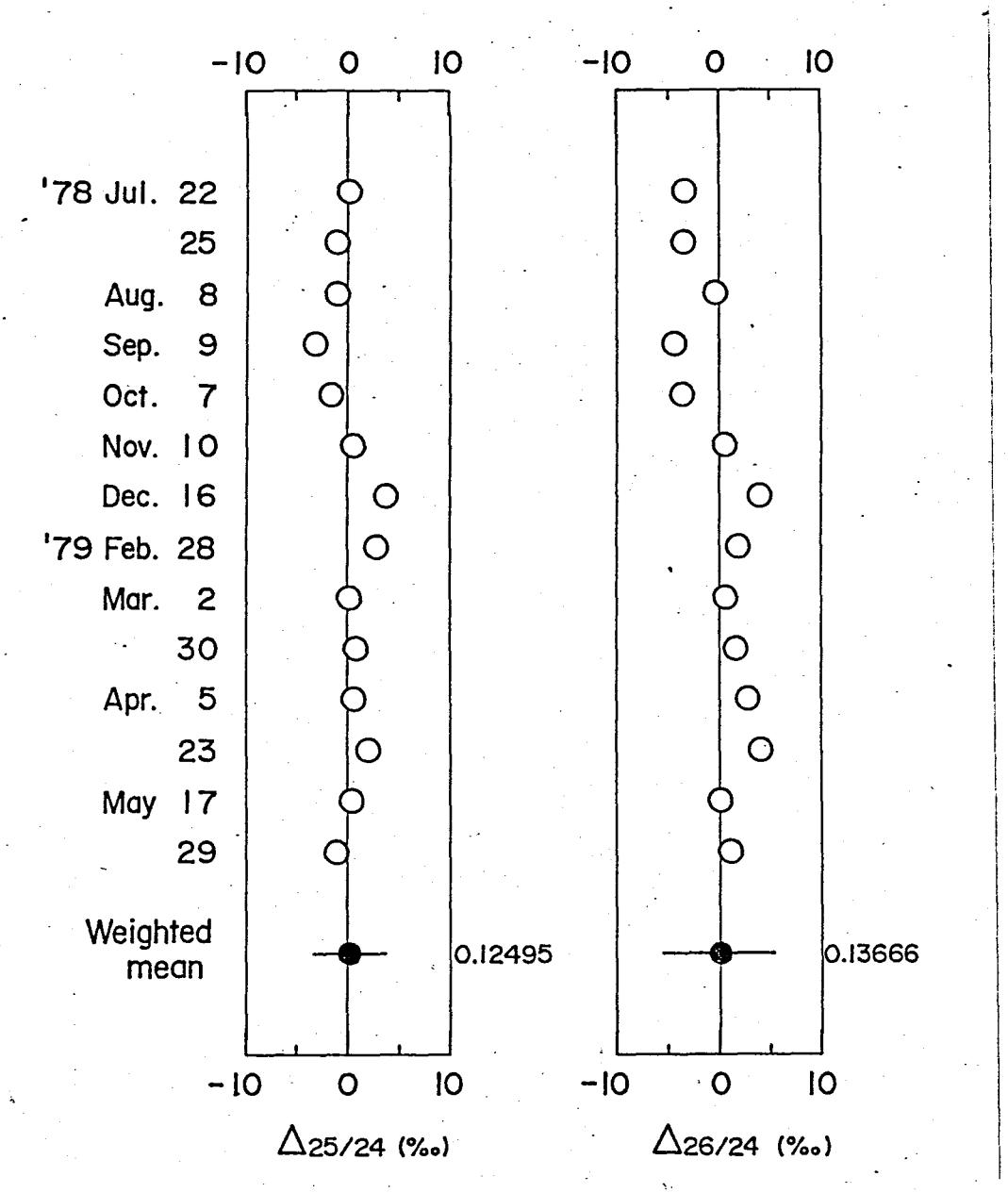

Fig. 4.6 Δ values obtained for the laboratory standard sample of terrestrial forsterite (FO). These data are plotted in the chronological order. The definition of Δ appears in the text. Values aside the closed circles are the weighted means of all these data, and these values were used as reference values in evaluating Δ values. Error bars for the closed circles represent twice the standard deviations.

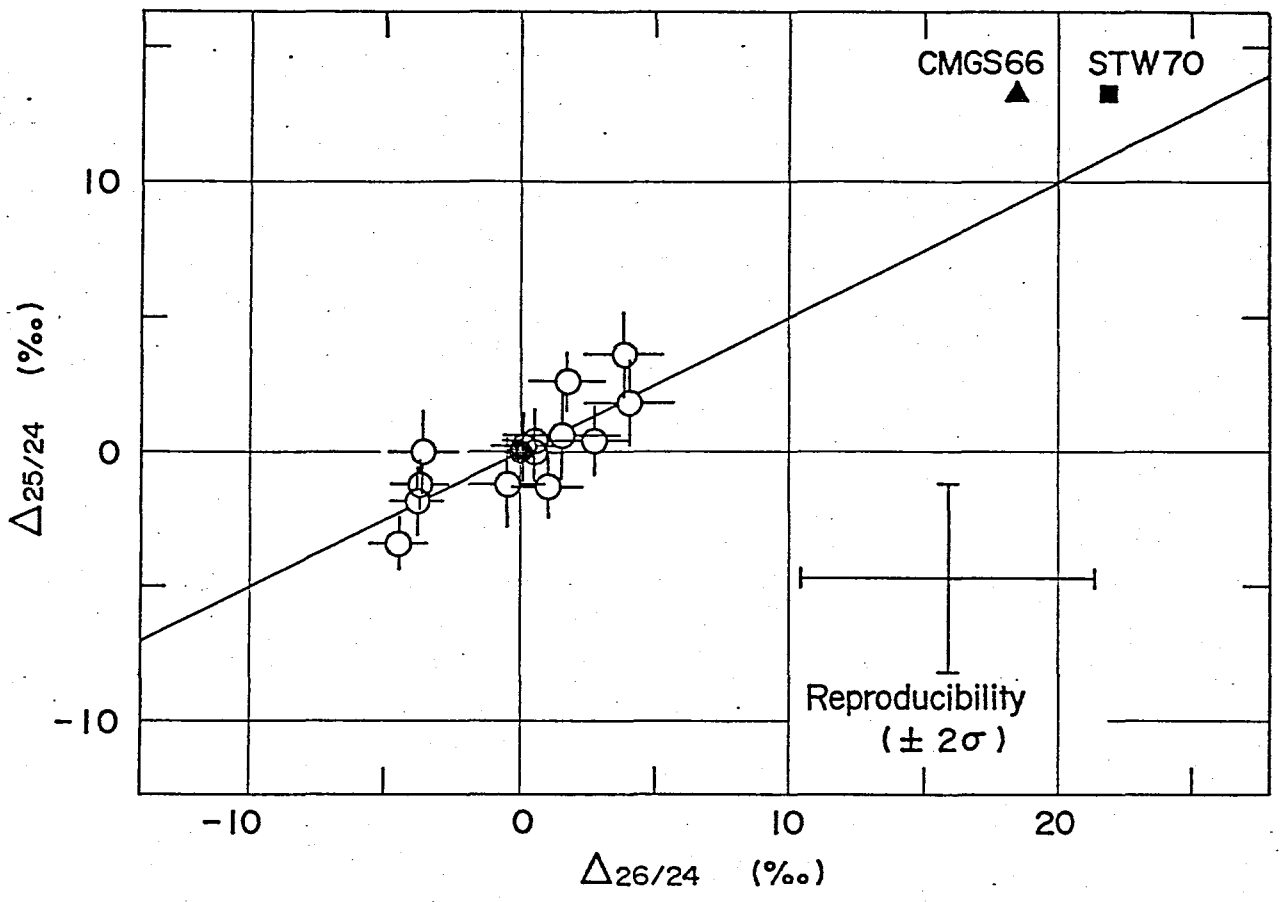

Fig. 4.7 Three isotope plot of the data for the terrestrial forsterite (FO). A straight line with the slope of 1/2 corresponds to the normal mass fractionation line. The absolute abundance ratios reported by Catanzaro et al. (CMGS 66) and Schramm et al. (STW 70) are also marked.

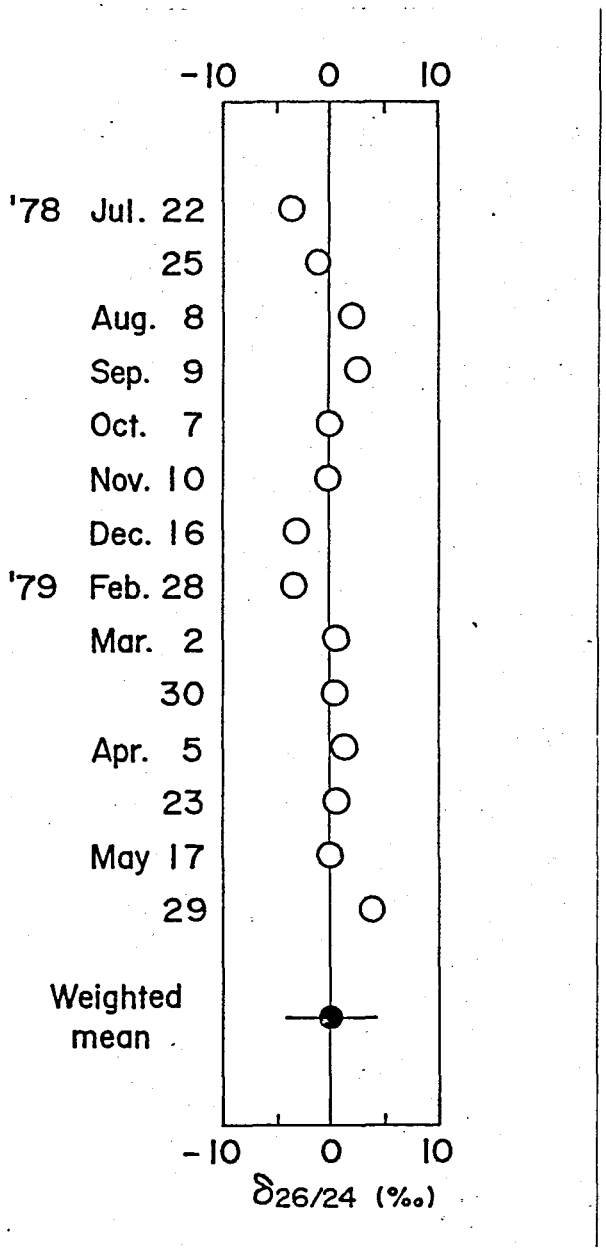

Fig. 4.8 Deviations, $\delta_{26/24}$, after the correction for the normal mass fractionation. These were obtained for the FO sample. The definition of $\delta_{26/24}$ appears in the text. These are plotted in the chronological order. The error bar for the closed circle represents the reproducibility.

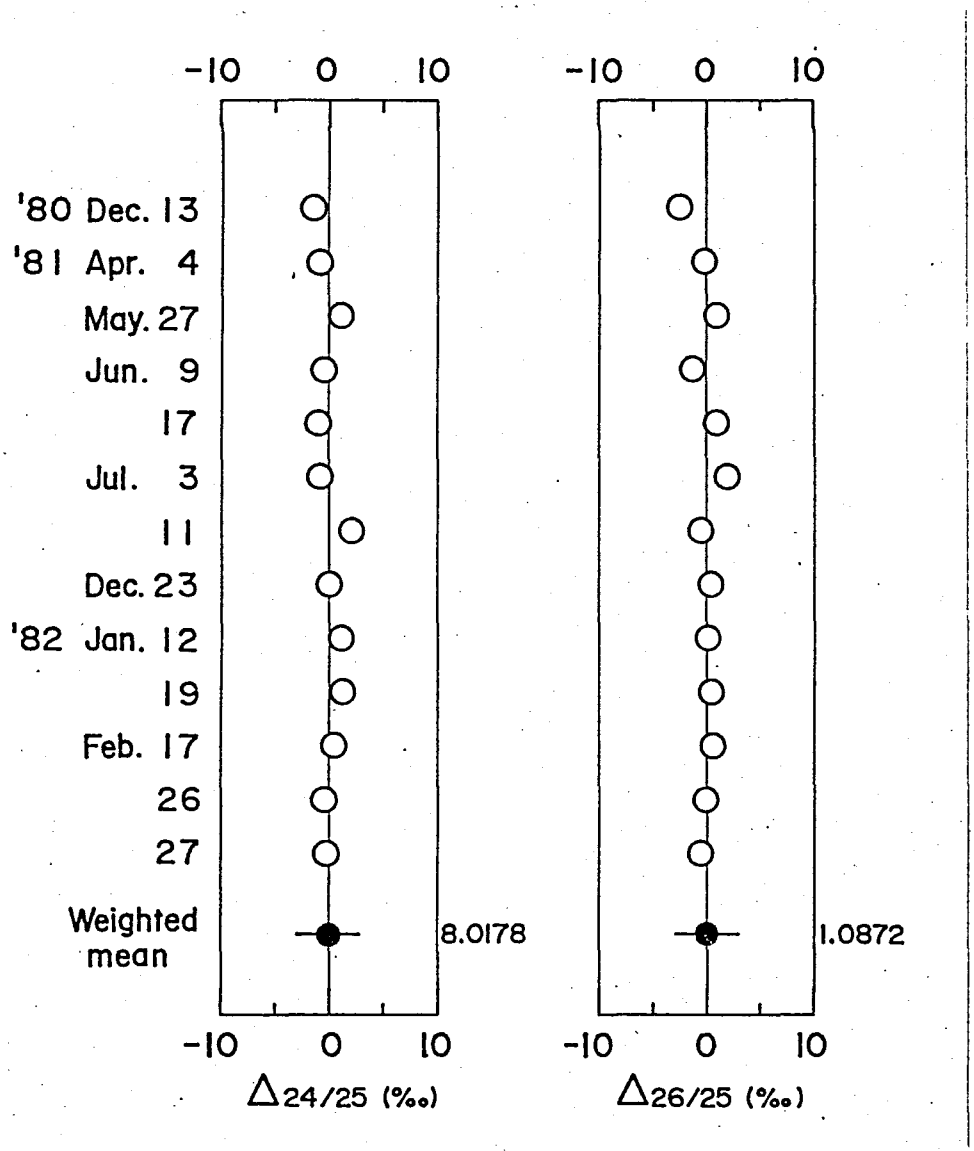

Fig. 4.9 Δ values for the FO sample. These data are plotted in the chronological order. The definition of Δ appears in the text. Values aside the closed circles are the weighted mean values of all these data, and these values were used as reference values in evaluating Δ values. Error bars for the closed circles represent twice the standard deviations.

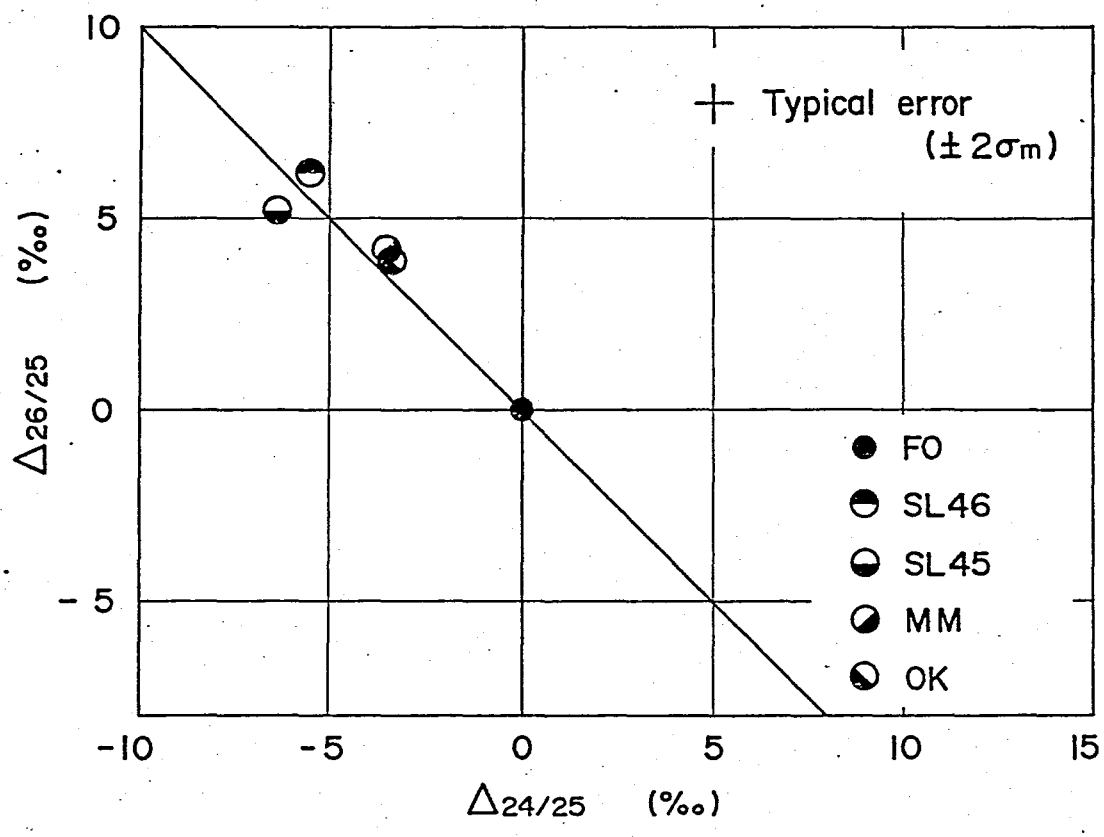

Fig. 4.10 Three isotope plot of magnesium obtained for four terrestrial olivines. These were analyzed as sub-standards. FO: forsterite (Ehime Pref.), SL46: olivine (Hawaii) SL45: olivine (Hawaii), MM: olivine (Antarctica) OK: olivine (Oki Island)

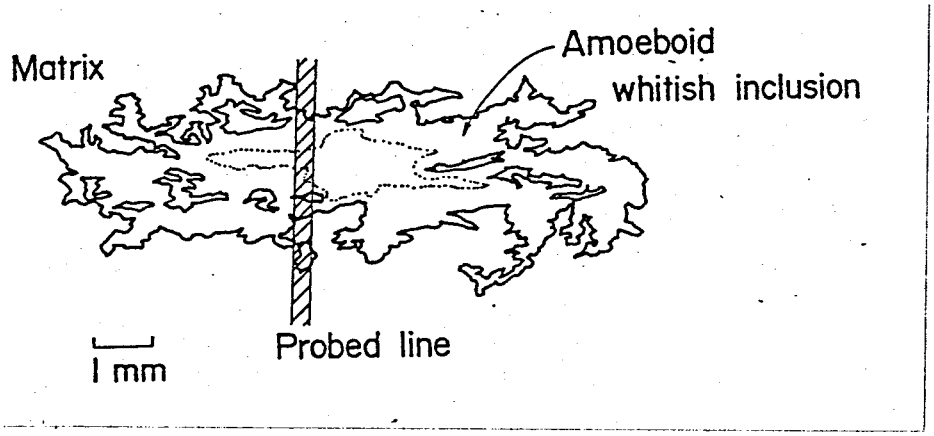

Fig. 4.11 Sketch of the amoeboid whitish inclusion in AL0.

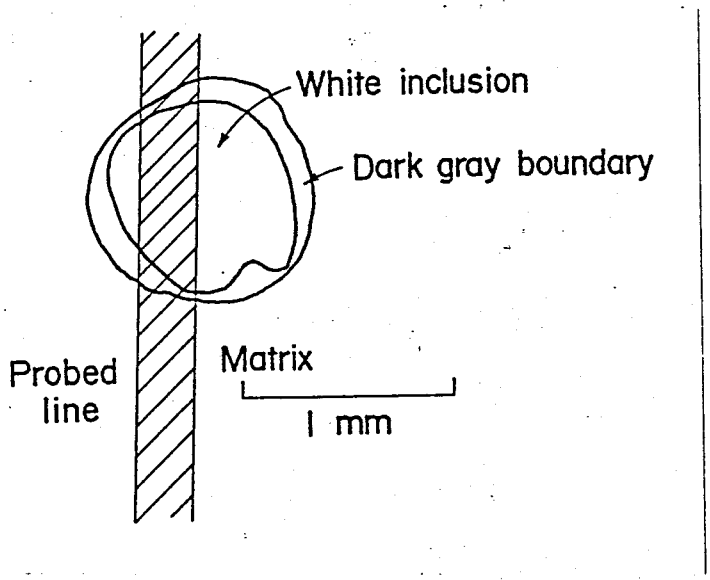

Fig. 4.12 Sketch of the chondrule-like white inclusion in AL1.

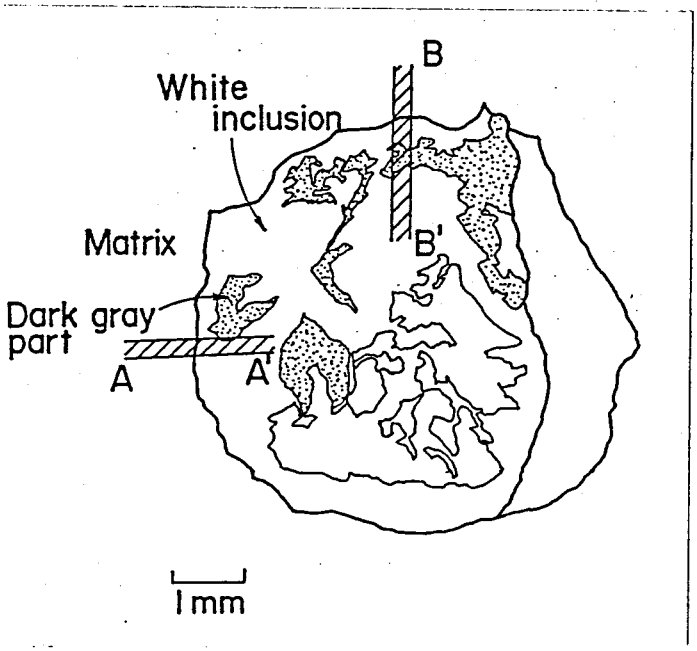

Fig. 4.13 Sketch of the comparatively large white inclusion in AL2.

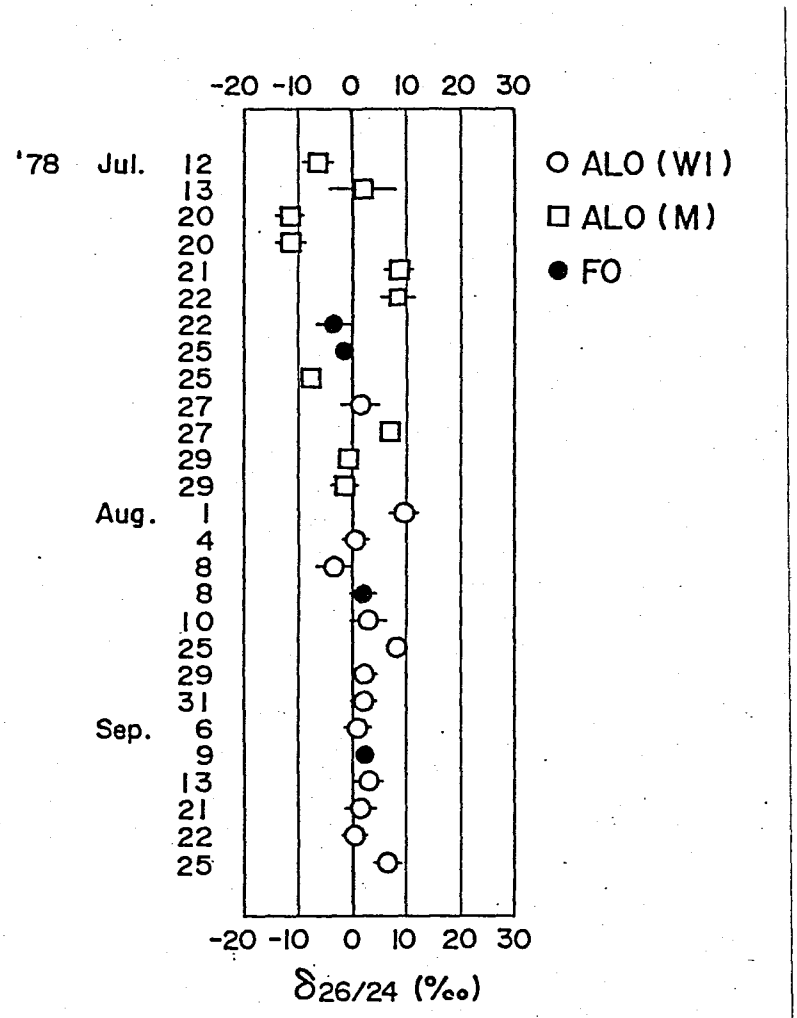

Fig. 5.1 $\delta_{26/24}$ values obtained for ALO including the amoeboid whitish inclusion. The definition of $\delta_{26/24}$ appears in the text.

ALO(WI): whitish inclusion in ALO

ALO(M): matrix in ALO

FO: terrestrial forsterite (laboratory standard)

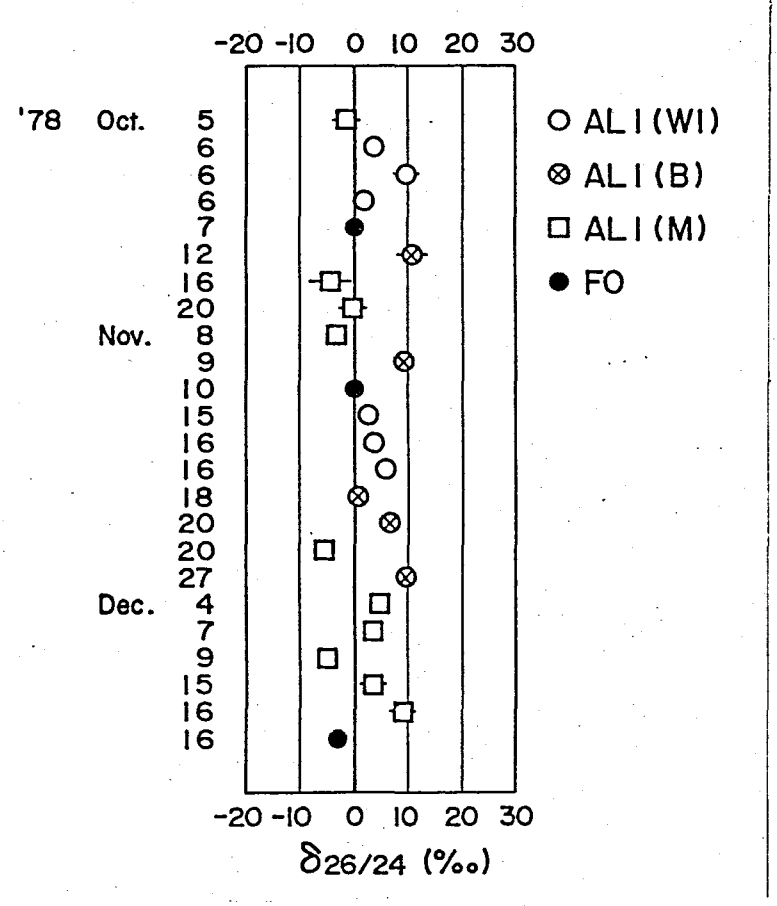

Fig. 5.2 $\delta_{26/24}$ values obtained for AL1 including the chondrule-like white inclusion surrounded by the boundary layer. The definition of the $\delta_{26/24}$ appears in the text.

AL1(WI): white inclusion in AL1

AL1(B): boundary layer surrounding the inclusion in AL1

AL1(M): matrix in AL1

FO: terrestrial forsterite (laboratory standard)

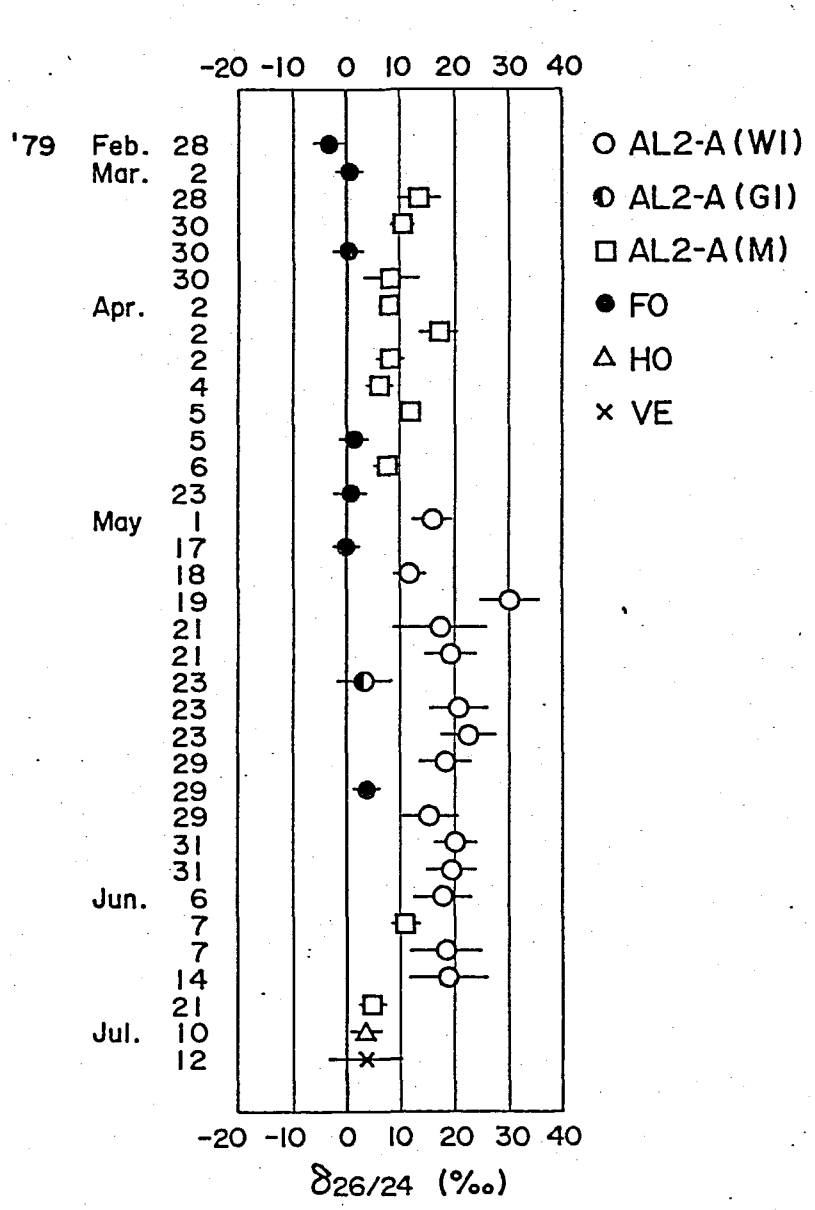

Fig. 5.3 $\delta_{26/24}$ values obtained for AL2 including the large white inclusion. The definition of $\delta_{26/24}$ appears in the text.

AL2-A(WI): white inclusion in AL2 (analysis along AA')

AL2-A(GI): dark gray part in AL2

AL2-A(M): matrix in AL2

FO: terrestrial forsterite (laboratory standard)

HO: terrestrial hornblende, VE: terrestrial vesuvianite

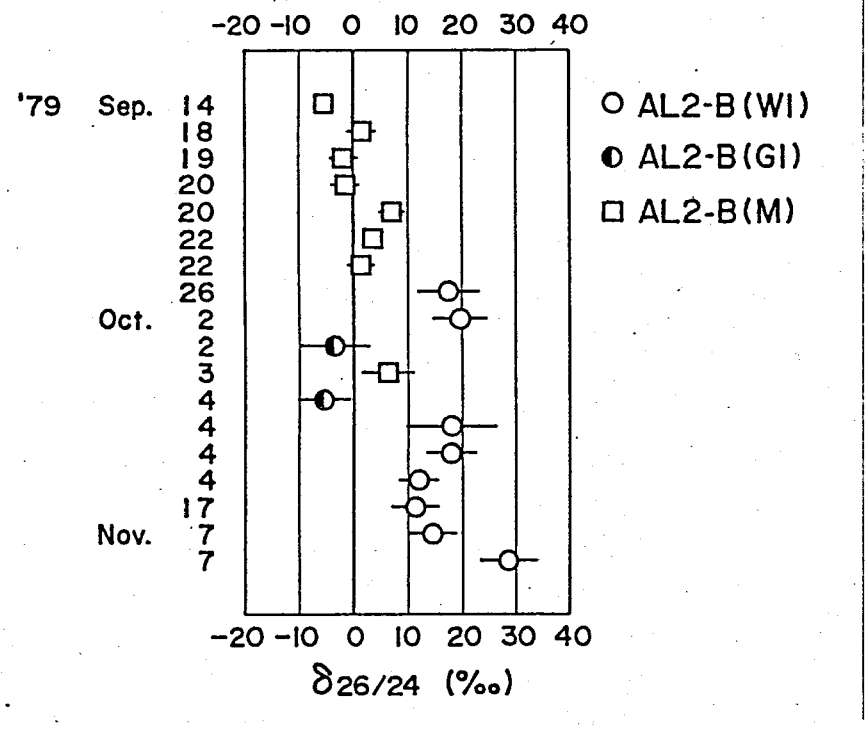

Fig 5.4 $\delta_{26/24}$ values obtained for AL2 including the large white inclusion. The definition of $\delta_{26/24}$ appears in the text.

AL2-B(WI): white inclusion in AL2 (analysis along BB')

AL2-B(GI): dark gray part in AL2

AL2-B(M): matrix in AL2

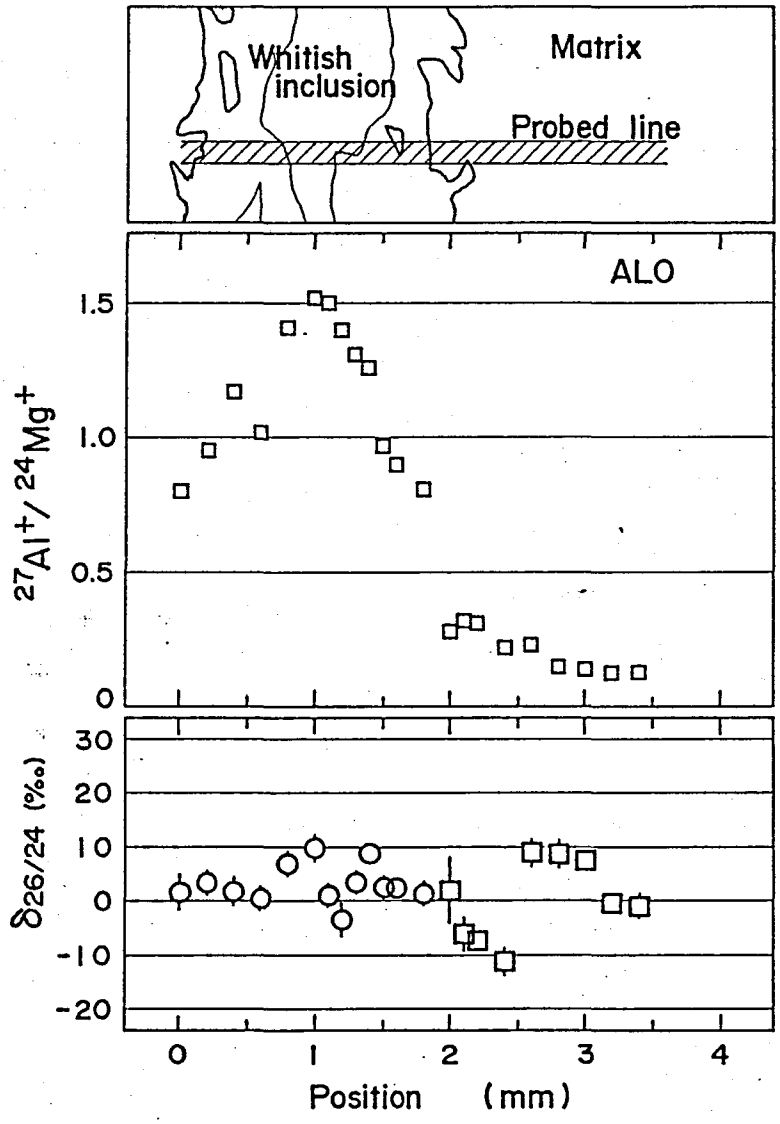

Fig. 5.5 $\delta_{26/24}$ and $^{27}Al^+/^{24}Mg^+$ as a function of probed position along the probed line for the AL0. Symbols for the plot of $\delta_{26/24}$ are the same as shown in Fig.5.1.

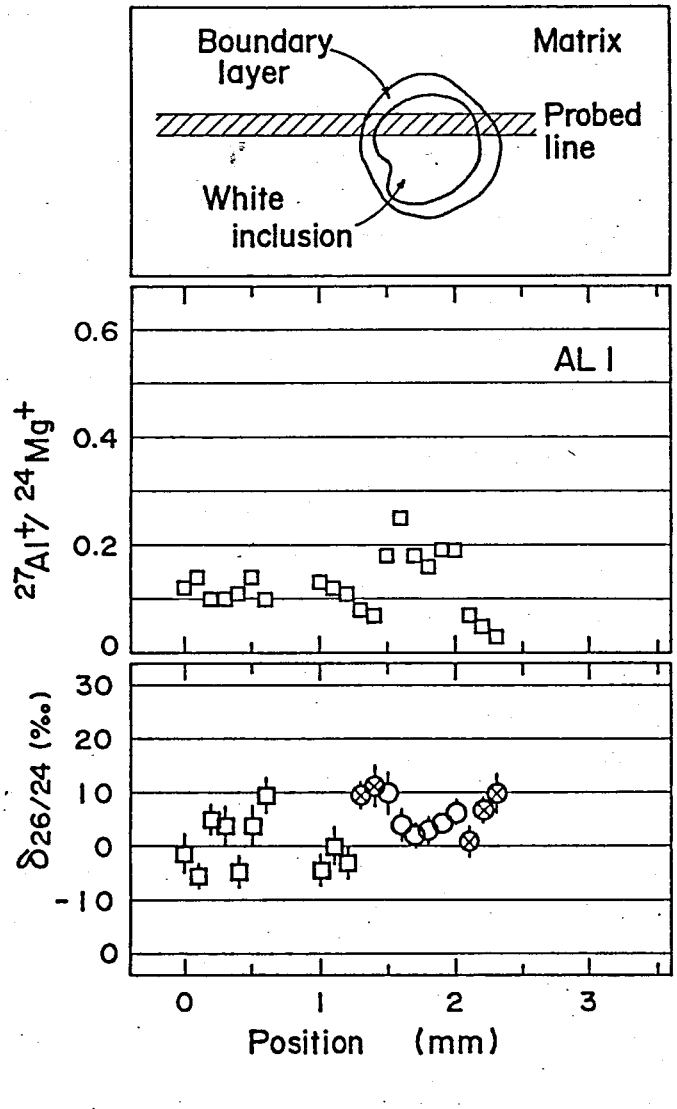

Fig. 5.6 $\delta_{26/24}$ and $^{27}Al^+/^{24}Mg^+$ as a function of probed position along the probed line for the AL1. Symbols for the plot of $\delta_{26/24}$ are the same as shown in Fig.5.2.

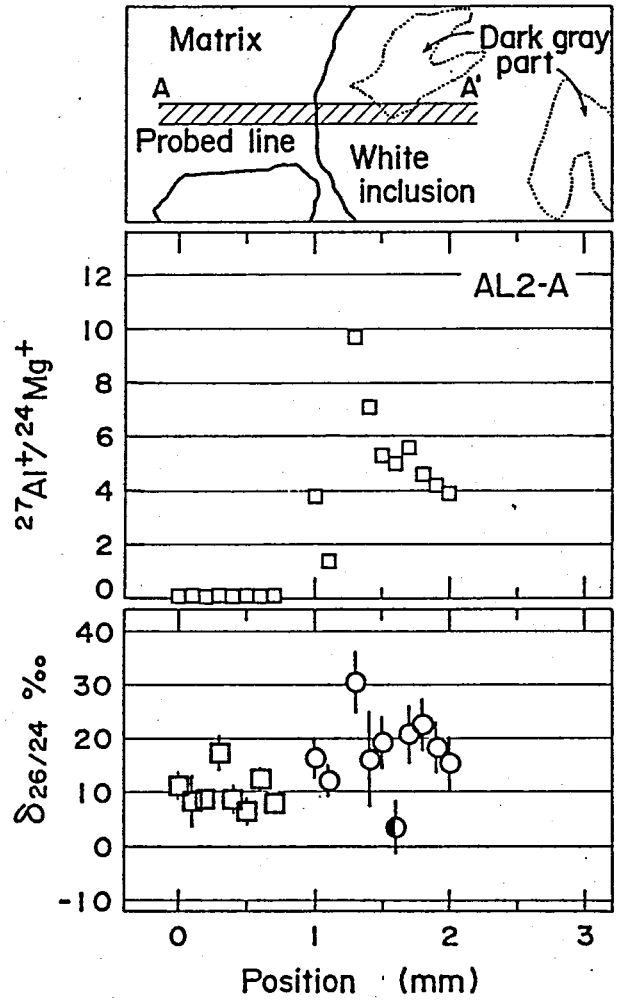

Fig. 5.7 $\delta_{26/24}$ and $^{27}Al^+/^{24}Mg^+$ as a function of probed position along the probed line AA' for the AL2. Symbols for the plot of $\delta_{26/24}$ are the same as shown in Fig.5.3.

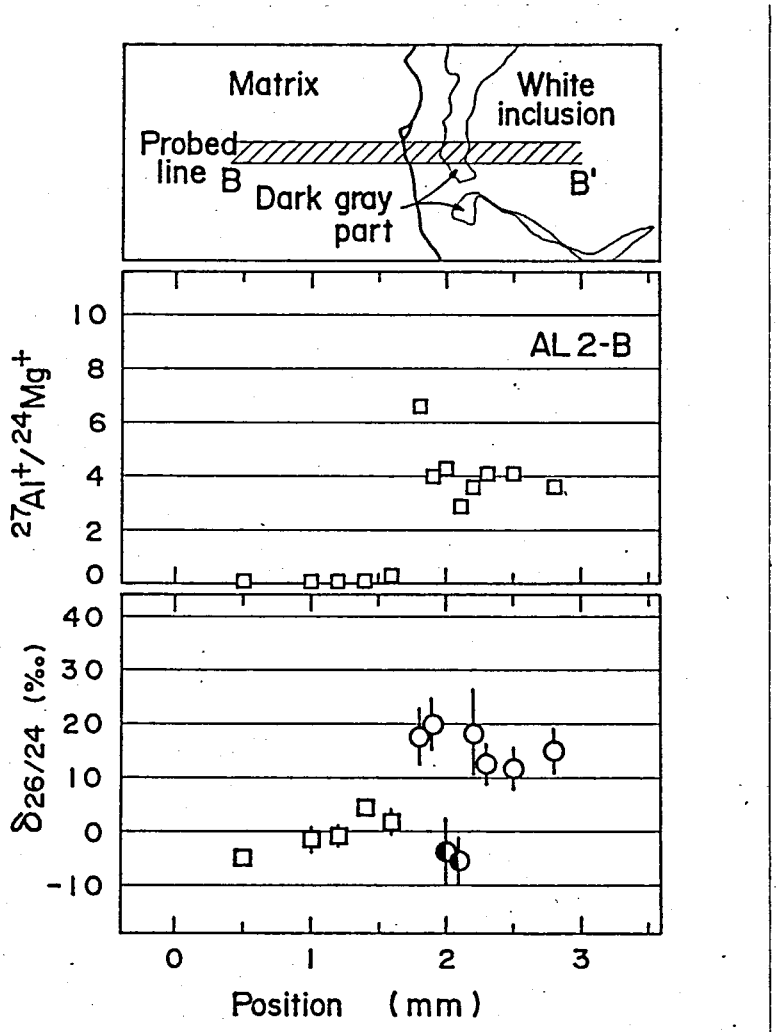

Fig. 5.8 $\delta_{26/24}$ and $^{27}Al^+/^{24}Mg^+$ as a function of probed position along the probed line BB' for the AL2. Symbols for the plot of $\delta_{26/24}$ are the same as shown in Fig.5.4.

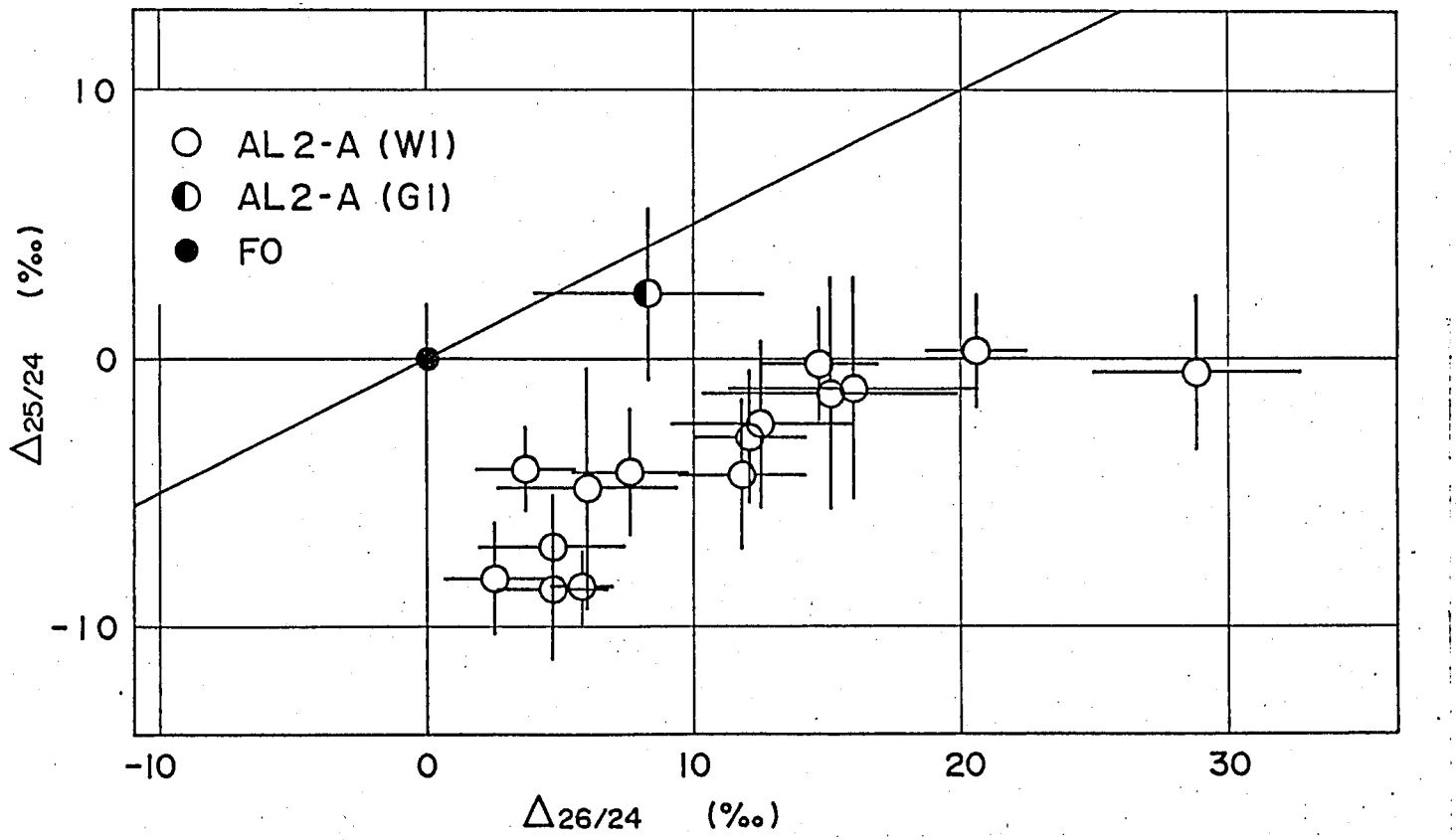

Fig. 5.9 Three isotope plot of magnesium for the white inclusion in the AL2. These data were obtained along the probed line AA'. A straight line with the slope of 1/2 represents the normal mass fractionation line.

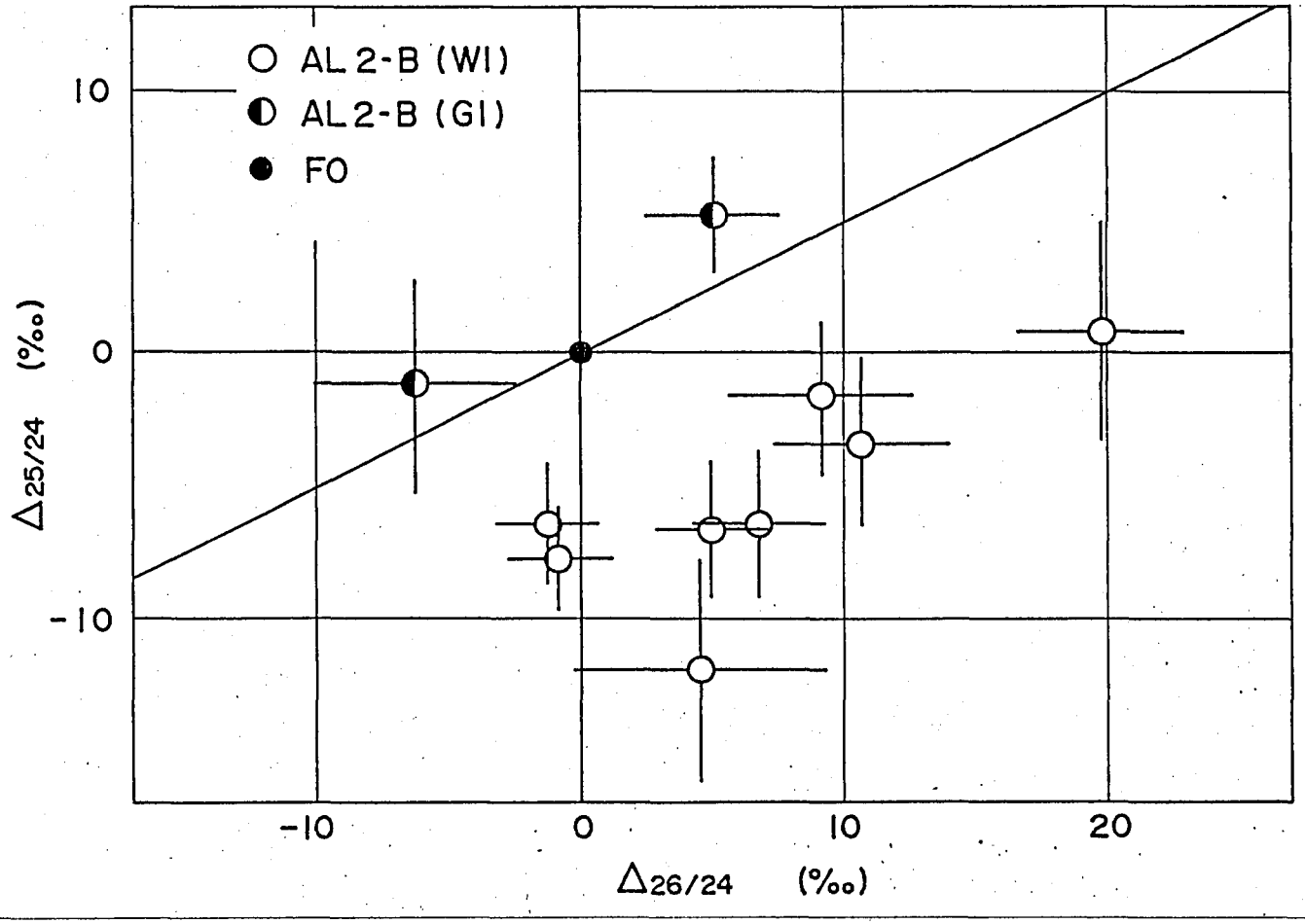

Fig. 5.10 Three isotope plot of magnesium for the white inclusion in the AL2. These data were obtained along the probed line BB'. A straight line with the slope of 1/2 represents the normal mass fractionation line.

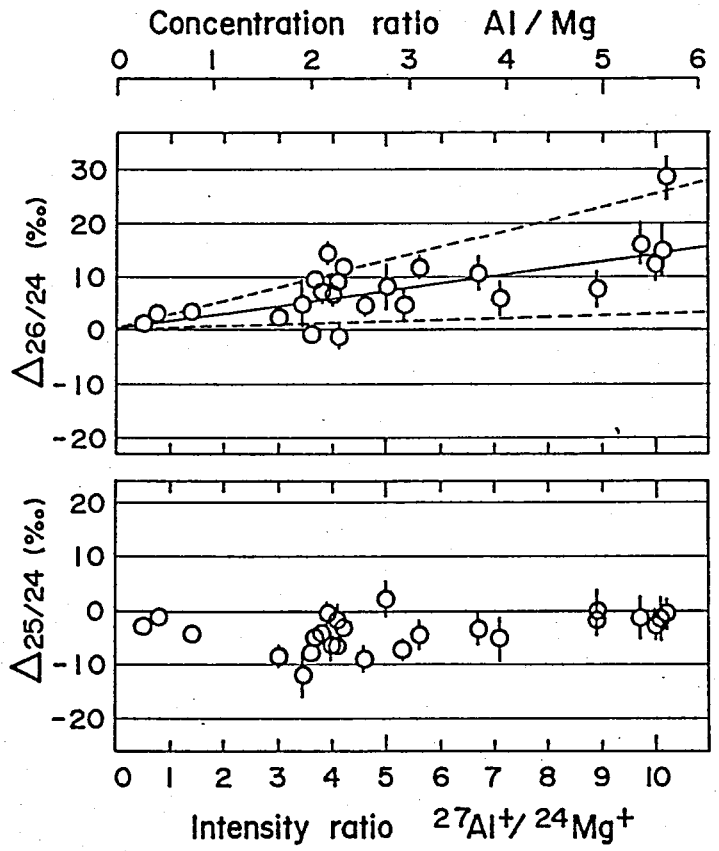

Fig. 5.11 $\Delta_{26/24}$ and $\Delta_{25/24}$ versus Al/Mg ratio showing the correlation between $\Delta_{26/24}$ and Al/Mg. These data are the same as plotted in both Figs.5.9 and 5.10.

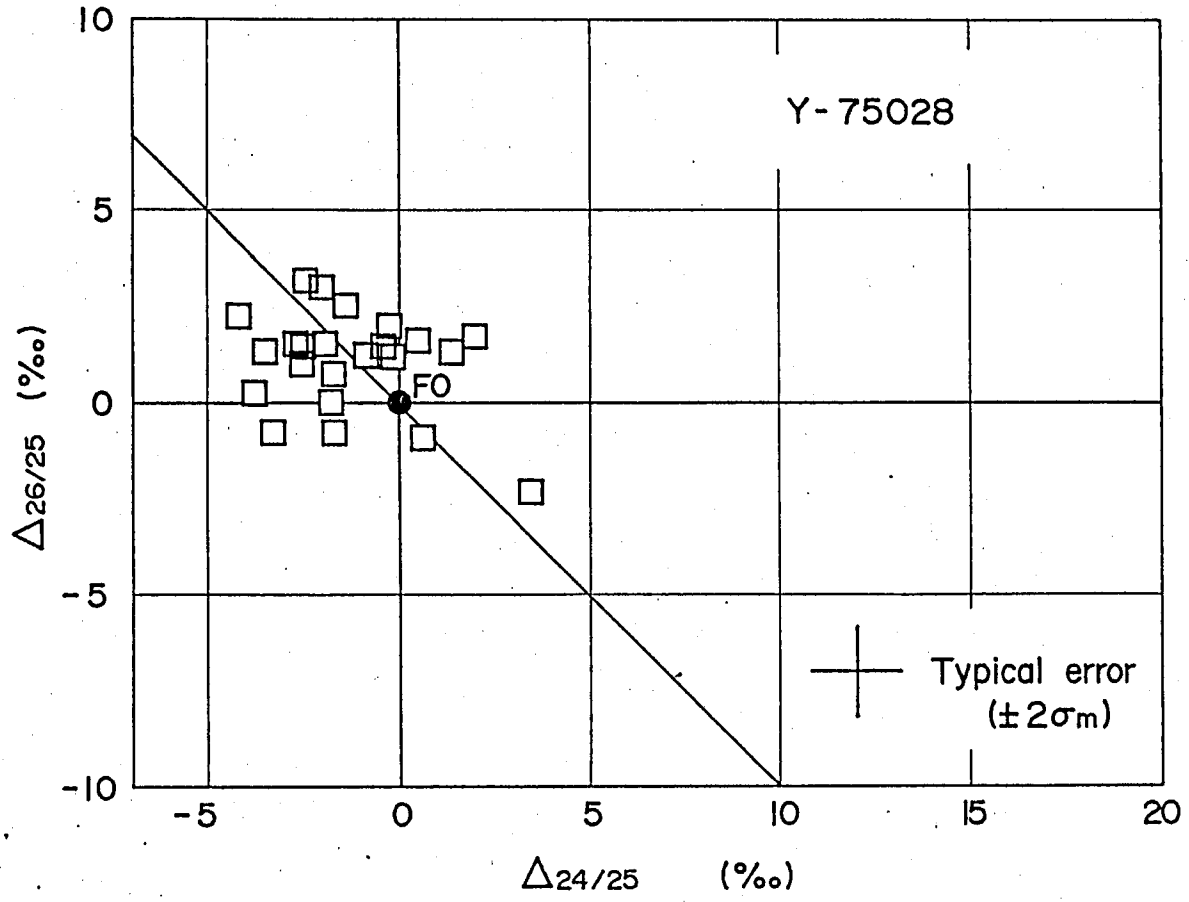

Fig. 5.12 Three isotope plot of magnesium for the matrix portions of Y-75028. The plotted data were obtained for the portions where the concentration ratio of Al/Mg is lower than 0.13.

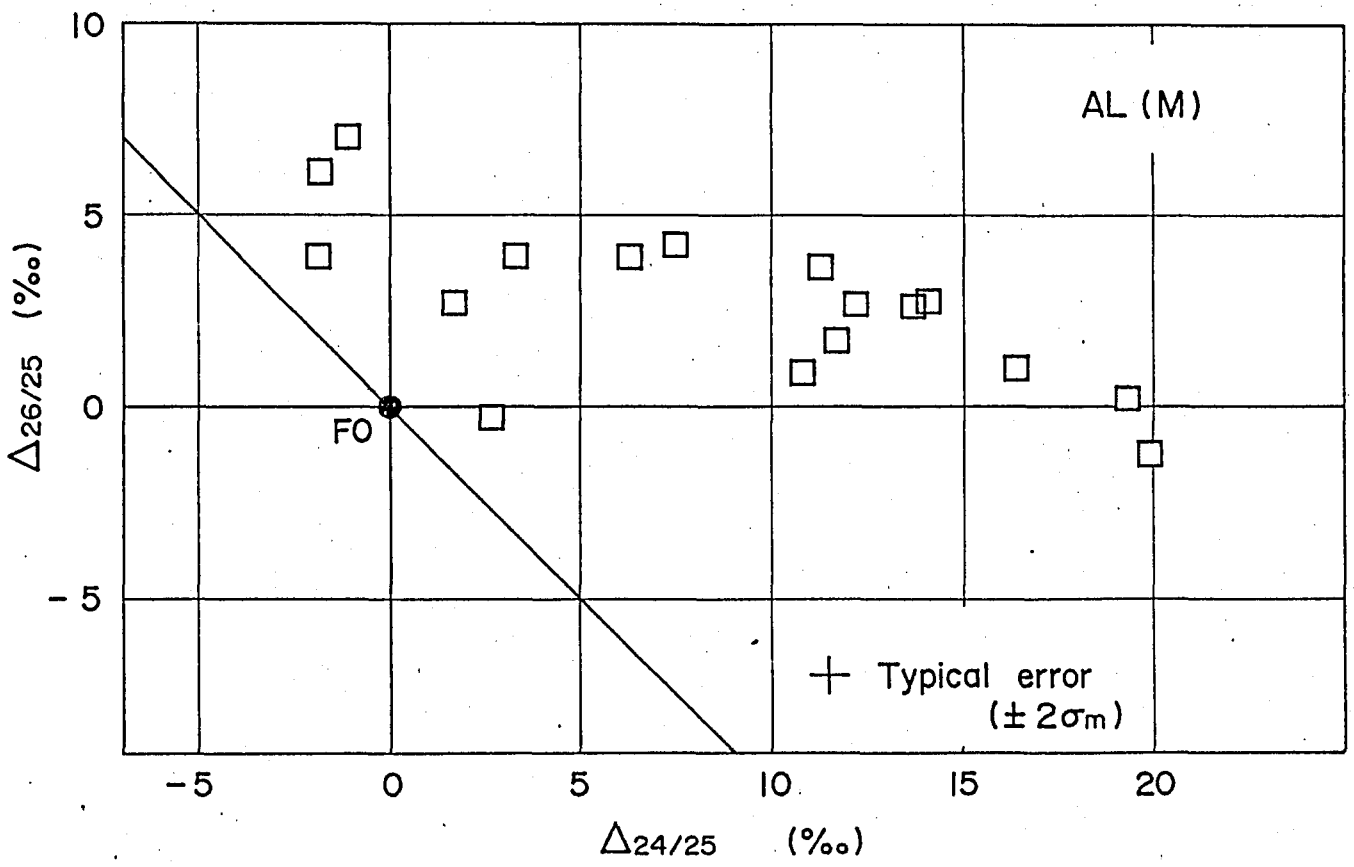

Fig. 5.13 Three isotope plot of magnesium for the matrix portions of Allende. The data were obtained for the portions where the concentration ratio of Al/Mg is less than 0.13.

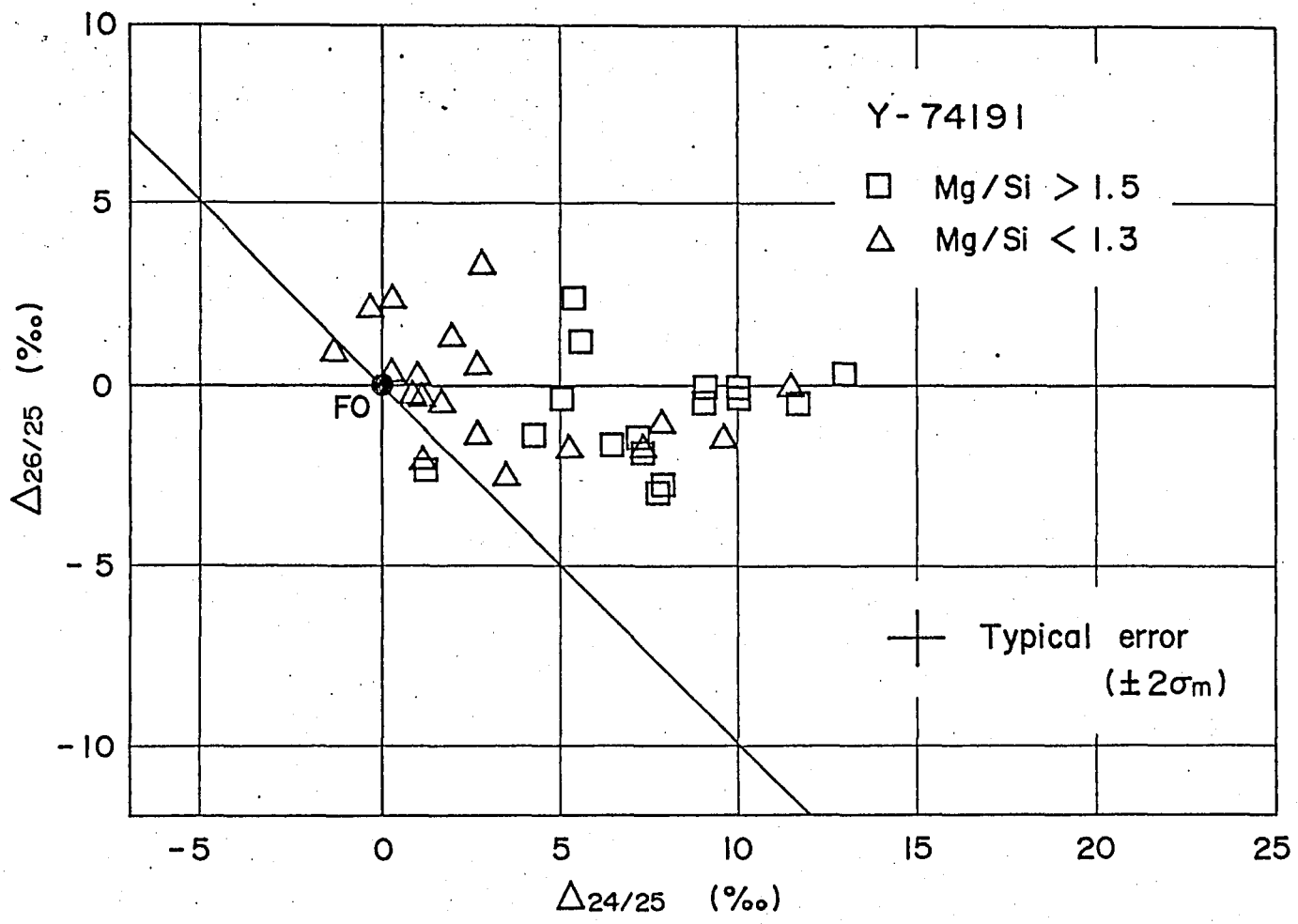

Fig. 5.14 Three isotope plot of magnesium for the matrix portions of Y-74191. The data were obtained for the portions where the concentration ratio of Al/Mg is less than 0.13.

LIST OF PUBLICATIONS

1) H. Nishimura and J. Okano, An ion microprobe analyzer, Japan. J. Appl. Phys., 8 (1969) 1335-1343.

2) H. Nishimura and J. Okano, Preliminary analysis of meteorites with an ion probe mass analyzer, Mass Spectroscopy, 18 (1970) 894-904 (in Japanese).

3) H. Nishimura, T. Fujiwara and J. Okano, Improvement of detectable limit of an ion probe mass spectrometer, mass Spectroscopy, 19 (1971) 205-212.

4) H. Nishimura and J. Okano, Isotopic ratio of lithium in chondrite measured by an ion probe mass spectrometer, Japan. J. Appl. Phys., 10 (1971) 1613-1622.

5) H. Nishimura, T. Fujiwara and J. Okano, Element and Isotope analysis with ion probe mass spectrometer, Proc. 6th Int. Cong. on X-ray Optics and Microanalysis (ed. G. Shinoda et al.) (1972) 431-437.

6) H. Nishimura and J. okano, Isotope analysis on iron meteorites with ion probe mass spectrometer, Proc. 6th Int. Vacuum Cong., (Japan. J. Appl. Phys. Suppl. 2) (1974) 399-401.

7) H. Nishimura and J. Okano, An oxygen ion source for the secondary ion mass spectrometer, Mass Spectroscopy, 23 (1975) 9-14.

8) H. Nishimura and J. Okano, Isotopic abundance of nickel in iron meteorites measured with a sputtering ion mass spectrometer, Adv. Mass Spectrom., 7A (1978) 569-572.

9) J. Okano and H. Nishimura, SIMS measurement of Mg isotopic ratio in chondrite, Secondary Ion Mass Spectrometry, SIMS II (eds. A. Benninghoven et al.) Springer Verlag, (1979) 216-218.

10) H. Nishimura, Application of SIMS to the fields of earth and planetary sciences, Mass Spectroscopy, 28 (1980) 41-52 (in Japanese).

11) H. Nishimura and J. Okano, SIMS measurements of magnesium isotopic abundance ratio in the Allende carbonaceous chondrite, Adv. Mass Spectrom., 8A (1980) 513-521.

12) H. Nishimura and J. Okano, SIMS measurement of magnesium isotopic ratios in chondrites, Mem. Natl. Inst. Polar Res., Special Issue (1981) 229-236.

13) H. Nishimura and J. Okano, SIMS measurement of magnesium isotopic ratios in chondrites, Meteoritics, 16 (1981) 368-369.

14) J. Okano and H. Nishimura, Distribution of Ni, Co, Ga and Cu in iron Meteorites, Secondary Ion Mass Spectrometry, SIMS III (eds. A. Benninghoven et al.) Springer Verlag (1982) 426-430.

15) H. Nishimura and J. Okano, SIMS measurement of magnesium isotopic ratios in Yamato-74191 and 75028 meteorites, Mem. Natl. Inst. Polar Res., Special Issue (1982) (in print).